The functional role and regulation of interferon induced transmembrane protein-1 in triple-negative breast cancer

By

Olivia K. Provance
B.A. William Jewell College, 2014

Submitted to the graduate degree program in Cancer Biology and the Graduate Faculty of the University of Kansas in partial fulfillment of the requirements for the degree of Doctor of Philosophy.

_____
Committee Chair: Joan Lewis-Wambi, PhD

_____
Shrikant Anant, PhD

_____
Christy Hagan, PhD

_____
Nikki Cheng, PhD

_____
Udayan Apte, PhD

Date Defended: 26 May 2021

The dissertation committee for Olivia K. Provance certifies
that this is the approved version of the following dissertation:

The functional role and regulation of interferon induced transmembrane protein-1 in triple-negative breast cancer

_____
Committee Chair: Joan Lewis-Wambi, PhD

_____
Graduate director: Joan Lewis-Wambi, PhD

Date Approved: 29 May 2021

Abstract

Breast cancer is the most common cancer diagnosed among women in the United States. Breast cancer is subdivided into groups based on receptor status including estrogen receptor (ER) and progesterone receptor (PR) positive, human epidermal growth factor-2 positive (HER2) or triple-negative. Triple-negative breast cancer (TNBC) affects 15-20% of women diagnosed with breast cancer each year and is the most aggressive subtype. TNBC lacks the common receptors used to diagnose and treat breast cancer and subsequently, does not have any targeted therapies. Therefore, our long-term goal is to identify drivers of TNBC aggression and subsequent treatments to target those drivers. Evidence suggests that breast tumors expressing high levels of interferon stimulated genes (ISGs) are more aggressive than tumors expressing low levels of ISGs, perhaps providing a molecular explanation into the aggressive nature of TNBC. We have identified that TNBC breast cancer cell lines and patient samples overexpress a specific ISG called interferon inducible transmembrane 1 (IFITM1). Though studies in cancer biology have identified that IFITM1 can promote tumor progression, the role of IFITM1 in TNBC is unknown. IFITM1 is normally only expressed upon exposure to type I interferons such as interferon (IFN)-alpha, but can also be regulated by other pathways including NFκB. The goals of this thesis are to assess the clinical and functional relevance of IFITM1 in TNBC, to investigate the mechanism by which IFITM1 contributes to TNBC progression, and to uncover novel ways to target its expression.

In this thesis we demonstrate that IFITM1 is significantly elevated in TNBC tumors as assessed by a TNBC tumor microarray and in silico analysis, and that IFITM1 is overexpressed in TNBC cell lines. Loss of function studies in SUM149, MDA-MB-157, and MDA-MB-468 TNBC cell lines reveal that IFITM1 regulates TNBC growth, migration, and invasion both *in vitro* and *in vivo.* RNA sequencing of CRISPR/Cas9 mediated IFITM1 knockout SUM149 cell lines suggest that loss of IFITM1 results in a decrease of NFκB mediated signaling and subsequently IL6 and

SNAI2 expression. Mechanistically, data presented herein suggest IFITM1 functions to regulate TNBC cell growth with the help of CD81 likely through regulating integrin, NFκB, and IL6 gene expression. Additionally, we uncovered, for the first time, that IFITM1 is secreted in TNBC extracellular vesicles. Collectively, these findings suggest that IFITM1 contributes to TNBC progression, therefore, selectively targeting IFITM1 may be a novel therapeutic avenue for patients with IFITM1 positive TNBC.

IFITM1 is normally only expressed upon exposure to type I interferons such as interferon alpha (IFNα). Canonical IFNα signaling activates a JAK/STAT phosphorylation cascade resulting in formation of a transcriptional complex comprised of phosphorylated (p-)STAT1, pSTAT2 and interferon regulatory factor-9 (IRF9). However, IFNα can promote gene expression in the absence of STAT phosphorylation due to chronic exposure to IFNα, or through crosstalk with other pathways including NFκB. Data presented herein show that IFITM1 is regulated in a STAT2/IRF9/p65 dependent manner. We identified that IFITM1 is regulated by autocrine IFNα in TNBC through unphosphorylated the STAT2/IRF9 complex, but also identified that IFITM1 is directly regulated by p65 and that IFNα can regulate p65 activation. Anchoring these data, a high throughput screen identified the NFκB inhibitor, parthenolide, to be cytotoxic to TNBC cells and we found it regulates IFITM1 expression both *in vitro* and *in vivo.* Lastly, loss of IFITM1 enhances parthenolide mediated apoptosis.

Data presented in this thesis begin to characterize the functional role of IFITM1 and IFNα signaling in TNBC progression as a means for developing a more comprehensive understanding of TNBC biology in hopes of identifying potential alternative therapies. Here, we provide evidence to suggest that IFITM1 is both a potential therapeutic target and biomarker for a subset of TNBC.

Acknowledgements

I would like to start by thanking my mentor. Dr. Wambi, I cannot thank you enough for your mentorship and support. You have encouraged me to develop my own ideas about how to solve a problem while trusting me and giving me the space to be creative in the pursuit. I have experienced the highs of success and the lows of failure and your encouragement and excitement for science has carried me along every step of the way. You are a mentor who truly cares about your trainees on a personal level. I remember after my first presentation on my work in your lab you gave me a hug and said “I’m so proud of you!” and you have done that nearly every presentation since. I am so lucky to have had a PhD mentor who cared just as much about the journey and my wellbeing as the science. It has been an honor being trained by you.

I would also like to thank my dissertation committee members Drs. Shrikant Anant, Christy Hagan, Udayan Apte and Nikki Cheng. Our meetings have been full of constructive criticism and thought-provoking questions, but most importantly, you all contributed to my growth as a scientist and have increased my confidence as a scientist dramatically. Thank you all for providing this guidance and support during my journey. A special thank you goes out to Dr. Hagan. Dr, Hagan, you and your lab have been an instrumental part of my graduate education. I knew that if I were stuck on a scientific question, if I was unsure about methodology, or needed help analyzing data, you would graciously help. You always showed excitement for my project and has never once hesitated to provide insight.

I would like to recognize the staff in the multiple cores at KUMC including the Biospecimen Shared Resources (Marsha Danley), High Throughput Screening Lab (Scott Weir, Anuradha Roy), Confocal Imaging Core (Pat St. John), as well as the staff and mice in the Animal Facility at KUMC. I would like to acknowledge the Welch lab, Hagan lab, and Anant Lab for help with experimental design advice and allowing me to use multiple machines for analysis. Furthermore, the support for this research could not have been completed without the funding from the National

Institutes of Health, Department of Defense, American Cancer Society, KUMC and KUCC, and the Biomedical Research Training Program.

I am grateful to the Cancer Biology Department for the support of their students and for the didactic training by wonderful instructors. Additionally, I would like to thank the administrative team for their role in ensuring the department and my path to graduation runs smoothly. Furthermore, the support given by Dr. Shrikant Anant for the formation of the Cancer Biology Student Society has been invaluable for my graduate experience and leadership development. And lastly to my fellow students in the department. Sharing in successes, failures, and all things in between has made many memories I will never forget. I am so thankful to have you all as colleagues and friends and I am excited to see what you go on to accomplish.

I would also like to thank both the past members (Eric Geanes and Asona Lui) and current member (Taylor Escher) of the Wambi lab. Eric and Asona, thank you for all of your time spent training me in methodology, for always being down for a coffee break, and for your continued help in manuscript preparation. Taylor, I am so thankful we had each other throughout our PhDs. Your kindness and encouragement over the last four years has been exceptional.

To my friends and family. Your loyalty, support, understanding, encouragements, and love has fueled me with the energy to complete this education. I could write a novel for each one of you. I love and appreciate you more than I can even begin to explain here.

And to my beloved husband, Jeremy. Pursuing PhD's together was not easy. On our wedding day you promised me you would challenge me to seek truth as a scientist, to be my energy when I am weary, to celebrate me in my successes, and to love and support me in my defeats. You have done all those things and more including the daily reminders to work hard and be nice.

Table of Contents

List of Figures

List of Tables

List of Supplemental Figures

Chapter 1: Introduction

Parts of this chapter are adapted from work previously published as an open access article.

Provance, OK, Lewis-Wambi, J. (2019). *Deciphering the role of interferon alpha signaling and microenvironment crosstalk in inflammatory breast cancer. Breast Cancer Res, 2019. 21(1):59.* PMCID*:* PMC6501286. doi: 10.1186/s13058-019-1140-1.

Breast Cancer

Breast Cancer: Statistics and subtypes

Breast cancer is the most common cancer diagnosed among women in America. The American Cancer Society predicts that approximately 282,000 new breast cancer cases will be diagnosed in 2021 and approximately 44,000 women will face mortality due to breast cancer. Contributing to the high mortality rate is the inter- and intra-tumor heterogeneity that is intrinsic to the disease. Assessment of both histopathological prognostic characteristics including grade and stage (1) and the presence of receptors including the estrogen receptor (ER), the progesterone receptor (PR), and the human epidermal growth factor (HER2) have provided a means to stratify patients in regard to prognostic predictions and treatment selection for many years (2). However, the use of recent technological and molecular advances including microarray analyses and next-generation sequencing has prompted a deeper investigation into the diversity and classification of breast cancer (3-7). This technology has identified five major intrinsic subtypes including Luminal A, Luminal B, HER2 enriched, basal-like and claudin-low, and normal breast like (3-7), all of which have unique incidence, risk factors, prognosis and treatment response (2) (Figure 1.1). In general, luminal tumors (estrogen receptor (ER+), progesterone receptor (PR+) are the most common (60% of cases) and are largely curable with a low rate of recurrence whereas those diagnosed with basal-like tumors (human epidermal growth factor-2 (HER2+) and triple negative) have a poor response to therapy and a higher rate of relapse free survival and lower overall survival (8). The most common subtype is luminal A comprising approximately 40% of breast cancer cases. These tumors are ER+ PR+ and HER2-, have a low proliferative index as identified by Ki67 staining, and respond well to estrogen inhibitor therapy. Similar subtypes include normal-like comprising 2-8% of breast tumors, and luminal B comprising approximately 20% of breast tumors with the major differences being in proliferation rate. Poorer prognosis arises with the presence of the HER2 receptor which comprises approximately 10-15% of breast tumors

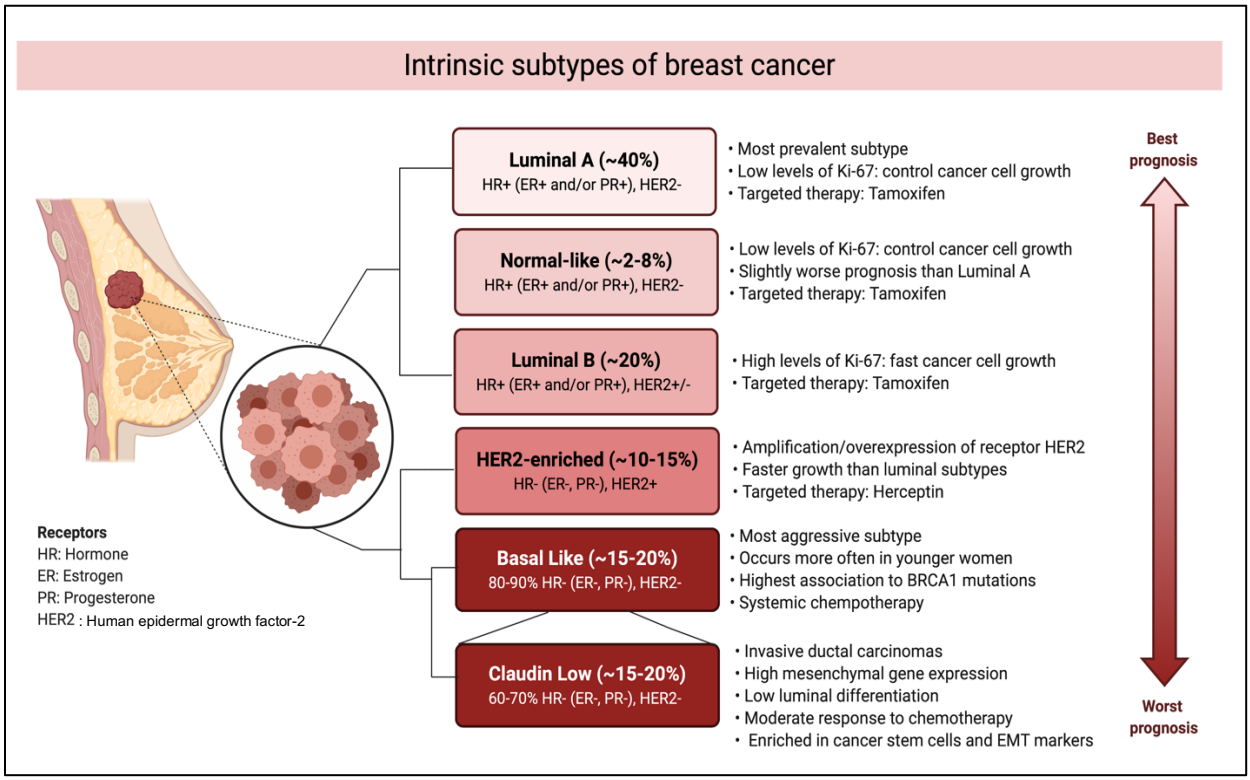

Figure 1.1 Intrinsic subtypes of breast cancer

Breast cancer is a heterogenous disease characterized by multiple distinct subtypes. Numerous groups have worked to classify breast tumors based on gene expression, receptor status, extent of differentiation, treatment response and prognosis (3-7). Here we represent the most prominent subtypes. Nodes represent similarity. In particular, within the basal like subtype is the claudin-low subtype. Claudin-low tumors are highly invasive with low luminal differentiation and elevated gene expression related to mesenchymal processes and stem cells. Figure created with BioRender.com template.

characterized by elevated cell growth and invasion, but can be targeted by HER2 targeting agents such as Herceptin. The most aggressive subtype is known as basal-like breast cancer which accounts for 15-20% of total cases (7, 9, 10). This subtype occurs more often in younger women, is associated with BRCA mutations, and is predominantly comprised of the triple-negative breast cancer (TNBC) subtype (80-90%) which lack the three most common receptors (ER, PR, HER2+) that are used for detecting and treating breast cancer. Though enhanced characterization has provided insight into the heterogeneity of breast cancer and has improved survival rates for luminal A and HER2+ tumors, TNBC patients still lack targeted therapy and continue to have high

mortality rates (11, 12). Therefore, there is an unmet need to identify drivers of TNBC aggression and subsequent treatment regimens for those markers.

Triple-negative breast cancer: Statistics and subtypes

Approximately 15-20% of breast cancer patients will be diagnosed with triple negative breast cancer (7, 9, 10). Unlike other subtypes, TNBC disproportionately affects younger women and African-American women, and demonstrates high pathologic grade (13). Patients diagnosed with TNBC have a lower 3-5 year overall survival rate than receptor positive breast tumors with a reported 12-month median overall survival compared to 20 months for ER/PR+ tumors and 56 months for HER2+ tumors (10, 12, 14-16). TNBC diagnosis depends on accurate assessment of ER, PR and HER2 by immunohistochemistry (IHC) or fluorescence *in situ* hybridization (FISH) (8). Tumors with <1% ER/PR/HER2 positivity as observed by IHC are classified as TNBC (8).

Like breast cancer in general, unique molecular subtypes within TNBC based on gene expression patterns and immune environment have been uncovered: immunomodulatory, mesenchymal stem like, basal like, luminal androgen receptor (AR), and mesenchymal (4, 10, 15, 17-19) (Figure 1.2). It is worth noting that the main difference between mesenchymal-stem like and mesenchymal TNBC subtypes is that the mesenchymal stem-like subtype has decreased proliferation genes and higher levels of genes related to mesenchymal stem cells (20). Despite this effort in identifying biologically distinct subtypes of TNBC, there is still high uncertainty of molecular drivers of the disease and each subtype will likely display differential responses to novel targeted agents (13).

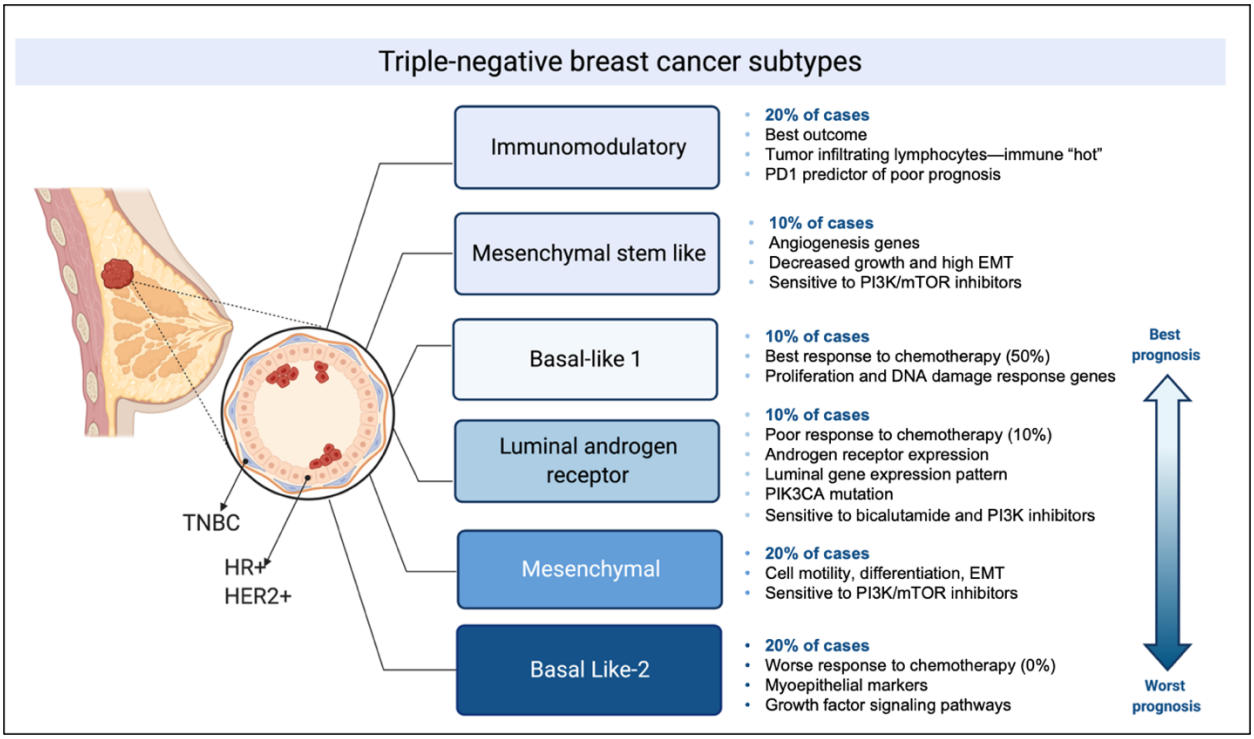

Figure 1.2 Triple negative breast cancer subtypes
Like breast cancer in general, TNBC is a highly diverse group of cancers. Subtyping of TNBC is necessary for development of molecular-based therapies to enhance patient prognosis. Here, we present an overview of the most prominent TNBC subtypes and descriptive of outcomes, gene signatures, and treatment response (4, 7, 10, 15, 17-19). Subtype response to chemotherapy was derived from Masuda et al. (21). Figure created with BioRender.com template.

Triple-negative breast cancer: Current therapies

Continued development of targeted therapies for HR+ and HER2+ breast cancer has contributed to a decrease in mortality. However, TNBC has not benefited from these discoveries due to the lack of receptors and extensive heterogeneity. To date, there is absence of targeted treatment for TNBC patients (22). The current standard of care for grade I-III TNBC patients is an anthracycline-taxane-based systemic chemotherapy regimen and for local TNBC, mastectomy, and radiation therapy (13, 23, 24). Despite this treatment, approximately 30-40% of early stage TNBC patients who receive treatment develop metastatic disease leading to demise, which is substantially worse than HR+ and HER2+ breast cancer (10). However, TNBC has an inherent

paradox when assessing response to chemotherapy (25). A study published in the Lancet assessed the relationship between pathological complete response (pCR) and residual disease (RD) in TNBC patients (26). pCR and RD are measured after neoadjuvant chemotherapy and are used as predictive outcomes for TNBC patients (26). The 35% of TNBC patients that achieve a pCR have good prognosis whereas the 65% with RD have a significantly decreased overall survival compared to other breast cancer subtypes (7, 26, 27). Regardless of pCR, 20-40% of patients with TNBC have tumor recurrence three to five years following diagnosis (28). In an effort to enhance patient response and effectiveness of systemic chemotherapy in TNBC patients, clinical trials have investigated the addition of other agents to chemotherapy though these additions had no significant improvement in overall survival (13, 29, 30). Though with the help of genomic studies, development of more targeted treatments have emerged including, PARP inhibitors (PARPi), pathway specific (AKT, PI3K and mTOR) inhibitors, and immune checkpoint therapy (31). Recent studies suggest that TNBC tumors are more likely to respond to immunotherapy than other breast cancer subtypes due to increased number of tumor infiltrating lymphocytes in the tumor stroma and increased levels of programmed death ligand-1 (PD-L1) expression on both tumor and immune cells providing direct targets for immune checkpoint inhibitors (32-35). However, TNBC patients have a poor response to PD-L1 targeted therapy. Interestingly, PD-L1 as well as other immune checkpoints are known to be regulated by interferon (IFN) signaling (36). IFNs have been implicated in enhancing tumor cell DNA damage resistance in multiple cancer types including breast cancer perhaps contributing to this treatment difficulty in TNBC (37).

Interferon signaling

The interferon family

Interferons (IFNs) are cytokines known to confer an adaptive immune response in all cell types (12, 13). The IFN family is divided into three groups: type I interferons (IFN-α, -β, -ε, -κ, and-ω) type II interferon (IFNγ) and type III IFNs (IFNλ's -1,-2,-3,-4). Each IFN has specific genetic loci contributing to differential activation (38).

Type I IFNs are best known for signaling through the interferon alpha receptor (IFNAR) complex of IFNAR1/IFNAR2 to activate signal transducer and activator of transcription (STAT)-1/STAT2 phosphorylation and subsequent binding with interferon regulatory factor (IRF)-9, forming the interferon stimulated gene factor-3 (ISGF3) complex. ISGF3 can bind to the DNA at the interferon stimulated response element (ISRE) to drive transcription of ISRE dependent genes. Activation of type I IFN signaling is essential for the antimicrobial defense and for modulation of the adaptive immune response. All nucleated cells express type-I interferon receptors and can produce IFNα upon viral stimulation (14). Type I IFNs are produced in cells upon viral or pathogenic infections through pattern recognition receptor pathways, including RIGI (retinoic acid inducible gene 1), PKR (protein kinase R), toll like receptor (TLR) 3, -7, -9, and STING (stimulator of interferon genes) (39).

Type II IFNs signal through the interferon gamma receptor (IFNGR) complex of IFNGR1/IFNGR1 activating STAT1 activation and subsequent dimerization allowing binding to gamma activated sites (GAS) sites in a subset of interferon stimulated genes (40). Though hematopoietic cells are the key producers of IFNγ nearly all cells in the body express an IFNGR receptor and therefore, are responsive to IFNγ (38, 41). IFNγ plays a key role in regulating T-cell response and myeloid activation since antigen-activated T-lymphocytes are key producers of IFNγ (39). Additionally, IFNγ is a potent macrophage activator which enhances the cellular response against mycobacteria and intracellular pathogens (39).

Type III IFNs include (IFNλ-1, -2, -3, -4) otherwise known as IL-29, IL-28A, IL-28B, and IFN-λ4 respectively. This family is the most newly characterized and are similar in structure and function to the IL10 family of cytokines (39). These interferons bind to the IFNLR1 (IL-28Ra) and IL-10R2. Though type III IFNs are capable of signaling through the ISGF3 complex, IFNLR1 has specific affinity to IFNλ and is only found on epithelial cells and subsets of myeloid and neuronal cells (38, 39). Similar to type I IFNs, type III IFNs are produced as a cellular response to viral or pathogenic infection, and through pattern recognition receptor pathways (39).

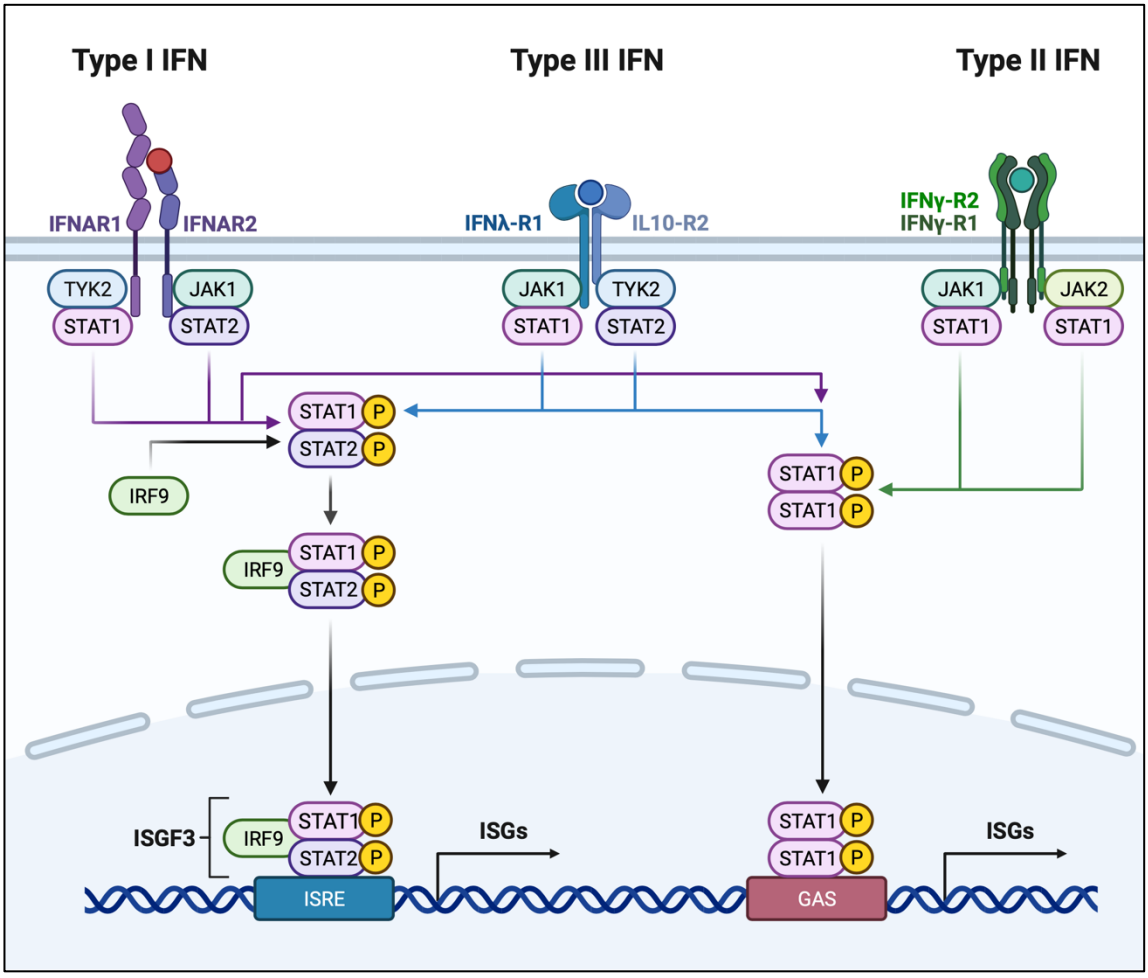

Figure 1.3 General overview of interferon signaling
Each IFN binds to a specific cellular heterodimer receptor complex with high affinity. The binding of IFN to its receptor complex initiates a phosphorylation cascade with activation of JAK, TYK and STAT proteins. Homodimerization and heterodimerization of STATs and other factors (i.e: IRF9) allow for nuclear entry and variable DNA binding affinity to specific promoter elements for gene transcription. Figure created with BioRender.com template.

As described above, each family of interferons induces specific but somewhat overlapping cellular responses. However, multiple regulatory mechanisms exist to control the cellular response to the IFN including the duration and concentration of IFNs, post-translational modifications, negative regulators, and mutational burden (42). Though the biological role of IFNs has evolved to regulate the immune response, implications for their role in cancer biology have emerged.

The paradoxical roles of IFN signaling

IFNs operate on a temporal spectrum contributing to their observed paradoxical roles in cancer biology (43). IFNs from both immune cells and tumor cells function concurrently to regulate the early steps of cellular transformation and elimination of malignant cells but can eventually lead to tumor cell immune escape and subsequent progression.

During initial tumor formation, immune cells surrounding the tumor will recognize tumor specific antigens and eliminate the transformed cells (44). IFN-signaling is required for this initial immune-recognition and destruction of nascent tumors by immune modulatory cells including dendritic cells and T-cells (45). Specifically, IFNα produced by tumor cells activates innate immunity to promote an anti-tumor immune response through elevating MHC molecules, co-stimulation, cross presentation, and activation of CD8+ T-cells (46), and through activating natural killer cells, dendritic cells, and B-cells (46, 47). In regard to TNBC, high infiltration of tumor infiltrating lymphocytes contributes to better response to chemotherapy (48). However, this may only be for specific subtypes of TNBC as previously outlined.

Alternatively, chronic inflammation is associated with cancer progression due to progressive immune dysfunction. Tumor cells which are not eliminated often undergo senescence (49). During senescence, normal epithelial cells become transformed through destabilization of chromatin, increased DNA damage, or through mutations necessary for survival, promoting secretion of a subset of inflammatory cytokines. This secretory phenotype of transformed cells

can promote a pro-tumorigenic microenvironment through immune suppression. In particular, studies show that IFNα may promote tumor immune escape through up-regulation of PD-L1 on tumor cells (50) which subsequently protects against further IFN induced cytotoxicity (51).

Moreover, persistent DNA damage can also contribute to chromosomal instability (CIN) in cells which maintain proliferative capacity (52). It is hypothesized that CIN can induce IFNα production (53) and a previous study identified that that ER-negative, triple-negative and basal-like tumors have significantly higher CIN scores (54) which correlates with tumor metastasis (52). Supporting this evidence, the IFNα signature has been identified as a pathway upregulated in an a highly aggressive subset of breast cancer known as inflammatory breast cancer (IBC) (55).

Though IFN signaling has the ability to eliminate tumor cells, aforementioned evidence highlights how IFN signaling, specifically IFNα, may contribute to tumor progression of TNBC. Perhaps sustained IFNα signaling could be induced by cellular injury (i.e.: chronic inflammation, DNA damage, etc.) and if its downstream effects are understood and appropriately targeted, may increase responsiveness to current therapies.

Interferon alpha signaling pathways: canonical, non-canonical, alternative

As previous discussions highlight, IFNα is a highly pleiotropic cytokine. Though IFNα preferentially signals through the JAK/STAT pathway, its signaling does not occur in isolation (46). The presence of other inflammatory and intracellular signals like crosstalk between pathways such as PI3K, MAPK and p65 ultimately mediate downstream gene expression (41). Adding to this complexity, IFNα modulates the activity of the JAK/STAT signaling pathway in both phosphorylated and an unphosphorylated mechanisms while this alone has implications in ISG induction. The plasticity of the cellular response to IFNα has been extensively reviewed by Cheon *et al.* (56) and Medrano *et al.* (57) so here, we discuss only the key aspects of mechanisms of IFNα intracellular signaling.

Canonically, the JAK/STAT pathway becomes activated once IFNα binds to IFNAR1 which then dimerizes with IFNAR2. IFNAR1 and IFNAR2 do not have intrinsic kinase activity but are constitutively associated with janus activated kinase-1 (JAK1) and tyrosine kinase-2 (TYK2) (41). Thus, the dimerization of IFNAR1 with IFNAR2 activates cross-phosphorylation of JAK1 and TYK2 resulting in phosphorylation of the intracellular domain of IFNAR1 and IFNAR2. STAT1 and STAT2 are recruited to the receptors through their SH2 domain allowing phosphorylation by JAK1 and TYK2. Phosphorylated STATs may then homodimerize or heterodimerize. The homodimer of STAT1 is known as IFN-activated factor (AAF) and the heterodimer of STAT1/STAT2 associated with interferon regulatory factor (IRF)-9 is termed interferon stimulated gene factor-3 (ISGF3). These complexes translocate into the nucleus and bind to gamma activated sequences (GAS) or interferon stimulated response elements (ISREs) on the DNA, respectively, transcribing specific interferon stimulated genes (ISGs), some of which are listed in Table 1.1 (Adapted from (37, 58, 59) and outlined in Figure 1.3 and 1.4. The ISGF3 complex binds a composite DNA sequence in which IRF9 contributes most of the DNA binding specificity by recognizing the core sequence of ISRE. Though STAT1 contributes necessary contacts with DNA, STAT2 does not directly bind to the DNA but instead, contains a transactivation domain which is essential for full ISGF3 transcriptional activity (60-62). Additionally, studies have uncovered essential roles of STAT2 and IRF9 in the absence of STAT1 which are highlighted by non-canonical interferon signaling (61, 62).

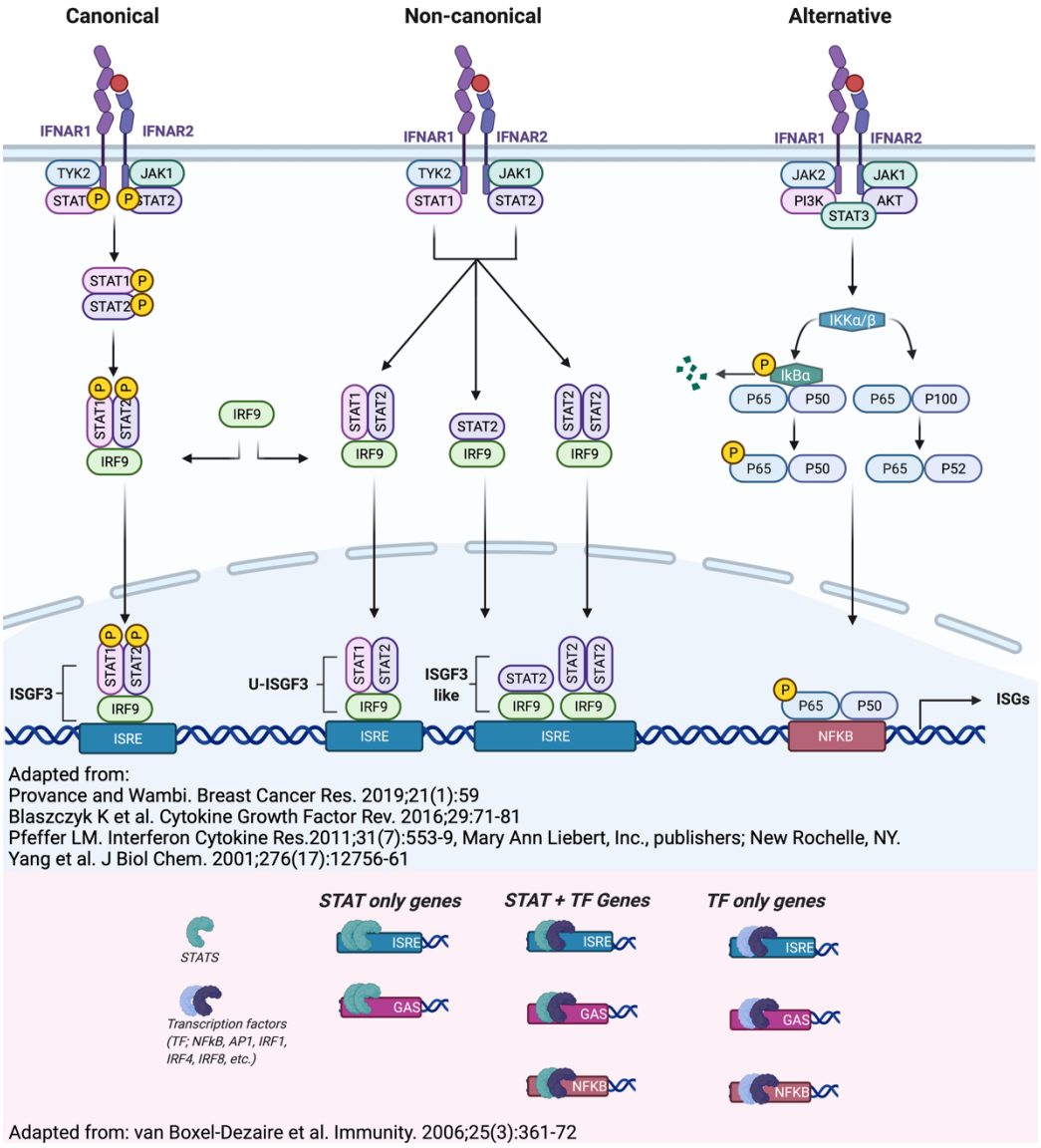

Figure 1.4 Canonical, non-canonical, and alternative mechanisms of IFNα signaling

Canonical: Canonical IFNα signaling begins with IFNα binding to IFNAR1/IFNAR2 receptor. After it binds to the receptor, JAK1 and TYK2 cross-phosphorylate each other and phosphorylate the intracellular domains of the receptors to allow for STAT1 and STAT2 binding through their SH2 domain for subsequent phosphorylation. Once STAT dimers form, they translocate into the nucleus and bind to their respective DNA binding elements. IRF9 and STAT1 are the only two proteins that directly interact with the DNA whereas STAT2 is necessary for stabilizing the ISGF3 complex and further recruitment of co-activators. ***Non-canonical:*** During chronic IFNα signaling, STAT proteins are no longer robustly phosphorylated however the interferon signature may remain upregulated due to the similarity between ISGF3 and U-ISGF3. In the absence of IFNα, there will either be no signal or, depending on STAT2 and IRF9 levels, the interferon response may stay elevated due to the continued formation of STAT2 and IRF9. TNBC cells have robust levels of IRF9 and IRF9 increases in tumor clusters. Therefore, IRF9 could be the key driver of this response (61). ***Alternative:*** IFN has also been identified to activate NFkB in a dose-dependent mechanism through adaptor proteins including STAT3, PI3K and AKT (63-65). Supporting this evidence, multiple ISGs have NFkB binding sites within their promoter (63, 66, 67). ***Below:*** Additionally, specific genes can be regulated in response to IFN signaling by STATs only, STATs and alternative transcription factors including NFkB, and IRF's, or through transcription factors only (68). Figure created with BioRender.com.

Table 1.1 Transcription factor complexes and their control of interferon stimulated genes

ISGF3		U-ISGF3	GAS
MX1/2		MX1/2	IFITM1
IFITM1	IRF9	IFITM1	STAT4
PLSCR1	IRF4	PLSCR1	IRF1
OAS1/2/3	cGAS	OAS1/2/3	IRF8
SOCS	STAT1	IRF7	IDO
USP18	STAT2	STAT1	NOS2
ISG15	NOS2	IFI27	PDGFRA
IRF3		IFI44	KRT14
IRF7			IRF2

Provance and Wambi. Breast Cancer Res. 2019;21(1):59

ISGF3: Interferon stimulated gene factor 3, consists of phosphorylated STAT1 and STAT2 dimers bound to IRF9. U-ISGF3: Unphosphorylated-interferon stimulated gene factor 3, consists of a dimer of unphosphorylated STAT proteins bound to IRF9. GAS: gamma activated sequence, consists of phosphorylated STAT1 dimers. Derived from Provance and Wambi (53).

Non-canonical interferon signaling occurs under chronic exposure to IFNα when STAT1 and STAT2 lose their phosphorylation status promoting formation of the unphosphorylated-ISGF3 (U-ISGF3) complex. Non-canonical interferon signaling can be STAT2/IRF9 driven through forming a complex known as ISGF3-like (Figure 1.4). In the absence of STAT1, a certain threshold amount of STAT2 and IRF9 must be reached to allow STAT1 independent transcription (61). This is of functional relevance because in the case of prolonged IFNα signaling, STAT2/IRF9 alone could be promoting transcription of specific, pro-tumorigenic ISGs in the absence of phosphorylation and STAT1 (61, 69). Perhaps, this stems from STAT2/IRF9 binding to distinct, yet undefined, promoter regions allowing transcription of a unique subset of ISGs (61, 62). Supporting the importance of STAT2 and IRF9 in breast cancer, loss of STAT2 but not STAT1 significantly inhibits progesterone activation of the interferon response (70, 71) and IRF9 overexpression contributes to resistance against anti-microtubule agents (72). Additionally, cells lacking STAT2 do not respond to IFNα activation of ISGs whose transcription is ISRE dependent (73). Therefore, stabilization of the U-ISGF3 or ISGF3-like complex could be a potential mechanism whereby TNBC utilizes IFNα for aggression.

Aside from non-canonical IFNα signaling, IFNα is known to mediate activation of other cellular pathways through intracellular crosstalk (Figure 1.4, Figure 1.5). Of recent, there has been an increase in the amount of evidence regarding IFN crosstalk with NFκB (74-76). For instance, multiple regulators of IFN signaling can also enhance NFκB activation including chromosomal

instability, stress or DNA damage response, and alterations in the microenvironment (Figure 1.5) (53). Moreover, IFNα could perhaps be controlled via NFκB indirectly since NFκB transcribes IFNβ which can promote transcription of IRF7 and IRF3, key regulators of IFNα (Figure 1.5) (77). This could also contribute to ISGs regulated by NFκB and a positive feedback mechanism driven by an IFN related gene signature (Figure 1.5). Moreover, previous reports suggest that IFNα can activate PI3K through the p85 subunit which in turn, activates NFκB reducing IFNα mediated apoptosis (Figure 1.5) (63). This crosstalk with NFκB and PI3K can occur independent of JAK activation and is not dependent on the ISRE element for gene transcription (78). These alternative pathways of transcription have likely evolved to control infection when canonical JAK/STAT is inhibited by pathogens exist by promoting expression of a subset of ISGs.

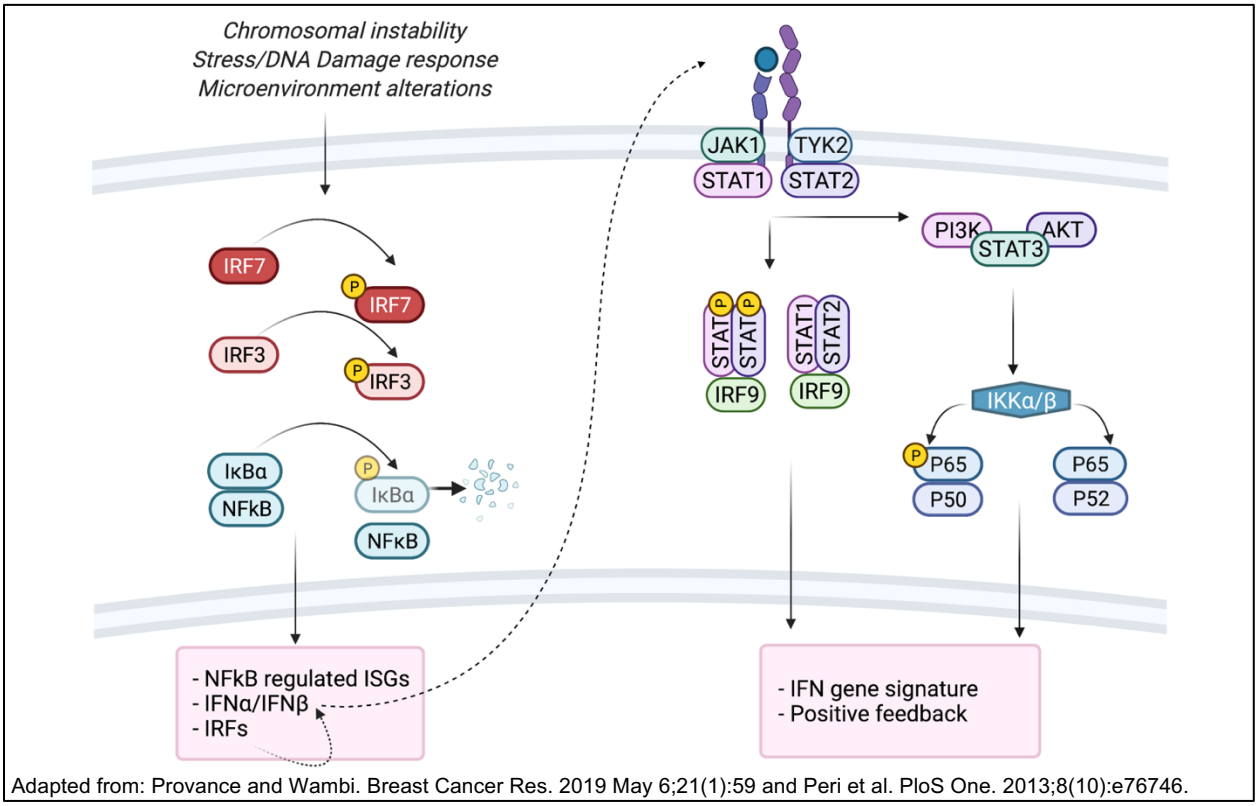

Adapted from: Provance and Wambi. Breast Cancer Res. 2019 May 6;21(1):59 and Peri et al. PloS One. 2013;8(10):e76746.

Figure 1.5 IFN crosstalk with NFκB

Induction of IRF and NFκB transcription factors may occur through insults including chromosomal instability, stress or DNA damage, and alternations in the microenvironment. Upon activation, specific NFκB ISGs may be induced as well as IFNα and IFNβ and their transcription factors amplifying a positive feedback loop. This may also induce continuous interferon signaling and subsequent downstream pathways. This IFN induced gene signature also has ability to contribute to a positive feedback mechanism. Figure adapted from Peri et al (79) and Provance and Wambi (53). Figure created with BioRender.com.

IFN/NFκB crosstalk may also occur on the DNA of specific genes. The NFκB related protein, p50, could regulate response to IFN by binding to ISG promoters on a basal level, suppressing gene expression until displacement occurs by IFN stimulation (63). Furthermore, biochemical analyses suggest that the interaction between the full ISGF3 complex (phosphorylated or unphosphorylated) and p65 is necessary to recruit Pol-II machinery for gene transcription (80, 81) (Figure 1.6). Additionally, STAT2 can bridge the ISRE and NFκB element in the IL6 promoter by binding to both IRF9 and p65 providing evidence for STAT2/IRF9 mediated IFNα signaling crosstalk (82) (Figure 1.6).

Collectively, though cells may have an elevated interferon gene signature, multiple mechanisms exist which could be driving gene expression. Therefore, it is of high importance to understand cellular responses to IFNα since uncovering the upstream IFN dependent regulation of ISG's promoting tumor aggression may lead to discoveries of disease etiology and subsequent treatment options.

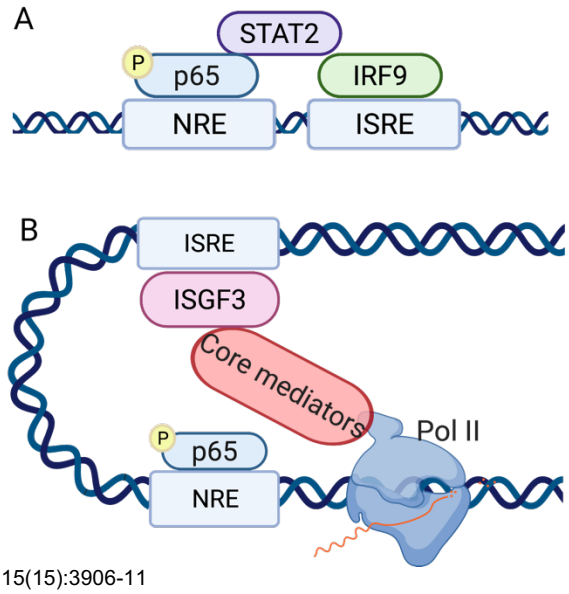

A. Nan et al. PNAS, 2018;115(15):3906-11
B. Platanitis and Decker. Frontiers in immunology. 2018;9:2542, and Wienerroither et al. Cell Reports. 2015;12(2):300-12

Figure 1.6 ISGF3 and NFκB DNA binding

Depiction of the coordinated efforts in driving gene expression mediated by ISGF3 components and NFκB mediated transcription factors. Panel A is adapted from Nan et al. (82) and panel B is adapted from Platanitis and Decker (81) and Wienerroither et al. (83). Figure created with BioRender.com.

Interferon stimulated genes in cancer biology

Interferon stimulated genes (ISGs) are abundantly expressed in all cell types in response to IFNs and mediate the effects of IFN signaling. Thousands of ISGs are capable of being induced by IFNs to promote an antiviral state effective against both RNA and DNA viruses and intracellular bacteria and parasites (58), but only a handful have been studied in detail. From what is known, ISGs have the ability to both sensitize and desensitize cells to IFN stimulation, inhibit viral entry, translation, replication, and egress (58). Though thousands of ISGs are capable of being transcribed by IFN, this transcription is heavily dependent on the duration and concentration of the IFN stimulus, the DNA elements within the specific gene promoter, and the levels of transcription factors, all of which fine tune the cellular response. Additionally, cell endogenous levels of IFN and pathway components may lead to variation in the nature and number of genes that are regulated leading to a distinct biological result. Overall, the complex control of ISG expression in controlling cell death and survival responses makes these genes an interesting point of study in tumor progression. Recent evidence suggests that later stage and more aggressive tumors utilize IFN signaling and ISG expression to enhance tumor growth, migration, invasion, metastasis, and resistance to chemotherapy in numerous tumor types including breast cancer (58, 70, 84-90). Notably, TNBC in specific has been identified to have a high IFN signature which contributes to poor overall survival (91).

We have herein established that a balance of interferons is essential for the correct cellular response. For example, if a cell receives high volumes of IFN then there is a rapid increase in genes essential for senescence or death which evolved to protect the cell against viral infection. Alternatively, prolonged IFN signaling can contribute to transcription of a separate subset of genes that can mediate tumor progression and DNA damage resistance. One specific gene, interferon induced transmembrane protein 1 (IFITM1) has been shown to individually regulate growth and invasion in multiple tumor subtypes.

Table 1.2 Interferon stimulated genes and known functions in cancer

Function	ISGs				Reference
DNA Damage Resistance	STAT1	PLSCR1	P2RY6	IFIT3	*Weichselbaum, 2008*
	IFI27	OAS1/2/3	XAF1	PSMB8	*Post, 2018*
	MX1/2	IRF9	OAS2	IFI6	
	IFI44L	DDX60	DDX58	IFIT1	
	APOL6	LGALS3BP	BTS2		
Migration and Invasion	IFI27	CD133	ISG15		*Ogony, 2016*
	CD24	IFITM1			*Lui, 2017*
	CD44	STAT2			*Kariri, 2020*
					Bektas, 2008
Positive feedback	IRF3	STAT1	IFNβ		*Lui, 2017*
	IRF7	STAT2			*Choi, 2015*
	IRF9	NFκB			
Immune checkpoint blockade	PD-L1				*Gruosso, 2019*
	CTLA4				
Immune recognition	HLA-Class I				*Gruosso, 2019*
	MHC-1				
	CXCL-10				

Interferon induced transmembrane protein-1

Interferon induced transmembrane protein-1 (IFITM1, Leu-13, CD225) is a member of the interferon induced transmembrane (IFITM) family. The IFITM family includes IFITM1, 2 , 3, 4, 5 and 10. IFITM1, 2, 3 and 5 are present in humans and are clustered in a 26kb region at the end of the short arm of chromosome 11, while IFITM10 is located 1.4Mb (megabase) downstream (92). IFITM1, 2 and 3 are highly conserved across species and are known as the immunity related IFITMs due to their established role as inhibitors of viral entry and replication on all cell types (67). IFITM5 and 10 are not interferon inducible and IFITM5 is mainly found in osteoblasts relating to bone mineralization, while IFITM10 has an unknown function and tissue distribution (67). The antiviral role of the IFITM members has been extensively reviewed (67, 93).

IFITM proteins have a highly conserved region named after IFITM1 known as the CD225 domain, an N-terminal domain (NTD), C-terminal domain (CTD), conserved intracellular loop (CIL) and two transmembrane spanning domains (TMD). The most highly conserved IFITM proteins to IFITM1 include IFITM2 and IFITM3. Notably the N-terminal domains of IFITM2 and IFITM3 are 20 and 21 amino acids longer than IFITM1, respectively, and the CTD of IFITM1 is elongated by 18 AA compared to IFITM2 and IFITM3 (67) (Figure 1.9 A). To date, the topology of IFITM1 remains elusive. The most current theories propose that due to the palmitoylated cysteine residues present at the CIL and TMD junctions, only one transmembrane domain spans the membrane, leaving the N-terminal and CIL on the inner leaflet and the CTD on the outer leaflet (94, 95) (Figure 1.9 B,C). Notably, IFITM1 has a caveolin binding domain in its TMD2 domain (Figure 1.6 B). Importantly, studies suggest that the location of IFITM1-3 are dependent on either the CTD or NTD which subsequently regulates the function of these proteins. This is supported by immunological studies which found that it was the C-terminal end of IFITM1 and the N-terminal of IFITM2/3 that regulates plasma membrane and endosome localization (92, 96, 97).

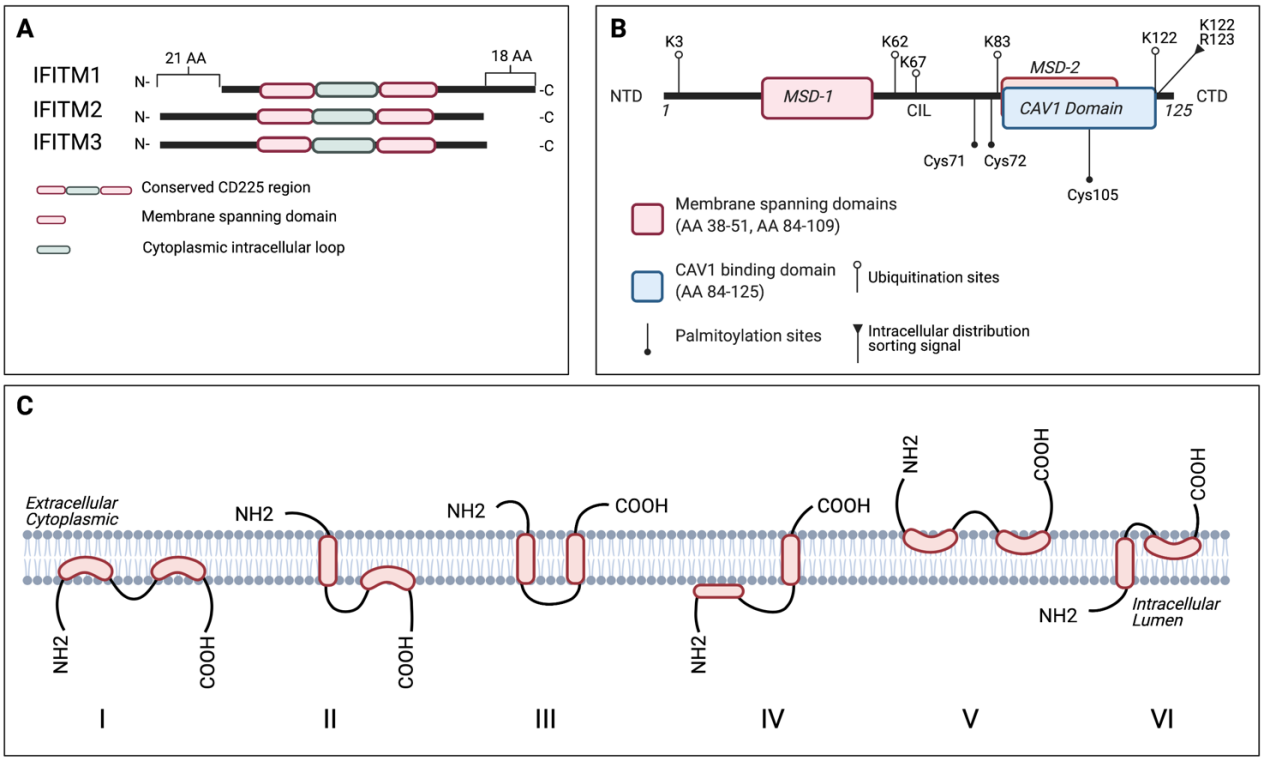

Adapted from: **A**. Narayana et al. J. Biol Chem. 2015;290(43):25946059. **B.** Li et al. J. Biol Chem. 2015;290(7):4248-5, and **C.** Zhao et al. Front Microbiol. 2019;9:3228,

Figure 1.7 IFITM1 protein domains and predicted topologies

A, Structure of protein length and conserved regions across IFITM1, IFITM2 and IFITM3. Each protein has two membrane spanning domains (red) and a cytoplasmic intracellular loop (green) The two membrane spanning domains and the CIL constitute the conserved CD225 region. As noted in the figure, IFITM1 has a shorter n-terminal end (21 AA) compared to IFITM2 and IFITM3 but has an 18 AA elongated c-terminal domain. **B,** Depiction of IFITM1 domains, post-translational modification sites, and intracellular distribution sorting signal. **C,** Predicted topologies of IFITM1. Since IFITM1 has been identified on internal membranes and on the plasma membrane, the top portion of the panel represents the extracellular or cytoplasmic facing regions whereas the bottom portion of the panel represents intracellular or lumen facing regions. Panels A-C are adapted from the following citations (93, 96, 98). Figure created with BioRender.com.

In addition to regulating viral entry and replication, IFITM1 has been shown to have a prominent effect in many cancer cell types (Table 1.3). Though the mechanism is elusive, insight gained from studies in viral biology provide some evidence. IFITM1 was first described as a leukocyte antigen and a component of a membrane complex of tetraspanins responsible for regulating cell adhesion and proliferation (99). Early reports identified direct interactions between IFITM1 and tetraspanin proteins in a complex comprising CD19, CD21 and CD81 in B-cells (100). Tetraspanins are cell surface molecules known to organize signaling complexes thus playing a

fundamental role in biological processes through regulating cellular adhesion, proliferation, and migration and CD81 has been established as a tumor promoter in multiple cancers (101-103).

Regarding the role of IFITM1 in cancer, our lab has previously identified that loss of IFITM1 can increase the levels of nuclear p21 and p27 through activation of JAK/STAT signaling thus decreasing growth and promoting apoptosis (104) (70, 105). Additionally, in an *in vivo* model of tumor growth, loss of IFITM1 was correlated with decreased blood vessel density (104). However, the most studied function of IFITM1 is in the context of tumor migration and invasion. In both head and neck cancer and ovarian cancer, high levels of IFITM1 are directly correlated clinically with increased invasion and metastasis (106, 107), and pre-clinical studies in breast cancer, glioma, and colorectal cancer show that IFITM1 regulates migration and invasion (70, 105, 108, 109). A recurring theme in all these studies is the regulation of matrix metalloproteinases, otherwise known as MMP's. Loss of IFITM1 in glioma significantly suppresses MMP9 and MMP2 levels and enzymatic activity *in vitro* and increases tissue inhibitor of metalloproteinase (TIMP)-1 and TIMP2 (110). Furthermore, loss of IFITM1 in AI resistant ER+ breast cancer significantly suppresses the levels of MMP1 in *in vivo* tumor samples (104). IFITM1 overexpression enhanced MMP12 and MMP13 expression in HNSCC cells, supporting that IFITM1 plays a role in regulating MMPs (106).

Additionally, IFITM1 has an important role in regulating drug resistance. These investigations began with the discovery that approximately 30% of ER+ patients develop resistance to their aromatase inhibitors (AI). Within these resistant cells, the IFN pathway and IFITM1 is upregulated. Correlative studies have shown that high levels of IFITM1 are associated with poor overall survival and decreased responsiveness to AI treatment (104). Mechanistic studies have shown that elevated IFITM1 expression in AI resistant ER+ breast tumors can be driven by PITX2 expression (111). PITX2 (Paired-like homeodomain transcription factor 2) is a transcription factor known for regulating skeletal muscle development but also regulates tumor development (111, 112). Importantly, loss of IFITM1 re-sensitizes these tumors to aromatase inhibitor mediated cell death.

Aside from chemotherapy resistance, IFITM1 also contributes to radioresistance as studied in oral cancer (113). In comparing oral cancer tumors that were sensitive or resistant to radiotherapy, the IFN gene signature was found to be elevated in the resistant tumors. TCGA analysis demonstrated that IFITM1 expression was more highly expressed in oral neoplasm compared to normal samples, and this expression level contributes to poor overall survival. It has been shown that loss of IFITM1 restores responsiveness to radiotherapy in oral squamous cell carcinoma (113).

Despite these findings highlighting the cellular responses to the loss of IFITM1 in mediating tumor growth, migration, and invasion, the specific mechanism of action of IFITM1 remains elusive.

Table 1.3 Functions of IFITM1 in cancer

Tumor type	Comparison	Sample type	Suppressor/ Promoter	Citation
Gastric	Normal vs. tumor	N/A	Promoter	Lee 2014
Colorectal	Normal vs. tumor vs. mets	Metastatic cell lines and patient samples	Promoter	Sari 2016
Colorectal	High vs. low expression	Cell lines and patient samples	Promoter	Yu 2015
Triple-negative inflammatory breast cancer	TN-IBC vs. HER2+ IBC	Cell Lines	Promoter	Ogony 2016
Endocrine resistant ER/PR+ breast tumors	Resistant vs. responsive	Cell lines and patient samples	Promoter	Lui 2017 Escher & Lui 2019
Letrozole resistant ER/PR+ breast cancer	Resistant vs. responsive	Cell lines	Promoter	Xu 2019
Head and neck	Normal vs. tumor	Cell lines and patient samples	Promoter	Hatano 2008
Oral cancer	Radioresistant vs. radiosensitive	Cell lines and patient samples	Promoter	Yang 2018
Ovarian	Metastatic vs. non-metastatic	Tumor explants and cell lines	Promoter	Kim 2014
Cervical squamous cell carcinoma	Normal vs. tumor	Patient samples and HeLa cells	Suppressor	Zheng 2017
Glioma	None	Cell lines	Promoter	Yu 2011
Non-small cell lung cancer	Adenocarcinoma vs. squamous cell carcinoma	Cell lines and patient samples	Promoter	Yang 2018
Lung adenocarcinoma	Expressed vs. not expressed	Patient samples	Promoter	Koh 2019
Chronic myeloid leukemia	Expressed vs. not expressed	Patient samples	Suppressor	Akyerli 2005

Project rationale and hypothesis

Triple-negative breast cancer (TNBC) is a highly aggressive and lethal subtype of breast cancer. Due to the lack of common receptors used to treat breast cancer, there are no targeted therapies thus contributing to poor overall survival. There is an unmet need to understand the molecular underpinnings of the disease to develop specific targeted therapies. Evidence suggests that cancer tumors expressing high levels of interferon stimulated genes (ISGs) are more likely to metastasize than tumors expressing low levels of ISGs, perhaps providing a molecular explanation for high rates of metastasis and poor survival in patients with TNBC. Therefore, our project investigates the IFNα pathway and one of its downstream genes, IFITM1 in TNBC, to contribute to the knowledge necessary for novel therapeutic development. Our long-term research goal is to identify novel drivers of TNBC which can be harnessed for therapeutic development. The goal of this thesis is to characterize the relevance, function, and biology of IFITM1 in TNBC, and to unravel and target the signaling pathways driving its expression. However, a critical barrier in defining molecular drivers and/or biomarkers of TNBC is the inherent TNBC heterogeneity of gene expression patterns and treatment outcomes. To overcome this barrier, our lab uses TNBC cell lines encompassing the two most prominent TNBC subtypes (basal and mesenchymal).

This thesis validates the clinical relevance of IFITM1 expression in TNBC though *in silico* mining of large databases and in house immunohistochemistry staining of TNBC patient samples. Three TNBC cell lines constitutively expressing elevated levels of IFITM1 (SUM149, MDA-MB-157, and MDA-MB-468) were used in this study for pre-clinical investigations. The biology of IFITM1 was studied on an endogenous level whereas loss of function analyses were utilized to demonstrate the functional importance of IFITM1. Next, mechanisms to target IFITM1 expression were investigated. Here, we took the approach of investigating intracellular signaling pathways promoting its expression supplemented with implementation of pre-clinical drug investigations *in*

vitro and *in vivo* based on data obtained from a high-throughput screen of FDA approved and abandoned drugs.

Aside from the therapeutic implications uncovered in this study, the hope is that data presented herein may contribute to a greater understanding of unique drivers of TNBC and for the continued development of IFITM1 as a prognostic and predictive biomarker for IFITM1 positive TNBC. Moreover, we identified that African American patients have elevated levels of IFITM1 compared to Caucasian women. Therefore, this data may be extracted for an investigation into the role of IFITM1 on breast cancer health disparities.

Overall, we hypothesize that IFNα mediated IFITM1 overexpression contributes to TNBC progression and targeting IFITM1 expression is a viable therapeutic strategy for treatment of a subset of TNBC patients. This hypothesis was tested in three specific aims (Figure 1.7): 1) Assessment of the clinical and functional relevance of IFITM1 in TNBC, 2) Investigation of the mechanism by which IFITM1 contributes to TNBC progression, and 3), Investigation of how to target IFNα driven IFITM1 expression *in vitro* and *in vivo.* Data obtained from these aims are presented in the following chapters:

Chapter 2: The clinical and functional relevance of IFITM1 in TNBC

This chapter utilizes *in silico* analysis of large databases to assess IFITM1 expression and contribution to invasive breast cancer. Data mining for TNBC is utilized as well as a TNBC tissue microarray. Additionally, IFITM1 expression is defined in TNBC cell lines to be used for functional analyses. CRISPR/Cas9 technology and siRNA were employed for loss of function analyses both *in vitro* and *in vivo.* RNA sequencing of CRISPR/Cas9 IFITM1 KO cells identifies global gene expression alterations mediated by IFITM1.

Chapter 3: IFITM1 cooperates with CD81 to mediate TNBC breast cancer growth and integrin gene expression. The role of IFITM1 appears to be context dependent. Therefore, this aim highlights important characteristics of IFITM1 in TNBC. IFITM1 subcellular location and binding proteins are defined. Insights into its mechanism of action are heavily focused on IFITM1 relationship with CD81. This chapter provides essential groundwork for future studies to manipulate these interactions to further define the mechanism of action of IFITM1.

Chapter 4: IFITM1 is regulated by non-canonical interferon signaling

This chapter investigates the involvement of interferon alpha signaling in driving IFITM1 expression. Particular attention is given to the non-canonical interferon pathway and alternative interferon crosstalk with the NFκB pathway.

Chapter 5: High throughput screen of drug repurposing library identifies inhibitors of IFITM1 positive TNBC

Here, approximately 3,500 FDA-approved and abandoned drugs were screened in two TNBC cell lines and a HER2+ cell line to assess TNBC and IFITM1 specific drug candidates. Parthenolide, an NFκB inhibitor, was identified to be highly cytotoxic to TNBC and we found it can be used to target IFITM1. Lastly, investigation into the feasibility of targeting IFITM1 expression with parthenolide *in vivo* was assessed.

Chapter 6: Conclusions and future directions

A recap of results, a discussion on how this research contributes to the field with particular focus on clinical relevance and future directions to continue this work.

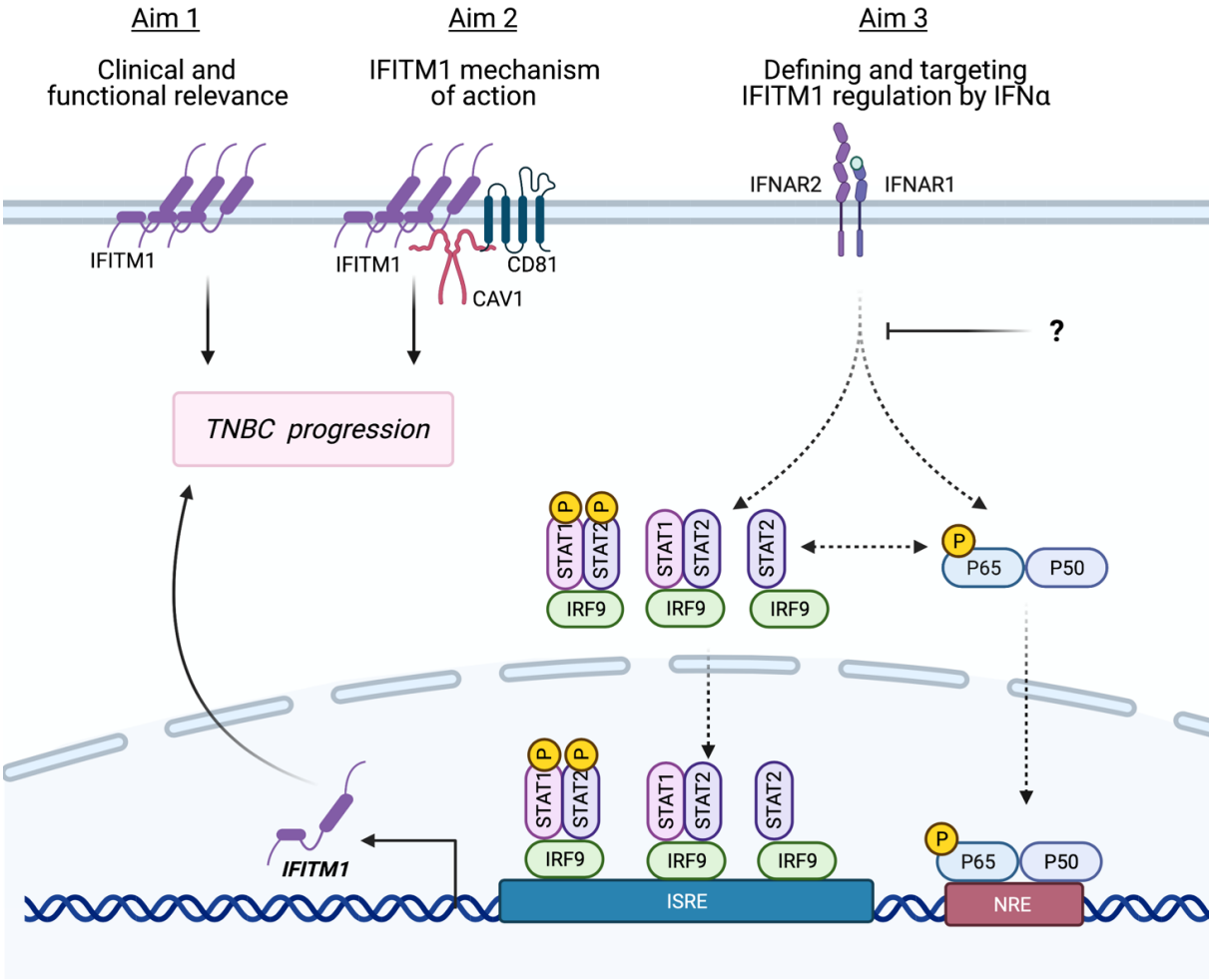

Figure 1.8 Visual depiction of specific aims
Chapter 2 will address Aim 1, chapter 3 will address Aim 2, and chapters 5 and 6 will address Aim 3. Figure created with BioRender.com.

Chapter 2: The clinical and functional relevance of IFITM1 in TNBC

Parts of this chapter have previously been published as an open access article and are reprinted here alongside never-before published results.

Provance OK, Geanes ES, Lui AJ, Roy A, Holloran SM, Gunewardena S, Hagan CR, Weir S, Lewis-Wambi J: *Disrupting interferon-alpha and NF-kappaB crosstalk suppresses IFITM1 expression attenuating triple negative breast cancer progression.* Cancer Lett. 2021, August 28; 514:12-29. DOI:10.1016/j.canlet.2021.05.006.

Introduction

Approximately 12% of total breast cancer diagnoses are classified as triple-negative breast cancer (TNBC). These tumors lack the three most common receptors used for detecting and treating breast cancer: estrogen receptor (ER), progesterone receptor (PR), and the human epidermal growth factor receptor-2 (HER2) (7, 9). Patients diagnosed with TNBC have a 12-month median overall survival rate. This survival rate is significantly lower than patients diagnosed with ER+/PR+ breast cancer (56-month median survival) and HER2+ (20-month median survival) tumors (10, 12, 14-16). TNBC poor survival is attributed to the lack of molecular targets and a poor response to systemic chemotherapy (7, 27). Therefore, there is an urgent need to identify novel mechanisms promoting TNBC onset and progression to facilitate the development of more efficacious therapies.

TNBC is a highly heterogenous disease with multiple pathways implicated in its aggressive phenotype perhaps contributing to varied treatment response and survival outcomes (7). However, evidence suggests that unbalanced type I interferon (IFN) signaling influences TNBC aggressiveness, patient survival, and response to therapy (86, 91). IFNs are cytokines that can be released by all cells in the body to inhibit viral infection, through upregulating interferon stimulated genes (ISG) as a mechanism of controlling cell death and survival pathways (114). Though both IFNα and IFNβ are classified as type I IFNs, previous studies suggest a specific role of IFNα in breast cancer biology in direct relation to specific ISGs that are produced (55, 70, 104).

Studies from our lab have identified a functional role for interferon-induced transmembrane protein-1 (IFITM1) in aromatase inhibitor resistant ER+ breast cancer and *in vitro* with a triple-negative inflammatory breast cancer cell line (70, 104). Though IFITM1 has a functional role in various types of cancer (Table 1.4), it's specific role in triple-negative breast cancer is unknown. Through use of a TNBC tumor microarray and public data set mining, we identified that IFITM1 is overexpressed invasive breast cancer and TNBC and contributes to decreased overall survival in specific TNBC subtypes. Furthermore, *in vitro* and *in vivo* loss of

function analyses suggest a prominent role of IFITM1 in mediating TNBC growth, migration and invasion.

Results

IFITM1 is overexpressed in invasive breast cancer

IFITM1 overexpression in cancer has been shown to promote an aggressive phenotype (Table 1.4). To further confirm this observation in breast cancer, we performed analysis on breast cancer cohorts using multiple online platforms. IFITM1 gene expression in invasive primary tumors was significantly elevated compared to normal tissue as assessed through the Oncomine database (Figure 2.1 A-C). To assess the relevance of IFITM1 in regard to grade and nodal status we utilized the Breast Cancer Gene-Expression Miner (bcGenExMiner) and found that IFITM1 is significantly elevated in breast tumors with higher grades (Figure 2.1 D) and nears significance when comparing node negative to node positive breast cancer (Figure 2.3 E). Lastly, using the UALCAN database, we assessed whether IFITM1 is elevated in metastatic breast cancer samples from the MET50 study. Samples without ERBB2 (HER2) amplification had elevated levels of IFITM1 (Figure 2.1 F). These analyses with the use of multiple datasets suggest that IFITM1 is clinically relevant in invasive and aggressive breast tumors.

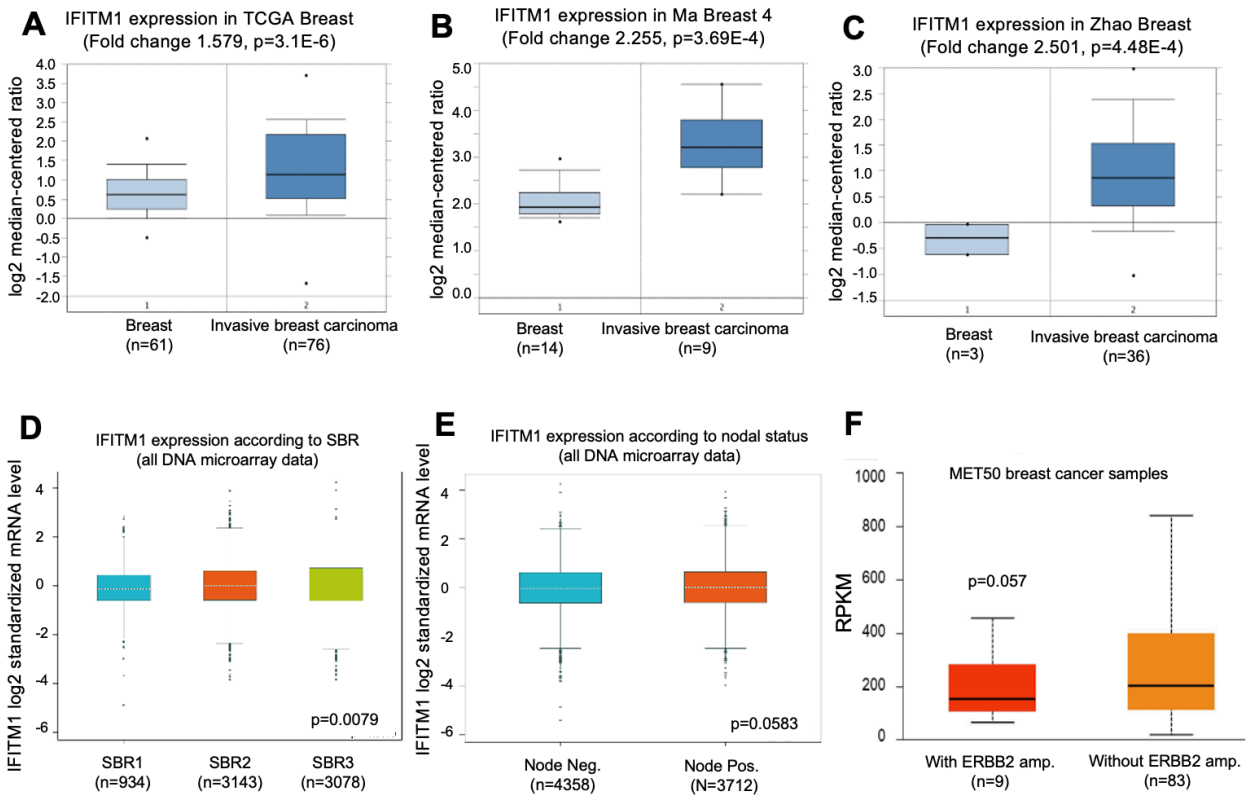

Figure 2.1 IFITM1 is overexpressed in invasive breast cancer
A-C: IFITM1 expression in invasive breast cancer in comparison to normal breast tissue assessed in publicly available datasets on the Oncomine Platform. Differences were assessed between groups with a student's t-test and results were considered significant with a p-value of <0.05. **D**, IFITM1 expression in breast cancer samples stratified according to grade (Scarff-Bloom-Richardson grade, SBR) analyzed using bcGenExMiner. **E**, IFITM1 expression in breast cancer samples according to nodal status using bcGenExMiner. **F**, IFITM1 expression in breast cancer samples stratified according to HER2 status in metastatic breast cancer samples from the MET50 study as analyzed using the UALCAN database.

Clinical and pre-clinical relevance of IFITM1 in triple-negative breast cancer

To define the clinical relevance of IFITM1 in TNBC, we first stained 34 primary TNBC breast tumor samples and 6 normal breast tissue samples through immunohistochemistry (IHC) for IFITM1 expression (Figure 2.2 A). We found that 0% (0/6) normal breast tissue samples had IFITM1 while 38% of TNBC breast tumors overexpressed IFITM1 as measured by a staining intensity of 2+ and 62% of TNBC breast tumors had 1+ intensity. To expand our analysis to a larger patient cohort, we analyzed TCGA data and found that IFITM1 is significantly elevated in TNBC patient samples compared to normal breast tissue (Figure 2.2 B). Moreover, utilizing the Kaplan-Meier Plotter

breast cancer survival database we found that IFITM1 expression correlates with decreased relapse free survival for patients with mesenchymal, mesenchymal-stem-like, and basal like-1 TNBC (Figure 2.2 C, Supplemental Figure 2.1) (115). For comparison, we also assessed IFITM1 expression in several breast cancer cell lines. We found that IFITM1 protein is highly expressed in SUM149, MDA-MB-157 an MDA-MB-468 TNBC cells, but not expressed in estrogen receptor (ER) positive MCF-7 and T47D breast cancer cell lines, or the normal, immortalized ER-negative MCF10a cells (Figure 2.2 D). qRT-PCR analysis confirms IFITM1 mRNA is elevated in TNBC cells compared with ER+ MCF-7 cells (Figure 2.2 E). Next, we assessed whether IFITM1 is more stable in TNBC relative to ER+ counterparts (Figure 3.1 C). The ER+ cell lines used here are derived from an aromatase inhibitor resistant model which express IFITM1 (104). SUM149, MDA-MB-468, and MDA-MB-157 cells have increased stability of IFITM1 as compared to the ER+ aromatase inhibitor resistant cell lines (Figure 2.2 F,G).

However, IFITM1 is not expressed in all TNBC cell lines. Unique to the cell lines expressing IFITM1 is that they are derived from African American (AA) patients. For example, IFITM1 is not expressed in MDA-MB-231 cells which were derived from a Caucasian woman (Figure 2.1 A). Further supporting this evidence, though our tissue microarray is only 18% from AA patients, these patients have significantly higher IFITM1 staining than non-AA patients (Figure 2.3 B). Overall, these data suggest that IFITM1 is clinically relevant in TNBC and may have a role in TNBC health disparities outcomes.

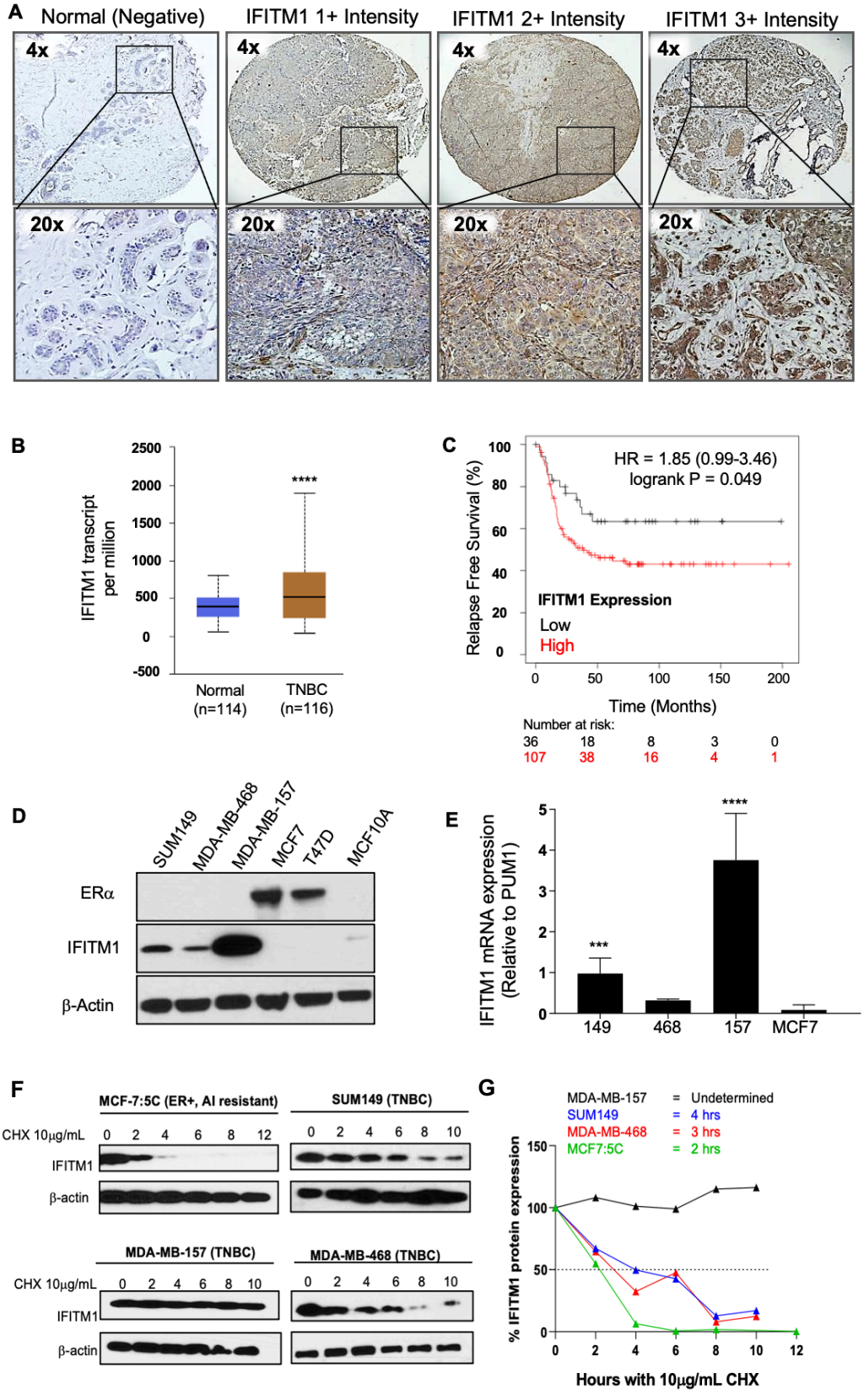
A
Normal (Negative)
IFITM1 1+ Intensity
IFITM1 2+ Intensity
IFITM1 3+ Intensity
4x
20x
B
IFITM1 transcript per million
2500
2000
1500
1000
500
0
-500
****
Normal (n=114)
TNBC (n=116)
C
Relapse Free Survival (%)
HR = 1.85 (0.99-3.46)
logrank P = 0.049
IFITM1 Expression
Low
High
Time (Months)
Number at risk:
36 18 8 3 0
107 38 16 4 1
D
SUM149
MDA-MB-468
MDA-MB-157
MCF7
T47D
MCF10A
ERα
IFITM1
β-Actin
E
IFITM1 mRNA expression (Relative to PUM1)
***
****
149
468
157
MCF7
F
MCF-7:5C (ER+, AI resistant)
SUM149 (TNBC)
CHX 10μg/mL
0 2 4 6 8 12
0 2 4 6 8 10
IFITM1
β-actin
MDA-MB-157 (TNBC)
MDA-MB-468 (TNBC)
G
MDA-MB-157 = Undetermined
SUM149 = 4 hrs
MDA-MB-468 = 3 hrs
MCF7:5C = 2 hrs
% IFITM1 protein expression
Hours with 10μg/mL CHX

Figure 2.2 IFITM1 is overexpressed in triple-negative breast cancer
A, Human TNBC breast tissue (34 samples) and normal tissue (6 samples) was obtained from the Biosample Repository at KUMC and stained for IFITM1 expression using immunohistochemistry. 62% had 1+ staining, 26% had 2+ staining and 12% had 3+ staining. **B,** The UALCAN database was used to assess IFITM1 expression. UALCAN analyzes TCGA data. **C,** IFITM1 on relapse free survival derived from KM Plotter. Patients were first stratified into basal-like breast cancer and further by the mesenchymal TNBC phenotype as defined by Pietenpol (1). **D,** Immunoblotting was used to assess IFITM1 protein expression in multiple TNBC cell lines (SUM149, MDA-MB-468, MDA-MB-157), ER+ breast cancer cell lines (MCF7, T47D) and normal-immortalized human breast cells (MCF10A). **E,** IFITM1 mRNA expression measured by qRT-PCR in SUM149, MDA-MB-468, MDA-MB-157, and MCF-7 cell lines. Values represent means ± SD of three biological replicates and data are presented as fold change to PUM1 using the DCT method. **F,** Immunoblot of MCF7:5C (AI resistant MCF7 ER+ cells), SUM149, MDA-MB-468 and MDA-MB-157 treated with cycloheximide (10μ g/mL)for up to 12 hours. **G,** Quantification of western blot with ImageJ.

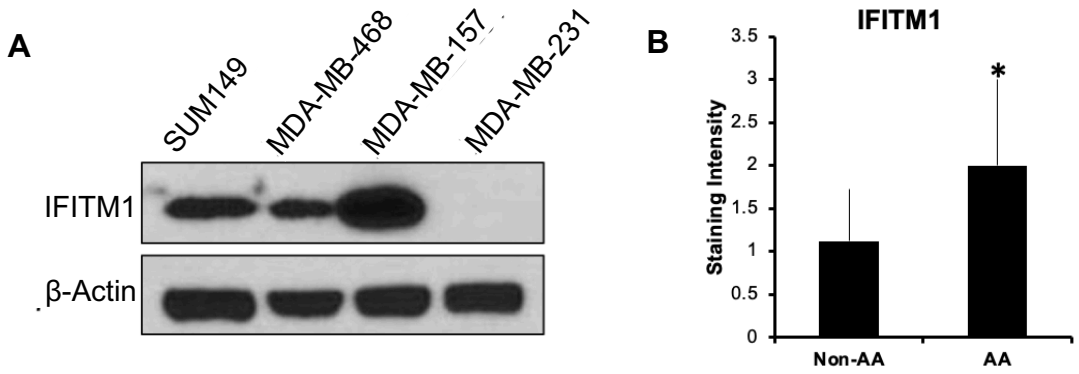

Figure 2.3 IFITM1 is overexpressed in African American TNBC patients
IFITM1 staining intensity from the tissue microarray delineated by race (non-African American (Non-AA) to African American (AA). T-test was used to assess significance. *p<0.05.

Loss of IFITM1 decreases TNBC in vitro growth, colony formation, and migration

To investigate the functional significance of IFITM1 expression in TNBC, siRNA was used to knockdown IFITM1 in MDA-MB-157 and MDA-MB-468 cells (Fig. 2A). We found that loss of IFITM1 significantly inhibits cell growth in MDA-MB-157 and MDA-MB-468 cells (Figure 2.4 B-C) and cell migration in MDA-MB-157 cells (Figure 2.4 D) but not in MDA-MB-468 cells (Supplemental Figure 2.2). To expand our analysis, we utilized CRISPR/Cas9 gene editing to stably knockout IFITM1 expression in the SUM149 and MDA-MB-157 cell lines (Figure 2.4 E). We found that SUM149 IFITM1 KO cells have a slower growth rate than CAS9/Control cells as assessed by cell counting (Figure 2.4 F) and that the IFITM1/KO cells have an impaired ability to form colonies (Figure 2.4 G) and to migrate after 24 and 48 hours (Figure 2.4 H). Additionally, CRISPR/Cas9 knockdown of IFITM1 in MDA-MB-157 cells had similar results such that loss of IFITM1 impaired the growth after 48 hours, 14-day colony formation, and 24 hour wound healing (Figures 2.4 I-M). Overall, these data confirm that the presence of IFITM1 in MDA-MB-468, MDA-MB-157 and SUM149 cells regulates growth and migration *in vitro*.

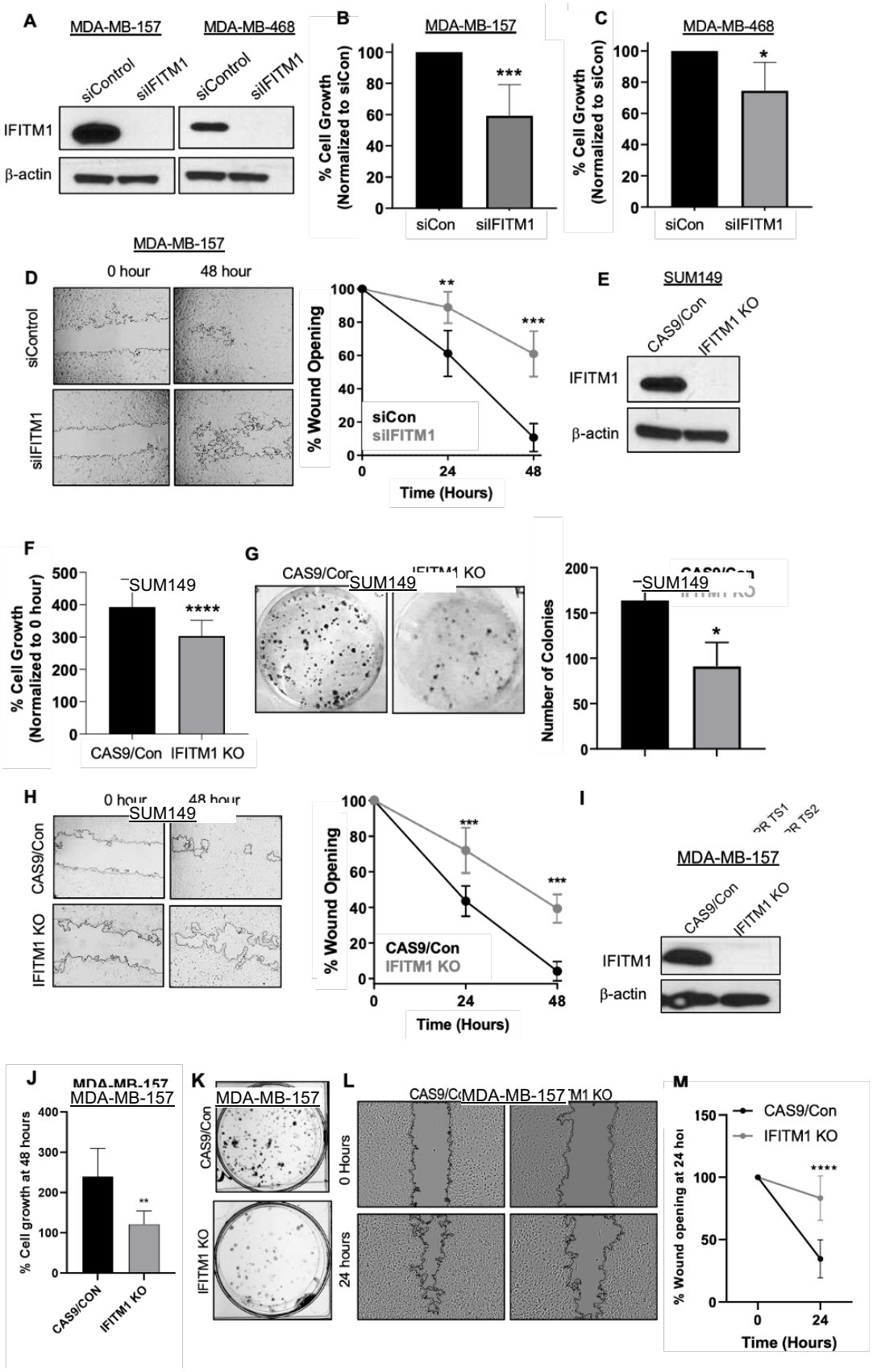
A
MDA-MB-157
MDA-MB-468
siControl
siIFITM1
siControl
siIFITM1
IFITM1
β-actin
B
MDA-MB-157
% Cell Growth (Normalized to siCon)
***
siCon
siIFITM1
C
MDA-MB-468
% Cell Growth (Normalized to siCon)
*
siCon
siIFITM1
D
MDA-MB-157
0 hour
48 hour
siControl
siIFITM1
% Wound Opening
**
***
siCon
siIFITM1
Time (Hours)
E
SUM149
CAS9/Con
IFITM1 KO
IFITM1
β-actin
F
SUM149
% Cell Growth (Normalized to 0 hour)
****
CAS9/Con
IFITM1 KO
G
SUM149
CAS9/Con
IFITM1 KO
SUM149
Number of Colonies
*
H
SUM149
CAS9/Con
IFITM1 KO
% Wound Opening
***
***
CAS9/Con
IFITM1 KO
Time (Hours)
I
MDA-MB-157
CAS9/Con
IFITM1 KO
IFITM1
β-actin
J
MDA-MB-157
% Cell growth at 48 hours
**
CAS9/CON
IFITM1 KO
K
MDA-MB-157
CAS9/Con
IFITM1 KO
L
MDA-MB-157
CAS9/Con
IFITM1 KO
0 Hours
24 hours
M
CAS9/Con
IFITM1 KO
% Wound opening at 24 hou
****
Time (Hours)

Figure 2.4 IFITM1 contributes TNBC growth, migration and colony formation in vitro
A, Immunoblot of MDA-MB-157 and MDA-MB-468 cells depicting siRNA knockdown of IFITM1 expression after 48 hours. **B-C,** MDA-MB-157 and MDA-MB-468 proliferation was measured through cell counting after transfection with either siControl or siIFITM1. Values represent means ± SD of three independent experiments done in triplicate. A t-test was used to assess statistical significance. *p<0.05, ***p<0.001 **D**, A scratch assay was conducted on 80% confluent plates after knockdown of IFITM1 with siRNA. Plates were imaged at 0, 24, and 48 hours and the wound was quantified by ImageJ (right). Values represent means ± SD of four independent experiments conducted in quadruplicate. A t-test was used to assess statistical significance at each timepoint; ***p<0.001. **E,** IFITM1 expression was assessed by immunoblotting. **F,** Cell growth was measured through counting CAS9/Con and IFITM1 KO cells. Values represent means ± SD of four independent experiments done in triplicate. A t-test was used to assess statistical significance. ****p<0.0001. **G,** The clonogenicity of SUM149 CAS9/Control and IFITM1 KO cells was assessed by plating 1,000 cells in a 6-well plate. After 10 days, cells were stained with crystal violet and quantified based on colony number using ImageJ (right). Values represent means ± SD of three independent experiments conducted in duplicate. A t-test was used to assess statistical significance; *p<0.05. **H,** Scratch assay was conducted on 80% confluent plates of SUM149 CAS9/Control and IFITM1 KO cells. Plates were imaged at 0, 24, and 48 hours and wound was quantified by ImageJ (right). Values represent means ± SD of four independent experiments conducted in quadruplicate. A t-test was used to assess statistical significance at each timepoint; ***p<0.001. **I,** Western blot of MDA-MB-157 parental (lane 1), CAS9/Con (lane 2), and two CIRPSR sequences targeting IFITM1 (Lanes 3 and 4). **J.** Cell growth was measured through counting CAS9/Con and IFITM1 KO cells. Values represent means ± SD of three independent experiments done in quadruplicate. A t-test was used to assess statistical significance. **p<0.001. **K.** The clonogenicity of MDA-MB-157 CAS9/Control and IFITM1 KO cells was assessed by plating 1,000 cells in a 6-well plate. After 14 days, cells were stained with crystal violet and imaged. **L**: Scratch assay was conducted on 80% confluent plates of MDA-MB-157 CAS9/Control and IFITM1 KO cells. Plates were imaged at 0 and 24 hours and wound was quantified by ImageJ (right). Values represent means ± SD of two independent experiments conducted in quadruplicate. A t-test was used to assess statistical significance at each timepoint; ****p<0.001.

Loss of IFITM1 decreases TNBC tumor growth and invasion in vivo

To determine if the loss of IFITM1 has the same impact *in vivo*, we assessed tumor growth with the orthotopic fat pad model using NSG mice. SUM149 CRISPR cells were due to the permanent decrease of IFITM1 expression and ability to grow *in vivo.* Tumors were developed by inoculating the mammary fat-pad of female mice with either SUM149 CAS9/Control or SUM149 IFITM1 KO cell lines. At day 26, CAS9/Control tumors measured 350mm^3 and loss of IFITM1 resulted in a significant reduction in tumor volume by approximately 300mm^3 (Figure 2.5 A) and tumor weight by approximately 0.3g (Figure 2.5 A-C, Supplemental Figure 2.2 A). A decrease in Ki67 staining (Figure 2.5 D) and an increase in TUNEL staining (Fig. 3D) demonstrate that the decrease in tumor growth is a result of decreased proliferation and increased cell death. These data suggest that IFITM1 regulates SUM149 TNBC tumor growth *in vivo*.

Since the loss of IFITM1 significantly inhibits migration (Fig. 2.4) and invasion (70) *in vitro,* and clinical data suggest IFITM1 is elevated in invasive breast tumors (Figure 2.1), we utilized the mammary intraductal (MIND) model to assess the effect of IFITM1 on local SUM149 tumor cell invasion *in vivo* (Figure 2.5 E). In the MIND model, breast cancer cells are injected into the mammary duct through the nipple, where they populate the duct and can invade into the surrounding mammary gland (116). IHC for IFITM1 and smooth muscle actin (SMA; milk duct marker) (Figure 2.5 F) and H&E staining (Supplemental Figure 2.2 B), allowed visualization of IFITM1 expression, mammary gland architecture, and the extent of tumor invasion to quantify the total number of lesions and number of invasive lesions per field (Figure 2.5 G). Immunofluorescence of SMA (shown in green) and human keratin-19 (human breast cancer cell marker; shown in red) was used to assess the average invasion distance outside the duct (Figure 2.5 F-G). Together, these data demonstrate that loss of IFITM1 decreases the ability of SUM149 tumor cells to invade out of the mammary duct and into the stroma.

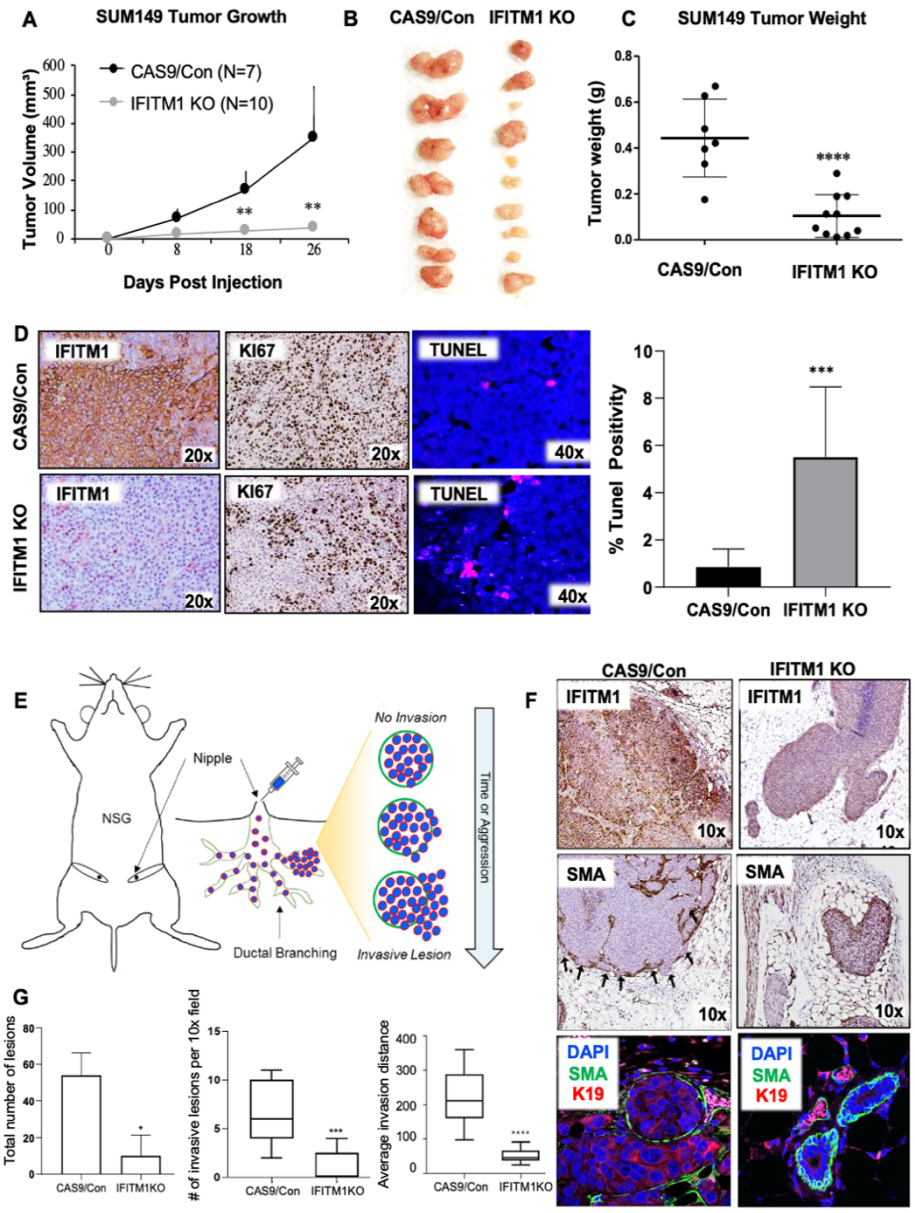

Figure 2.5 Loss of IFITM1 results in decreased growth and invasion in vivo
A, 3 million SUM149 CAS9/Control or IFITM1 KO cells were injected bilaterally into the 4th mammary fat pad of female NSG mice. Tumor growth was measured over the course of 26 days and the difference of tumor volume between groups was assessed using a t-test at each time point **p<0.01 **B,** Images of the tumors derived from fat pad injections **C,** Final tumor weight of CAS9/Control and IFITM1 KO tumors. Significance was assessed using a t-test ****p<0.0001. **D,** IHC analysis was used to assess IFITM1 and Ki67 expression. **D**, Click-iT™ Plus TUNEL kit was used to stain for apoptotic cells within the tumor. Quantification was completed using ImageJ software and a t-test was used to assess the significance of the percentage of cells with TUNEL staining ***p<0.001. **E,** Schematic of the mammary intraductal mouse model **F,** Immunofluorescent staining of the mammary glands. Nuclei were stained with DAPI, milk ducts were stained with smooth muscle actin (SMA; green) and human keratin 19 (K19) stained the injected human epithelial breast cancer cells. **F,** Mammary glands were fixed and processed onto glass slides. H&E staining and IHC was used to assess tissue architecture and IFITM1 expression, and smooth muscle actin was used to stain the milk duct **G,** Quantifications of invasive lesions per duct. Invasive lesions were quantified in a 10x field by counting the number of invasive lesions through SMA degradation in 5 fields per slide. *p<0.05 **p<0.01 in comparing control cells to IFITM1 KO cells.

RNA sequencing identifies signaling pathways affected by loss of IFITM1

To assess mechanisms whereby loss of IFITM1 decreases TNBC growth, migration and invasion, RNA sequencing was performed on SUM149 CAS9/Con and IFITM1 KO cells. 1,358 genes were differentially regulated in IFITM1 KO cells compared to CAS9/Control cells with a p-value of 0.05, an FDR of 0.05, a fold change threshold of 2.0 (Figure 2.6 A). Stringency was enhanced by ensuring FPKM (fragments per kilobase million) were >1 which provided 561 differentially regulated genes. Of those genes, the IFITM1 KO cells had 294 upregulated in 267 downregulated genes compared to CAS9/Control. Analysis of the 267 genes downregulated in the IFITM1 KO cells using Ingenuity Pathway Analysis (IPA) identified a negative Z-score (suggestive of downregulation or inhibition) for pathways of proliferation, migration, invasion and metastasis, corroborating both in vitro and in vivo data (Figure 2.6 B). Using the upstream analysis tool in IPA, we identified that loss of IFITM1 reduces activation of pathways including NFκB, TGFB, PI3K, FN1, IL6, and EGFR (Figure 2.6 C, Supplemental Table 2.1, Supplemental Figure 2.4). Interestingly, NFκB is known to have intracellular crosstalk with these pathways. Particularly, multiple NFκB related genes including RELA (p65), NFKB1 (p105), NFKB2 (p100) cREL and IkBα are downregulated (Figure 2.6 C-E). To visualize NFκB gene regulation we overlaid IFITM1 KO versus CAS9/Con fold change values to genes regulated by the NFκB complex as grouped by IPA. Figure 2.6 D depicts the genes in which their downregulation is mediated by loss of IFITM1 through the NFκB complex. Solid lines represent direct regulation and dashed lines represent indirect regulation (Figure 2.6 D). These results were validated through qRT-PCR as loss of IFITM1 significantly decreases the mRNA expression of RELA (p65), NFkB1 (p105), NFKB2 (p100) and key NFκB target genes involved in growth and invasion, IL6 and SNAI2 (Figure 2.6 E). Additionally, correlation between IFITM1 and factors of the NFκB signaling pathway shows a slight positive trend when assessing publicly available clinical RNA sequencing data (Figure 2.6 F). Collectively, these results suggest that loss of IFITM1 decreases multiple pathways with NFκB being a key player.

A

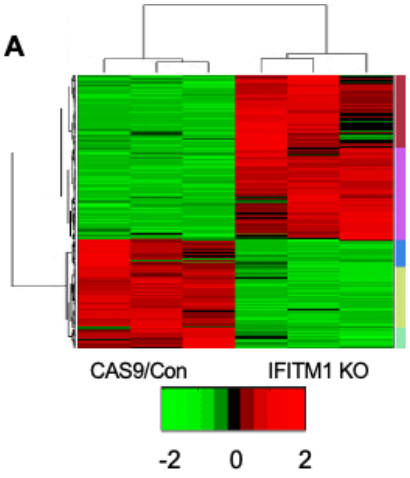

B

Downregulated in IFITM1 KO			
Pathway	**P-Value**	**Gene #**	**Z-score**
Proliferation of tumor cell lines	6.4E-13	78	-0.114
Migration of tumor cell lines	6.4E-6	37	-2.475
Invasion of tumor cell lines	8.4E-8	40	-2.1

C

Upstream Regulator	**Expr Fold Change**	**Activation z-score**	**p-value of overlap**
TGFB1	1.2	-4.4	1.95E-18
P38 MAPK		-3.1	6.75E-11
IL6	-23.9	-2.6	0.0000107
FN1	-2.6	-1.7	0.000141
EGFR	-1.4	-1.9	0.000611
NFKB Complex		**-3.954**	**4.39E-13**
P65 (RELA)	-1.493	-3.854	9.31E-11
IkBα (NFKBIA)	-1.153	-2.890	7.10E-10
c-Rel (REL)	-1.001	-2.010	5.91E-6
p105 (NFKB1)	-1.429	-2.4475	2.41E-09
P100 (NFKB2)	-2.381	-1.727	5.49E-05

D

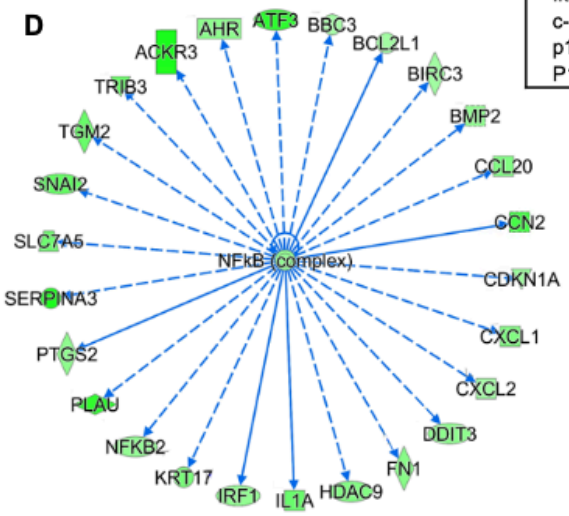

E

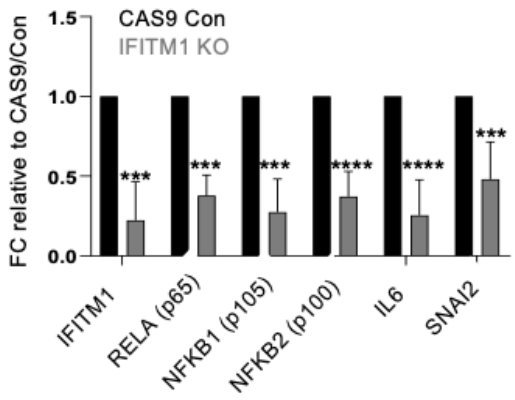

F

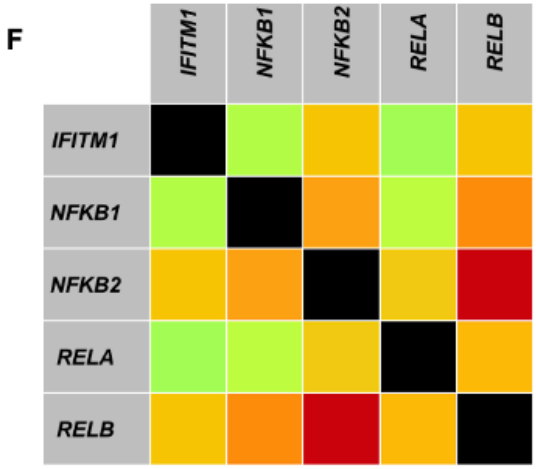

	RELA	**RELB**	**NFKB1**	**NFKB2**
IFITM1	R=0.13 P=0.01	R=0.37 P=<0.0001	R=0.16 P=0.054	R=0.37 <0.0001

Figure 2.6 RNA sequencing identifies signaling pathways affected by loss of IFITM1
A, Heat map of the differentially expressed genes between CAS9/Control and IFITM1 KO cells showing upregulated (red) genes and downregulated (green) genes. **B,** Ingenuity pathway analysis (IPA) on the differentially expressed genes comparing IFITM1 KO to CAS9/Control. Negative Z-scores correlate to a decrease in pathway activation in IFITM1 KO cells. P-value and Z-score were computed within IPA. **C,** IPA upstream analysis summary **D,** IPA determined pathway of NFkB complex regulated genes with overlay of gene expression values of IFITM1 KO compared to CAS9/Control (dark green = >5 fold downregulated). **E,** mRNA expression measured by qRT-PCR in SUM149 CAS9/Con and IFITM1 KO cell lines. Data represented as fold change compared to CAS9/Control via $2^{\wedge DDCT}$ method. Statistics were assessed on individual fold changes relative to PUM1 using a t-test with samples from three independent passages ***p<0.001, ****p<0.00001. **F,** The gene correlation targeted analysis on the BcGenExMiner platform was used to assess correlation between IFITM1 and NFkB elements. Search was performed using all available RNA-seq data (4,712 patients from TCGA, Brueffer et al. 2018 (Study code: GSE81538), and Saal et al. (Study code: GSE96058). R-values for Pearson's correlation values and p-values are listed below for IFITM1 and NFkB correlations.

Discussion

Triple negative breast cancer (TNBC) is the most aggressive subtype of breast cancer (27). The absence of well characterized, druggable targets and disease heterogeneity provide significant therapeutic barriers therefore requiring the identification of novel biomarkers to be investigated as potential targeted therapies. Here, we show for the first time that the ISG, IFITM1, is overexpressed in a subset of TNBC patient samples through use of a tumor microarray and *in silico* analyses as compared to normal and ER+ breast cancer (Fig. 1). We further identified that the presence of IFITM1 contributes to poor relapse free survival in the mesenchymal, mesenchymal stem-like, and basal-like-1 TNBC subtype (Supplemental figure 2.1). Our data is reflective of previous studies such that interferon gene expression higher in ER- breast cancer than ER+ breast cancer and contributes to poor overall survival (91).

First, to determine if IFITM1 is expressed endogenously in TNBC breast cancer cells, we screened multiple breast cancer cell lines for IFITM1 expression. We identified that IFITM1 is overexpressed in multiple TNBC cell lines and not expressed at measurable levels in ER+ or normal-immortalized breast cell lines. The TNBC cell lines with the highest IFITM1 expression (MDA-MB-157 and SUM149) are of the mesenchymal subtype with exception to SUM149 being "mixed" (i.e.: basal and mesenchymal). Since this data correlates with our *in silico* analyses of

subtype specific survival rates in TNBC, we hypothesized that loss of IFITM1 in these cell lines will inhibit the aggressive phenotype of these cells.

Briefly, we also observed higher IFITM1 levels in African American (AA) patients from our tissue microarray and highest IFITM1 expression in TNBC cell lines derived from AA patients. Women of African descent have on average, lower incidence of breast cancer but a higher rate of mortality by approximately 30% (117). The TNBC phenotype accounts for approximately 15% of diagnoses from Caucasian women but approximately 30% of AA tumors (117). Therefore, it is hypothesized that the higher rate of mortality observed in AA patients is related to the high prevalence of TNBC within this population. However, studies investigating the distinct genetic contribution between AA and Caucasian women is sparse, though one study has identified elevated JAK-STAT and interferon signaling in tumor samples derived from AA women compared to those derived from Caucasian women (117). Though these data supporting our observation of elevated IFITM1 levels in AA patients, confirmation of these findings in a larger cohort of patient samples is necessary to draw a definitive conclusion.

The functional role of IFITM1 was investigated through loss-of-function analyses using siRNA or CRISPR/Cas9. Both *in vitro* and *in vivo* studies demonstrate that IFITM1 promotes an aggressive phenotype in TNBC through enhancing growth, colony formation, migration, and invasion. Our present finding that IFITM1 promotes an aggressive phenotype in TNBC aligns with previous reports demonstrating that IFITM1 induces tumor growth, migration, invasion, and metastasis in head and neck, gastric, colorectal, and endocrine resistant breast cancers (104, 106, 108, 118).

Here, we observe that IFITM1 regulates NFκB signaling which is a key regulator of growth and invasion in breast cancer (119, 120). IFITM1 has also been shown to enhance EGFR signaling (121) and caveolin-1 activation (109) in some tumors. Additionally, studies in virology can also provide additional insight into how IFITM1 functions. IFITM1 inhibits viral infection at the plasma membrane through interaction with multiple tetraspanin family members including CD81

(122), a tumor promoter in TNBC, that regulates integrins and phosphoinositide signaling (123, 124). In a THP-1 model IFITM1 mediates ERK and PI3K signaling increasing MMP9 expression (125), and in letrozole resistant breast cancer, IFITM1 mediates AKT signaling (111). Though this is the first study to suggest a role of IFITM1 on NFκB signaling, these previous studies both directly (Supplemental Figure 2.4) and indirectly support our findings since ERK, AKT, and PI3K signaling have been identified to regulate NFκB activation through non-canonical mechanisms (125). We suspect that loss of IFITM1 may result in perturbation of membrane microdomains which are home to many receptors, kinases and co-factors thus inhibiting these downstream signaling pathways (30).

Another important observation regarding IFITM1 is that it is expressed in the both the stromal and tumor cells (Fig. 1). Though it is well known that the stroma plays an important role in facilitating response to therapies and tumor progression, there is limited data and discussion regarding the function of IFITM1 expression in the stroma (53). Recently, Grosso *et al.* identified specific tumor immune microenvironment (TIME) metasignatures based on CD8+ infiltration and identified that fully inflamed tumors have elevated IFN, JAK/STAT and NFkB signatures (126). Interestingly however, these fully inflamed TNBC tumors have enrichment of the immunomodulatory subtype and we have identified that the immunomodulatory subtype has better overall survival with IFITM1 expression (Supplemental Figure 2.1). Additionally, the stroma of these tumors has higher levels of IFITM1 expression and low levels of MHC-class I molecules and elevated levels of PD-L1. Supporting this study, we have identified that loss of IFITM1 increases gene expression of HLA molecules (HLA-A,B,C,E,F) and decreases PD-L1 expression (data not shown), suggesting a rationale for the investigation of the role of IFITM1 in immune checkpoint regulation in the tumor microenvironment. Therefore, IFITM1 expression and subsequent function in TNBC may be influenced by the specific TNBC subtype. Collectively, evidence presented in this chapter demonstrate that inhibition of IFITM1 substantially attenuates TNBC growth, migration, and invasion.

Materials and Methods

Cell lines and culture conditions

Human TNBC cell lines SUM149, MDA-MB-157, and MDA-MB-468 were used and were authenticated by STR allele profiling by Genetica DNA laboratories. SUM149 cells were obtained from Dr. Massimo Cristofanilli (Northwestern University, Chicago, IL, USA) who purchased them from Asterand Bioscience (Detroit, MI, USA). SUM149 cells were maintained in Ham's F-12 nutrient mixture (LifeTech) supplemented with 10% FBS (LifeTech), 5µg/mL insulin (Sigma), 1µg/mL hydrocortisone (Sigma), and 100 U/mL antibiotic-antimycotic (Sigma). MDA-MB-157 and MDA-MB-468 cells were obtained from Dr. Gustavo Miranda-Carboni (University of Tennessee Health Science Center). MDA-MB-157 and MDA-MB-468 cells were maintained in DMEM (LifeTech) supplemented with 20% FBS, 100 U/mL antibiotic-antimycotic and 1% glutamine (LifeTech). All cells were passaged twice weekly, with media changed every other day. All cells were cultured at 37^{o}C in a 5% CO_2 atmosphere.

Clinical Analyses

The UALCAN resource was used to assess expression of IFITM1 in TNBC compared to normal breast from the TCGA database and the expression of IFITM1 in HER2neg metastatic breast cancer (127). Relapse free survival data were obtained from the 2020 version of the Kaplan-Meier Plotter breast cancer survival database (115). The 143 breast cancer patient samples used in the analysis were obtained by first delineating basal subtype and further by the Pietenpol mesenchymal subtype. Patients were stratified by IFITM1 expression (probe set 214022_s_at) relative to the upper and lower quartiles (107 patients in upper quartile, and 36 patients in lower quartile). The p-value was calculated using a log-rank test. IFITM1 gene expression in invasive primary breast cancer compared to normal breast tissue was analyzed using the Oncomine^{TM} platform (128, 129).

Clinical Samples

Clinical samples were provided by the KUMC Biospecimen Shared Resource as approved by KUMC IRB. A total of 34 primary TNBC breast tumors and 6 normal breast tissue samples from routine reduction mammoplasties were examined. Tissues were formalin-fixed with 10% neutral buffered formalin and paraffin-embedded (FFPE) prior to performing IHC. Clinicopathological data including age, race, clinical stage, HER2 staining and vascular invasion are shown in Table 2.1. After review of the hematoxylin and eosin slides and marking of tumor areas, 2-mm tissue cores of representative tumor areas were extracted and inserted in recipient blocks. IHC analysis for IFITM1 was then performed on these samples (See IHC staining protocol below). Two cores from each tumor were analyzed to account for the impact of tumor heterogeneity on IFITM1 expression. IFITM1 staining intensity was quantified manually on a scale of 0–3 where 0 means no staining, 1+ is faint staining (light brown), 2+ is moderate staining (yellowish brown) and 3+ is strong staining (brown). Cores were scored by three independent individuals including a senior pathologist at KUMC. Any discrepancies were resolved by group consensus. Final distribution of IFITM1 expression is shown in Table 2.2.

Table 2.1 Characteristics of patients included in the tissue microarray

	Frequency	Percent
Age		
25-35	5	15%
36-45	6	18%
46-55	6	18%
56-65	8	24%
66-75	6	18%
75+	3	9%
Race		
European American	26	76%
African American	6	18%
Asian/Pacific Islander	2	6%
Stage		
2	3	9%
3	31	91%
Her2/Neu Intensity		
0+	12	35.29%
0+	15	44.12%
1+	5	14.71%
2+	2	5.88%
Vascular invasion		
Present	7	21%
Absent	27	79%
Total	**34**	

Table 2.2 IFITM1 staining intensity in normal and TNBC breast tissues

Tissue Type	Intensity	Frequency	Percent
Normal Breast			
	0	6	100%
	1+	0	0%
	2+	0	0%
	3+	0	0%
	Total	**6**	
Breast Tumors			
	0	0	0%
	1+	21	62%
	2+	9	26%
	3+	4	12%
	Total	**34**	

Immunohistochemistry (IHC), immunofluorescence (IF) and TUNEL staining of human and mouse tumors

IHC staining was performed after tissue deparaffinization by clearance in xylene and hydration through graded ethanol series. Antigen retrieval was conducted at 99°C in Dako Target retrieval solution for 20 min per manufacturer's instructions (Agilent Technologies: #S1700). For human samples, blocking was performed using 5% normal horse serum and antibody dilution was performed in 0.01% Triton-X. Sections were stained using primary human antibodies targeted against IFITM1 (Santa Cruz: sc-374026) and biotinylated secondary antibodies (Vector Labs). Immunoperoxidase signal was produced using 3,3′-Diaminobenzidine (DAB) and amplified using the Vectastain® Elite ABC Kit (Vector Laboratories). Sections were stained using human antibodies for anti-Ki67 (Dako: #M7240), anti-IFITM1 (Santa Cruz: sc-374026), or anti-smooth muscle actin (Spring Biosciences #E2464). Tissue sections were counter stained using

hematoxylin and mounted in xylene. Slides were imaged on a Nikon Eclipse 80i Upright Microscope in the KUMC imaging core.

IF staining of mouse tumors was performed after tissue deparaffinization by clearance in xylene and hydration through graded ethanol series followed by antigen retrieval as described above. IF method has been described previously (104). Due to the use of mouse antibodies on mouse tissue, blocking and antibody dilution were performed using the Mouse on Mouse (MOM^{TM}) kit per manufacturer's instructions (Vector Labs: BMK-2202). Sections were stained using human antibodies for anti-Keratin 19 (Neomarkers: #MS-198-P1) or anti-smooth muscle actin (Spring Biosciences: #E2464). Secondary antibodies were FITC (Vector Laboratories: FI-1000) or Texas Red conjugated (Santa Cruz: sc-362277). ProLong® Gold Antifade Reagent with DAPI (Cell Signaling: P36935) was used to stain the nuclei and mount the slides. Slides were visualized on a Leica TCS SPE confocal microscope in the Confocal Imaging Core at the University of Kansas Medical Center. Images were collected and analyzed using the Leica LAS AF Lite software (Leica Biosystems).

TUNEL staining was performed using the Click-iT^{TM} Plus TUNEL assay kit (Thermo Fisher: #C10617) on deparaffinized tissue or methanol fixed cell lines grown on chamber slides following the manufacturer's instructions. The average number of TUNEL positive cells was quantified using the binary transformation and cell counting method in ImageJ.

Western blotting

Cells were seeded in 6-well plates or 10cm culture dishes and collected using a cell scraper and lysed in RIPA buffer (Thermo Scientific, Cat. #89901) supplemented with protease inhibitor cocktail (Roche Diagnostics, Cat. #11836–153-001) and phosphatase inhibitor (Sigma, Cat. #P0044). Cells were homogenized over ice by sonication and purified by centrifugation. Protein

concentration was determined by Bio-Rad protein assay (Biorad: Cat. #5000006). Proteins were separated by 4–12% SDS–polyacrylamide gel electrophoresis (NuPage, Cat. #NP0335 and #NP0336) and electrically transferred to a polyvinylidene difluoride membrane. After blocking the membrane using non-fat milk or BSA target proteins were detected using anti-IFITM1 (1:200, SantaCruz: sc-374026) or β-actin (1:15,000, Cell Signaling Technologies: #3700). The appropriate horseradish peroxidase (HRP)-conjugated secondary antibody (Cell Signaling Technologies: Mouse #7076, Rabbit #7074) was applied and the positive bands were detected using Amersham ECL Plus Western blotting detection reagents (GE Health Care: RPN2106) or Immobilon® Crecendo Western HRP Substrate (MilliporeSigma: WBLUR0500) and exposed to autoradiography film (Midwest Scientific).

RNA isolation and RT-PCR analysis

Total RNA was isolated from cultured cells using a QIAGEN RNeasy Mini Kit Qiagen (Cat #74104) according to the manufacturer's protocol. First strand cDNA synthesis was performed from 3 µg total RNA using MulV Reverse Transcriptase (Invitrogen: Cat. #28025-013), RNAse inhibitor (Applied Biosystems: Cat. #N8080119), random hexamers (Invitrogen: Cat. #100026484), deoxynucleotide triphosphates, and colorless PCR buffer (Promega: Cat. #M792A) on a Bio Rad MyCycler™. RT-PCR was conducted using the ViiA™ 7 Real-Time PCR system (Applied Biosystems) and SYBR Green Reagent (Life Technologies: #4367659) with 25 pmol primers obtained from Integrated DNA Technologies. Specific human sequences listed in Table 2.3. Relative mRNA expression level was determined as the ratio of the signal intensity to that of PUM1 using the formula: $2^{-\Delta CT}$. For experimental comparisons, fold change in expression was normalized to PUM1 and then compared to control for that experiment using the formula: $2^{-\Delta\Delta CT}$.

Table 2.3 Primer sequences

Gene	Forward Primer (5'-3')	Reverse Primer (5'-3')
PUM1	TCACCGAGGCCCCTCTGAACCCTA	GGCAGTAATCTCCTTCTGCATCCT
IFITM1	GGATTTCGGCTTGTCCCGAG	CCATGTGGAAGGGAGGGCTC
IL6	CCTCCAGAACAGATTTGAGAGTAGT	GGGTCAGGGGTGGTTATTGC
SNAI2	TGGTTGCTTCAAGGACACAT	GTTGCAGTGAGGGCAAGAA
RELA	AGCTCAAGATCTGCCGAGTG	ACATCAGCTTGCGAAAAGGA
NFKB1	GCAGCACTACTTCTTGACCACC	TCTGCTCCTGAGCATTGACGTC
NFKB2	GGCAGACCAGTGTCATTGAGCA	CAGCAGAAAGCTCACCACACTC

Small interfering RNA (siRNA) transfections

SUM149, MDA-MB-468 and MDA-MB-157 cells were seeded overnight and transfected at 60-80% confluency with 60-100nM of targeted siRNAs or scrambled RNA (siControl Santa Cruz Biotechnology: sc-37007) introduced by Lipofectamine 2000™ (Invitrogen: #1668019) in OptiMEM Reduced-Serum Medium (Gibco: #11058-021). After overnight incubation the transfection mixture was replaced with normal culture medium. MDA-MB-468 and MDA-MB-157 cells were transfected with pooled small-interfering RNAs (siRNAs) targeting IFITM1 (Santa Cruz Biotechnology: sc-44549) which has been validated previously (70). siCon and siIFITM1 cells were then used for functional *in vitro* assays as described below.

CRISPR/Cas9-Mediated Gene Knockout

SUM149 and MDA-MB-157 cells were subjected to CRISPR/Cas9-mediated knockout of IFITM1 by lentiviral transduction using particles from OriGene™ Technologies (Catalog number: KN201617). The guide RNA vector 5'- TGATCACGGTGGACCTTGGA-3' or a scrambled control was cloned into a pCas-Guide vector which expresses Cas9 behind CMV and U6 promoters. This vector was co-transfected with the donor template including homologous arms and a functional

GFP-puromycin cassette using Turbofectin 8.0 (Origene: #TF81001) as the delivery reagent. For SUM149, cells were passaged at a 1:10 ratio 48 hours post-transfection for 8 passages. Cells were treated with 1000µg/mL puromycin daily. Single cells were grown in puromycin until colonies formed. Both clonal populations and a pooled population of all puromycin resistant cells were expanded and screened for absence of IFITM1 protein expression using the IFITM1 antibody. The pooled population of CAS9/Control cells and IFITM1 KO cells were then used for functional *in vitro* assays as described below. For MDA-MB-157, transfected cells were passaged at a 1:2 ratio for 8 passages prior to treatment with 250-350mg/mL puromycin for one week.

Proliferation, colony formation, and wound healing assays

Cell proliferation was measured by cell counting. Cells were seeded onto a 24-well plate at a density of 25,000 cells/well. The next day, cells were either transfected, treated, or harvested for the 0-hour timepoint. Cells were counted every 24 hours and the final values were normalized to the 0-hour timepoint.

For colony formation, cells were seeded onto a 6-well plate at 1,000 cells/well. Cells were grown for 10-14 days prior to staining colonies with 5% crystal violet and imaged using the ChemiDoc™ XRS system equipped with Image Lab™ software.

Wound healing was assessed by seeding cells onto a 24-well plate at a density of 90,000-120,000 cells/well (approximately 80% confluency) and making a single wound by scratching the attached cells using a 10-µl sterile pipette tip. The plates were washed with complete medium to remove cellular debris. Images of the cells were taken immediately after and 24, 48, and 72 hours later using a phase-contrast microscope and wound area was quantified using the Wound Healing Tool in ImageJ.

Animal Experiments

Recipients were 8-10-week-old virgin female NOD-SCID IL2Rgamma^{null} (NSG) mice which were purchased from Jackson Laboratories. Animal experiments were conducted following protocols approved by the University of Kansas School of Medicine Animal Care and Use (ACUP#: 2016-2341). Mice were maintained in the animal facility at KUMC under specific-pathogen free conditions.

To assess tumor growth, the orthotopic fat pad model was used. For this experiment, mice were randomly divided into two groups (8 mice/group). Each mouse was inoculated with SUM149 CAS9/Control cells or IFITM1 KO cells suspended in 50:50 PBS/Matrigel (Corning) through bilateral injection into the 4th mammary fat pads as described previously (130). Briefly, 3 x 10^6 cells were delivered per injection in a volume of 100µL. The length (L) and width (W) of tumors was measured weekly with digital calipers, and the tumor volume was calculated by the formula $L^2/(2W)$. Tumors grew for 26 days and then the mice were sacrificed, and tumors excised, measured, and weighed. Solid tumors were fixed in 4% paraformaldehyde prior to processing and staining.

To assess tumor cell invasion, the mammary intraductal (MIND) model was used as previously described (116). Briefly, SUM149 CAS9/Control cells or IFITM1 KO cells were resuspended as single cells in PBS and counted. A 30-gauge Hamilton syringe, 50-µl capacity, with a blunt-ended 1/2-inch needle was used to deliver the cells. The mice were anesthetized by ketamine/xylene injection and a Y-incision was made on the abdomen allowing exposure of the inguinal mammary fat pads. The nipple of the inguinal gland was snipped for direct needle insertion. Two microliters of cell-culture medium (with 0.1% trypan blue) containing 2,500 to 5,000 cells/µl were injected. Successful injection was confirmed by visual detection of trypan blue in the ductal tree branches. The skin flaps were then repositioned normally and held together with wound clips. After 6 weeks

mice were sacrificed mammary glands were excised and weighed. Mammary glands were fixed in 4% paraformaldehyde prior to processing and staining.

RNA Sequencing and Functional Transcriptomic Analysis

RNA-Sequencing was performed at a strand specific 100 cycle paired-end resolution, in an Illumina NovaSeq 6000 sequencing machine (Illumina, San Diego, CA). The CAS9/Control and the IFITM1 KO pooled samples were analyzed in triplicate. The initial read quality was assessed using the FastQC software (131). The average per sequence quality score measured in the Phred quality scale was above 30. Reads were mapped to the human genome (GRCh38) using the STAR software, version 2.3.1z. On average, 99% of the sequenced reads mapped to the genome, resulting in 30 to 42 million mapped reads per sample, of which on average 95.5% were uniquely mapped reads. Differential gene expression analysis was performed using the Cuffdiff software, version 2.1.1. The number of transcripts mapped to each gene was quantified using the RSEM software. Expression normalization and differential gene expression calculations were performed in edgeR to identify statistically significant differentially expressed genes. The resulting p-values were adjusted for multiple hypothesis testing using the Benjamini and Hochberg method (132).

Genes that were up- or downregulated by at least 2-fold (P 0.05, FDR0.05) and had a FPKM (Fragments per kilo base per million mapped reads) value of ≥ 1 when comparing IFITM1 KO cells to CAS9/Control provided 561 analysis ready molecules. Ingenuity pathway analysis (IPA) was performed using the ingenuity pathway analysis software (QIAGEN). Pathways were identified through the diseases and biological function analysis on IPA. The activation z-score was calculated to infer activation states of upstream regulators.

Supplemental Data:

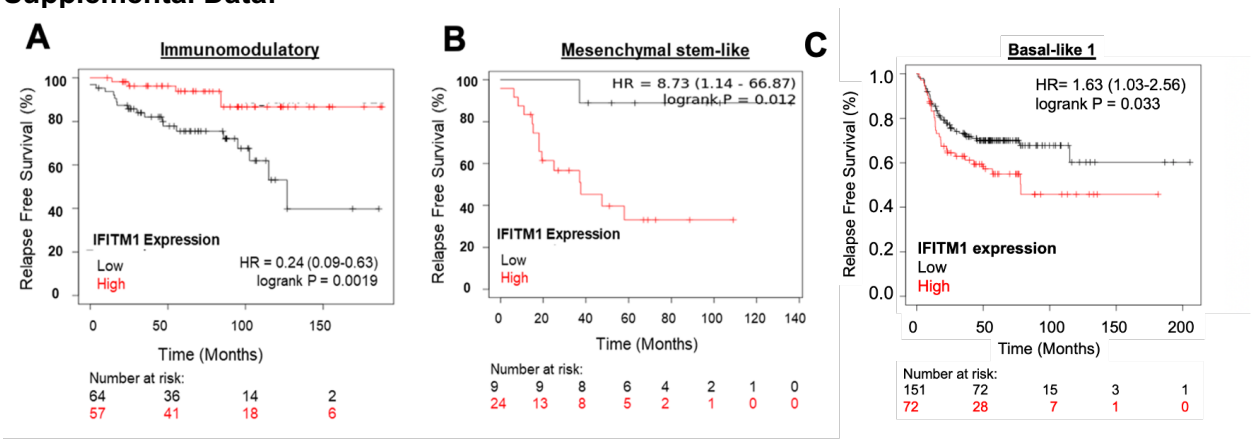

Supplemental Figure 2.1 IFITM1 expression and overall survival in TNBC subtypes
Data were generated using bcGenExMiner4.0. IFITm1 effect on relapse free survival in other TNBC subtypes including immunomodulatory (A), mesenchymal stem-like (B) and basal-like (C), were assessed.

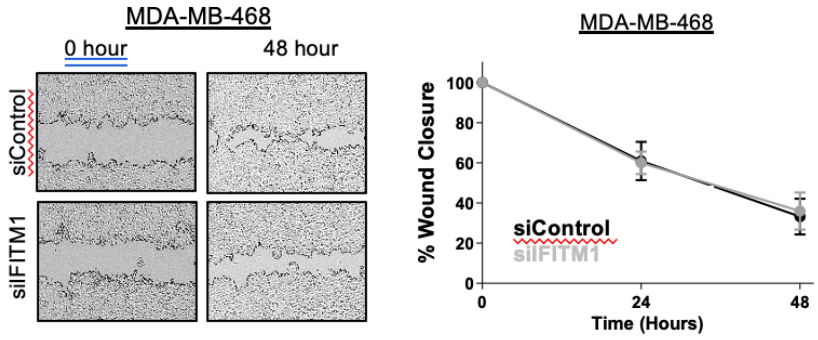

Supplemental Figure 2.2 Loss of IFITM1 on MDA-MB-468 wound healing
Wound healing assay was conducted on 80% confluent plates of MDA-MB-468 cells transfected with siControl or siIFITM1. Plates were imaged at 0, 24, and 48 hours and the size of the wound was quantified by ImageJ (right). Values represent four independent experiments conducted in quadruplicate.

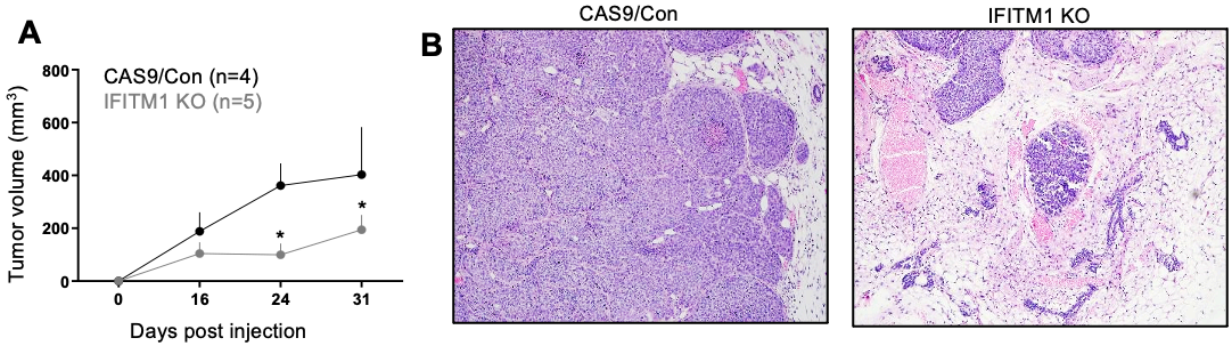

Supplemental Figure 2.3 Loss of IFITM1 decreases tumor growth in the fat pad model of breast cancer and decreases invasion and overall tumor burden in the MIND model of breast cancer
A, SUM149 CAS9/Control and SUM149 IFITM1 KO cells injected into the mammary fat pad of immunocompromised mice as a second replicate for previously presented in vivo data. **B,** Hematoxylin and eosin staining of mammary glands of CAS9/Con and IFITM1 KO MIND tumors.

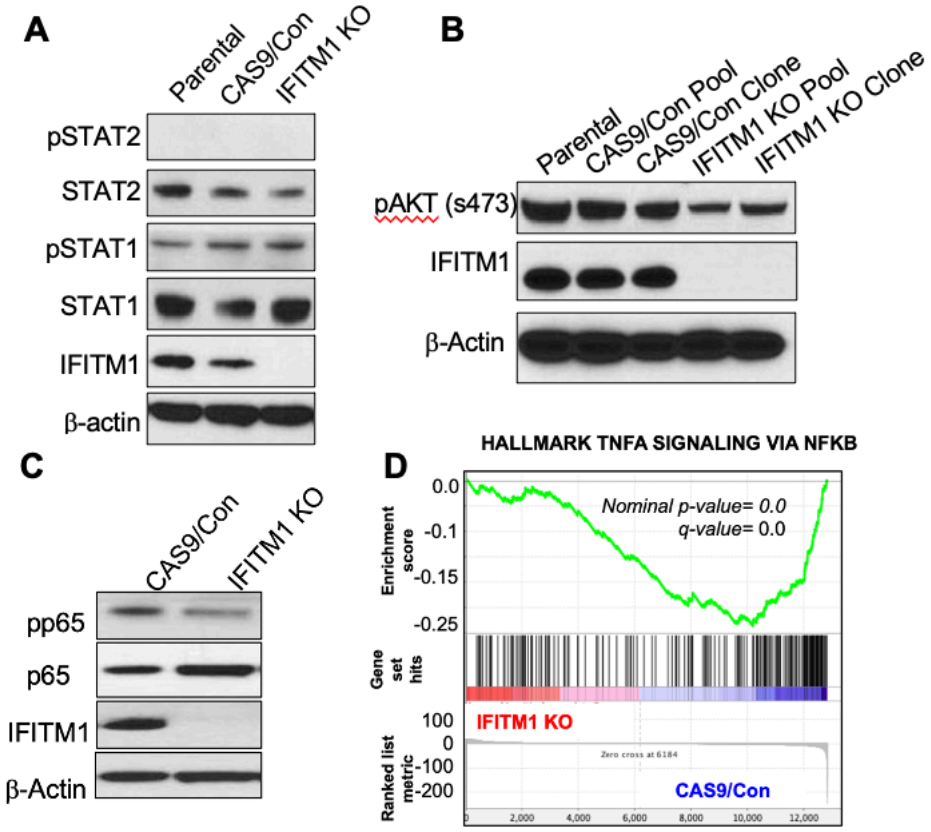

Supplemental Figure 2.4 Loss of IFITM1 on STAT, AKT and NFkB signaling in SUM149 cells
Western blots depicting how the loss of IFITM1 affects canonical STAT (**A**), AKT (**B**), and NFκB signaling (**C**). **D.** GSEA pathway analysis representation of TNFα signaling via NFκB.

Supplemental Table 2.1 Upstream regulators and target genes altered upon IFITM1 inhibition: derived from Ingenuity Pathway Analysis

Upstream Regulator	FC	Predicted Activation	Z-score	p-value of overlap	Target Molecules in Dataset
TP53	-1.334	Inhibited	-2.14	0.00000207	ABAT,ABCC2,ABCG2,ABHD4,ACE,ADRB2,APBB2,AR,ARHGEF2,ARRB1,ATF3,ATG4A,BBC3,BCL2L1,BDNF,BHLHE41,BIRC3,CARD11,CAT,CCDC80,CCN2,CCN5,CCNE1,CCNE2,CCNL1,CD44,CDKN1A,CGB7,CGREF1,CITED2,CKB,COL18A1,COL6A2,CPT1B,CSF1,CTIF,CXCL1,CXCL8,CYFIP2,DDIT3,DGCR6/LOC102724770,DLC1,DLX1,DNAJB2,DUSP1,DUSP2,EGR3,ENO3,EYA4,FGF2,FGFBP1,FHL1,FN1,FOXO1,FOXO3,FUCA1,FUT1,FYN,GADD45A,GAS1,GATM,GDA,GDF15,H2AX,H2BC5,H4C15,HBEGF,HDAC9,HMOX1,HSPA1A/HSPA1B,HSPA1L,HSPA8,HSPB1,HSPG2,IGF1R,IGFBP2,IL1A,IL21R,IL31RA,IL6,IL7,INKA2,ITGB1BP2,ITGB7,KCNG1,KLF4,LDLR,LHX1,LIMA1,MAFB,MAPK4,MATN4,MCAM,MOCOS,MPV17L,MST1,NEO1,NFAM1,NFKB2,NPNT,NPTX1,NUPR1,NYNRIN,PAK3,PCDH7,PDE2A,PDE6A,PDHX,PFKFB4,PIK3CD,PIK3R5,PLAAT3,PLAU,PPARGC1A,PPP1R15A,PRDM1,PRRX2,PSTPIP2,PTGS2,PTP4A1,PTP4A3,PTPRN,RBBP4,RNF144B,RPRM,RPS6KA2,RYR2,SCN3B,SERPINA3,SERPINE1,SESN2,SLC5A3,SLC7A5,SNAI2,TERT,TET1,TEX15,TFPI2,TFRC,TGM2,THBS1,TIMP3,TMEM151A,TNF,TNFRSF9,TOM1,TP63,TRIB3,TSC22D3,TTC28,UNC5B,UPP1,VASN,VWCE,XAF1,XBP1,ZAP70,ZMAT3,ZYX
SP1	-1.068	Inhibited	-2.482	0.000000414	ADAMTS1,ADCY4,AGER,AR,ATF3,BBC3,BDNF,BMP4,BMP7,CAT,CCL20,CCN2,CDH2,CDKN1A,CES1,CIITA,CITED2,CKB,COL7A1,COL8A1,CPLX1,CRABP2,CXCL8,CXCR4,CYP7B1,DLC1,DNM1,FGF2,FN1,FYN,GDF15,HBEGF,HMOX1,IGF1R,IL1A,IL21R,IRF1,ITPR1,KCNQ2,KLF4,KRT16,LCAT,LDLR,MAOA,MAT2A,MYLK,NES,NPR1,PDHX,PLAA,PLAU,PREX1,PSG5,PTGER4,PTGS2,SERPINE1,TERT,TFF1,TFPI2,TGFBR3,TGM1,TIMP3,TINCR,TNF,TNFSF14
RELA	-1.493	Inhibited	-4.144	7.19E-09	ABCG2,AHR,ALOX5AP,ANKRD2,AR,BACH2,BBC3,BCL2L1,BIRC3,BMP2,CCL20,CCN2,CD44,CDKN1A,CIITA,CITED2,CXCL1,CXCL2,CXCL8,CXCR4,DDIT3,DGCR6/LOC102724770,DUSP1,FGF2,FN1,GDF15,HMOX1,IGF1R,IGFBP2,IL1A,IL20,IL6,IRF1,MAT2A,MIA,NFATC1,NFKB2,NFKBID,NR4A3,OAS2,P2RY2,PLAU,PRDM1,PTGS2,SAA1,SAA2,SLC2A5,STAT5A,SYTL1,TERT,TFPI2,TGM2,TNF,TP63,TREM1,TSLP,WASF3,WT1
NFKBIA	-1.153	Inhibited	-3.242	0.0000288	ACKR3,BCL2L1,BIRC3,BMP2,CCL20,CCNE2,CDKN1A,CSF1,CSF3,CXCL1,CXCL2,CXCL8,CXCR4,CYP7B1,DDIT3,FGF2,FN1,FOXC2,GADD45A,GNRH1,HMOX1,HSPA8,IGFBP6,IL1A,IL33,IL6,IRF1,ITPR1,JDP2,LIMA1,MATK,MGP,MSC,MXD4,NFKB2,NGF,NID1,PCDH7,PLAU,PTGS2,RASA3,RCAN1,SORL1,SYCP2,TFRC,TIMP3,TLR4,TNF,TNFSF14
CEBPA	-1.795	Inhibited	-3.055	0.000166	AKR1C1/AKR1C2,AKR1C3,ALOX5AP,APLN,ARHGEF5,CA2,CCL20,CDKN1A,CIITA,CRABP2,CSF1,CSF3,CXCL8,CXCR4,FHL1,FOXO1,FOXO3,GADD45A,GAS1,GGH,HMOX1,IFI27,IL6,IVL,KLF4,KRT17,LCK,LEPR,MC1R,NFATC1,NFIL3,OAS2,PPARGC1A,PRDM1,PTGS2,RGS2,RORA,SAA1,SERPINE1,STEAP4,SULT1A3/SULT1A4,TFR2,THBS1,TNFAIP6,TSC22D3,UCP1,ZIC2
NUPR1	-3.715	Inhibited	-4.727	0.00945	ADRB2,ATF3,AVPI1,CASTOR2,CITED2,CXCL8,CXCR4,DDIT3,DUSP8,ENO2,FAM111B,FBXO3,FOXO3,FUCA1,GABBR1,GADD45A,GCNT2,GDF15,GPR1,GSTA4,H3C6,HBEGF,HSPA2,IFIT2,IGF1R,IGF2BP3,KLF4,MAT2A,NFIL3,NUPR1,PFKFB4,PODNL1,PPP1R15A,RAB39B,SERPINE1,SESN2,SPG7,TERT,TRERF1,TRIB3,UNC5B,UPP1,XBP1,ZNF488
FOXO3	-2.029	Inhibited	-2.109	0.00000221	AHR,ALDH3A1,APLN,AR,ATP6V0D2,BBC3,BMP2,CAT,CCN2,CCNE2,CDKN1A,CDKN1C,CLDN1,CXCL8,CXCR4,DDIT3,ENO2,FBXO32,FN1,FOXO1,FOXO3,FYN,GADD45A,IGF1R,IL6,ITGB2,MCAM,MXD4,NPNT,NRP2,NTN4,NUPR1,PLAU,PPARGC1A,PPP1R15A,PRDM1,SERPINE1,SLC1A4,TCIM,TFF1,TNF,TXNIP
SMAD4	-1.143	Inhibited	-2.181	0.000000548	ANGPTL4,ARHGEF2,BBC3,BMP2,BMP4,BMP7,CCL20,CCN2,CCNE1,CDH2,CDKN1A,CELF2,CITED2,COL7A1,CSF1,FN1,GADD45A,HMOX1,ITGB7,JAG2,LHX1,PAK3,PAX6,PILRA,PLAU,PTGS2,PTHLH,RGCC,SERPINE1,SNAI2,THBS1,TIMP3,TNF,TNFAIP6,TPM1
STAT1	1.102	Inhibited	-2.541	0.00461	APOL6,BCL2L1,C1R,C1S,CCL20,CCNE1,CDKN1A,CIITA,CMPK2,CXCL2,CXCL8,EGLN3,FGF2,FOXO1,IFI27,IFIT2,IGF1R,IL18BP,IL31RA,IL6,IRF1,ISL1,KLF4,OAS2,PAX6,PDX1,PTGS2,SAA2,SERPINA3,SLFN5,TFF1,TLR4,TNF,XAF1
SP3	-1.114	Inhibited	-2.592	0.00000225	ADCY4,ATF3,CCL20,CDH2,CDK5R1,CDKN1A,CES1,CITED2,COL7A1,CYP7B1,DNM1,DUSP1,GDF15,IGF1R,IL1A,KLF4,KRT16,LCAT,LDLR,MAT2A,MYLK,NES,PLAU,PREX1,PTGS2,SERPINE1,TERT,TFF1,TGFBR3,TGM1,TNFSF14,XYLT1
ATF4	-1.488	Inhibited	-3.395	7.89E-08	ABCG2,ATF3,BBC3,CDKN1A,CHAC1,DDIT3,FGF21,FYN,GADD45A,GDF15,HERPUD1,IGFBP2,IL6,KLF4,MITF,NUPR1,PCK2,PPP1R15A,PRRX2,PTGS2,SLC1A4,SLC1A5,SLC6A9,SLC7A11,SLC7A5,SNAI2,SSBP2,STC2,TRIB3
KMT2D	1.107	Activated	3.065	0.0000659	ACCS,CSPG4,DUSP2,ECHDC2,ECI2,ENO3,FHL1,GALNT12,IRF1,IVL,JAG2,KLF4,KRT16,KRT17,KRT6A,LCK,LRRN4,MEOX1,METRNL,NAALADL2,NPR3,PAOX,PCDH7,PTGR2,TFF1,TGM1,VTN
FOXA2		Activated	2.417	0.000252	AMY2B,C5,CDX2,CXCR4,FOXA1,FOXO1,GSTM3,IL13RA2,IL33,IL6,ISL1,LHX1,LIPE,MAP1B,NFKB2,PAX6,PDHX,PDX1,PPP1R14C,PROS1,RORA,SAA1,SERPINA1,TCF7,UST
FOXA1	2.049	Activated	2.815	0.0000171	BMP2,CDKN1A,CDX2,COL18A1,FOXA1,HNF4G,IL6,ISL1,KRT16,MGP,NES,PAX6,PPP1R14C,PRDM15,RORA,RPRM,SNAI2,SPDEF,TCF7,TFF1,TMEM74,UCP1,UST,XBP1
ATF2	-1.237	Inhibited	-2.351	0.00000165	ATF3,BCL2L1,CXCL8,DDIT3,DUSP1,DUSP8,FGF21,FN1,GADD45A,IL1RL1,IL6,MAT2A,MYLK,NUPR1,PLAU,PPARGC1A,PTGS2,SNAI2,TNF
MDM2	1.11	Activated	2.048	0.00000142	ATF3,BBC3,CDKN1A,CLIP3,CXCL8,FOXO3,H2AC18/H2AC19,H2BC21,HIPK2,IGF1R,IGFBP6,IL13RA2,INHBB,SNAI2,TERT,THBS1,TP63
KLF6	-1.583	Inhibited	-2.749	0.00000378	ATF3,BCL2L1,CDH2,CDKN1A,CXCL2,CXCL8,IGF1R,IL1A,IL6,PLAU,PRDM1,PSG5,PTGS2,TFPI2,TNF,VAV3
SMAD2	-1.43	Inhibited	-3.03	0.000177	CCN2,CDH2,CDKN1A,CDX2,FN1,GSC,HMOX1,IL6,PTHLH,S1PR1,SERPINE1,SNAI2,THBS1,TIMP3,TPM1
NFKB2	-2.381	Inhibited	-2.048	0.000436	AR,BCL2L1,BIRC3,BMP2,CCL20,CDKN1A,CXCL8,CXCR4,ICOSLG/LOC102723996,MAT2A,NFKB2,PTGS2,TNF

Chapter 3: IFITM1 cooperates with CD81 to mediate TNBC breast cancer growth and integrin gene expression

Introduction

Membrane proteins constitute approximately 30% of the proteome and most of which, are very well characterized (133). Receptors, pore forming proteins, enzymes, attachment proteins, and structural proteins are all members of this family and play a fundamental role in tumor development and progression and have therefore emerged as therapeutic targets. IFITM1 is a 14kDa, 125 amino-acid interferon inducible transmembrane protein overexpressed in TNBC and contributes to TNBC growth, migration and invasion. Historically, IFITM1 has been defined as component of protein complexes involved in homotypic adhesion, germ cell homing, and transduction of antiproliferative signals (99, 134-136), and as an important factor of regulation of viral infection. IFITM1 can restrict infection of a number of RNA viruses, including hepatitis C virus (94), HIV (92), Zika virus (137), and influenza viruses (138). Although aforementioned mechanisms of IFITM1 function are better understood, the mechanism by which IFITM1 regulates growth, migration, and invasion of tumor cells is yet to be uncovered.

IFITM1 contains three palmitoyl sites (C50, C51, T97), two membrane spanning domains, a caveolin-1 (CAV1) binding domain (84-125 aa) and a sorting signal near its c-terminus (67, 96, 109). IFITM1 has been identified both as plasma membrane resident protein and an internal membrane protein due to its distinct interaction with RAB5, LAMP1, and CD63; components of internal membranes and recycling machinery (96, 139). Additionally, early reports identified direct interactions of IFITM1 with tetraspanin proteins CD19, CD21 and CD81 on surface of B-cells (23). Tetraspanins are cell surface molecules known to function as molecular adaptors to cluster adhesion receptors, signaling molecules, and cell surface receptors to regulate EMT, cell adhesion, angiogenesis, invasion, and exosome mediated metastasis, thus playing a fundamental cancer progression (24). Not all tetraspanins are expressed on all cell types (23), but cluster of differentiation-81 (CD81) has been established as a tumor promoter in breast cancer (25). CD81 is a 26kDa cell surface protein and is well known for its function as an integrin adaptor and regulator, and an exosome marker (140). In breast cancer, CD81 is a key EMT marker in

which its loss decreases in vitro migration and in vivo tumor growth and metastasis (103, 141). Here, we hypothesize that CD81 is important for the function of IFITM1 in TNBC.

Due to IFITM1's complex nature, we aimed to define its localization, interacting partners, and the functional importance of these relationships in regard to proliferation and gene expression. First, we confirmed that IFITM1 resides in the membrane fraction of TNBC but is not localized at cell-cell junctions. Through public data mining, we found IFITM1 has a direct interaction with CD81, a potential interaction with CAV1, and identified clinical correlations between IFITM1 and CD81 in TNBC. Notably, RNA sequencing analysis of IFITM1 KO versus CRISPR/Con SUM149 cells suggests that loss of IFITM1 reduces pathways regulated by CD81. *In vitro* analyses suggest this observation may be due to a decrease in CD81 levels due to decreased protein stability upon loss of IFITM1. Mechanistically, we found that IFITM1 regulates β1, α3, α4 integrins with the help of CD81. Though strong co-localization was observed between IFITM1 and CD81, no direct interaction was found. However, a secondary complex formation mediated by CAV1 could be bringing CD81 and IFTM1 into close proximity. Lastly, we show for the first time that IFITM1 is found in the extracellular vesicles of TNBC cells. Collectively, our data suggest that the function of IFITM1 may be mediated in part by CD81 and that this relationship may have both intracellular and extracellular implications. The findings from this study provide evidence into the potential mechanism of action of IFITM1 and lay a solid foundation for further mechanistic and biomarker assessments of IFITM1 and CD81 in TNBC.

Results

IFITM1 is a membrane protein in TNBC

We first aimed to confirm the membrane localization of IFITM1 in TNBC. Utilizing a cytoplasmic, membrane, nuclear/cytoskeletal fraction assay we verified that IFITM1 is indeed localized to the membrane portion of TNBC cells (Figure 3.1 A). To further define the subcellular localization of IFITM1, confocal immunofluorescence was used. IFITM1 localizes heavily to the perinuclear region in all cell lines with some diffuse staining identified throughout (Figure 3.1 B).

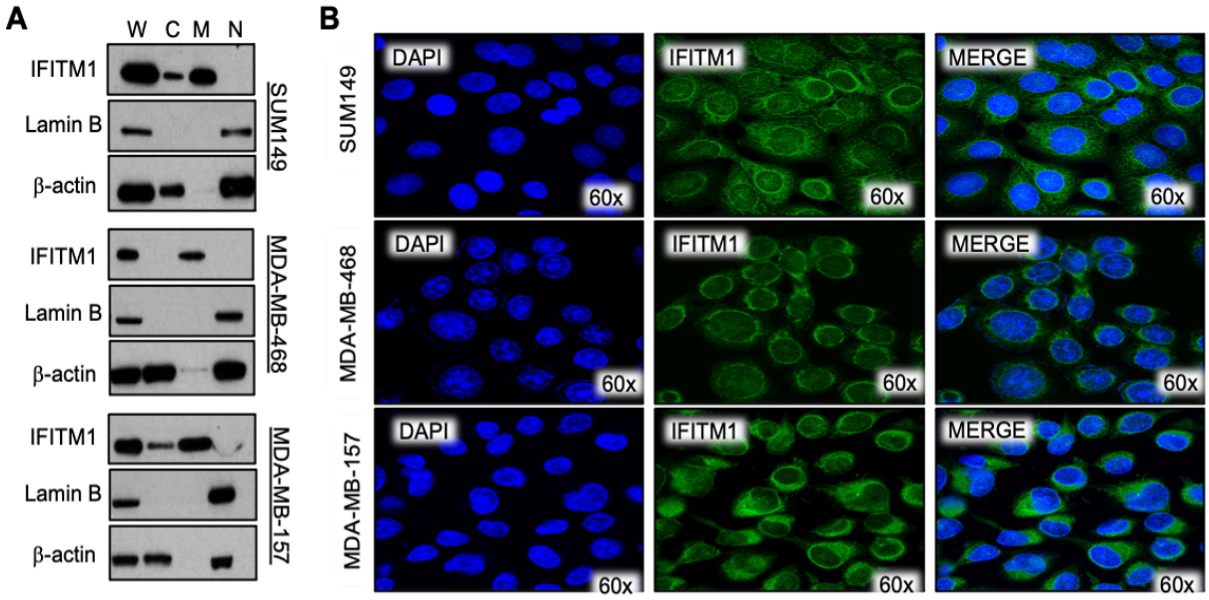

Figure 3.1 IFITM1 is a stable membrane protein in TNBC
A. Western blot of cytoplasmic, membrane, and nuclear/cytoskeletal fractions of SUM149, MDA-MB-468, and MDA-MB-157 cell lines. **B.** Immunofluorescence of IFITM1 in SUM149, MDA-MB-468, and MDA-MB-157 cell lines under permeabilized conditions.

IFITM1 and CD81 expression correlate clinically and pre-clinically

The STRING interaction network visually depicts potential IFITM1 interactions which identified an experimentally determined an interaction between IFITM1 and CD81 (Figure 3.2 A). Notably, CD81 is a widely expressed tetraspanin involved in numerous biological responses in cancer cells and is known to interact with IFITM1 on B-cells (142). As we thought that CD81 might be involved in the action of IFITM1 in TNBC cells, we examined the correlation between IFITM1 and CD81 and its relation to overall survival. First, we screened multiple TNBC cell lines including TNBC (SUM149, MDA-MB-468, MDA-MB-157), ER+ (MCF7, T47D), and normal immortalized mammary cells (MCF10A) and identified that CD81 is expressed in all screened cell lines (Figure 3.2 B). CD81 is a tetraspanin that is expressed in almost all cells of the body so expression in multiple breast cancer cell lines was not surprising. Next, the correlation between IFITM1 and CD81 in clinical data from TNBC patients was assessed. In basal like breast cancer, the expression of CD81 and IFITM1 have a slight positive, but significant correlation based on gene expression analysis from clinical samples obtained from bcGenExminer4.0 (Figure 3.2 C). Notably, when assessing how CD81 expression alters overall survival of basal like breast cancer and luminal a breast cancer, we found that high levels of CD81 contributes to poor overall survival in basal like breast cancer but better overall survival in luminal breast cancer (Figure 3.2 D,E), suggesting a context dependent role of CD81. Corroborating this evidence, the finding that IFITM1 and CD81 are only co-expressed in TNBC cell lines suggests that CD81 may function independently of IFITM1 in ER+ cancer and that the CD81/IFITM1 relationship may be functionally important in mediating IFITM1 function in TNBC, thus warranting future mechanistic analyses.

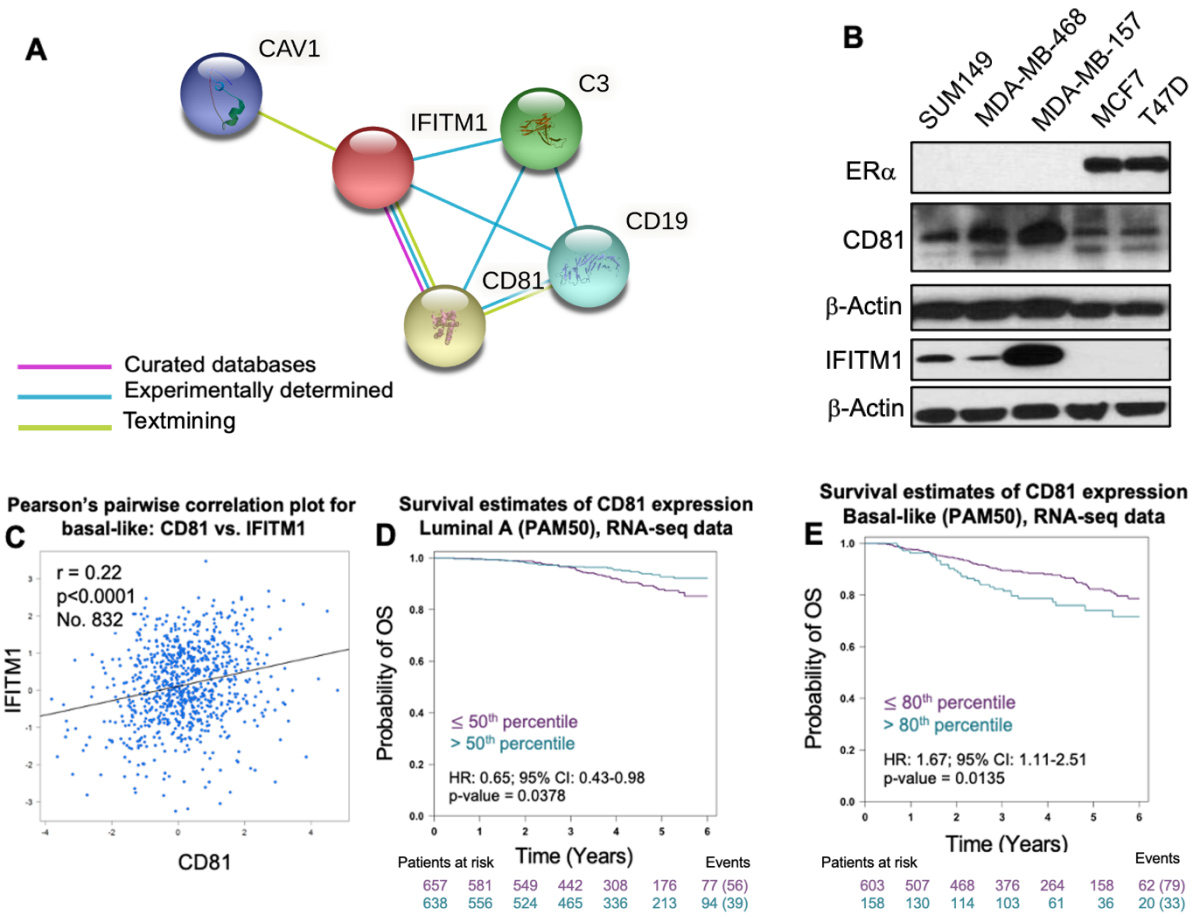

Figure 3.2 IFITM1 and CD81 clinical and pre-clinical relationship
A, STRING interaction network summary of IFITM1 interacting proteins. Physical network assessed in textmining, experiments, and databases with the minimum interaction score of 0.4). **B,** Immunoblotting assessed CD81 protein expression in multiple TNBC cell lines (SUM149, MDA-MB-468, MDA-MB-157), ER+ breast cancer cell lines (MCF7, T47D) and normal-immortalized human breast cells (MCF10A) **C,** bcGenExMiner4.0 was used to assess the correlation between CD81 and IFITM1 DNA expression in basal-like breast cancer **D,** CD81 on luminal breast cancer overall survival derived from bcGenExMiner4.0 **E,** CD81 on basal-like breast cancer overall survival derived from bcGenExMiner4.0.

Loss of IFITM1 decreases CD81 mediated signaling pathways and stability

Since IFITM1 and CD81 are positively correlated in clinical samples of TNBC, we assessed the nature of this correlation in vitro with the use of TNBC cell lines. First, comparing SUM149 IFITM1 KO and CRISPR/Con cells highlights that IFITM1 significantly decreases pathways known to be regulated by CD81 including TGFB, P38 MAPK, and PI3K (Figure 3.4 A). To assess if this observed downregulation could be a result of IFITM1 mediated CD81 levels, siRNA was used to transiently silence IFITM1 in SUM149, MDA-MB-157, and MDA-MB-468 cell lines, where loss of IFITM1 contributes to a slight decrease in CD81 expression (Figure 3.3 B). Since membrane proteins rely heavily on the membrane integrity for their stability, we hypothesized that loss of IFITM1 may alter the stability of CD81 contributing to CD81 downregulation. Therefore, we utilized CRISPR/Cas9 IFITM1 KO SUM149 cells treated with the translation inhibitor, cycloheximide, and identified that loss of IFITM1 reduces the stability of CD81 by about 4 hours (Figure 3.3 C,D). Interestingly, siRNA mediated decrease of CD81 resulted in a slight increase of IFITM1 expression in SUM149 and MDA-MB-468 cells (Figure 3.3 E). MDA-MB-157 cells have a higher basal expression of IFITM1, perhaps offsetting the necessity for IFITM1 upregulation upon CD81 loss (Figure 3.3 E). Collectively, these data are suggestive of a biological correlation between IFITM1 and CD81 in TNBC.

A

Upstream Regulator	mRNA fold change	Predicted activation	Activation z-score	p-value of overlap
TGFB1	1.224	Inhibited	-4.377	1.95E-18
P38 MAPK		Inhibited	-3.057	6.75E-11
PI3K			-1.345	2.15E-12

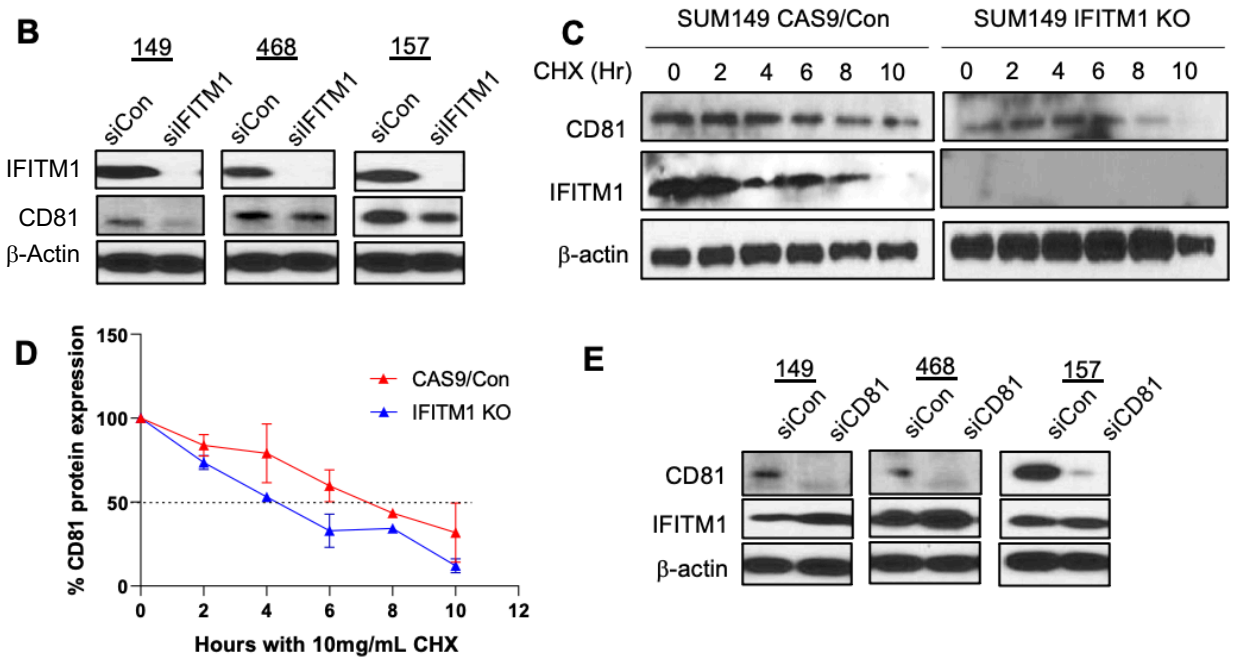

Figure 3.3 Loss of IFITM1 CD81 regulated signaling pathways through mediating its stability
A, Table of pathways known to be regulated by CD81 which were significantly downregulated in SUM149 CRISPR IFITM1 KO cells compared to SUM149 CAS9/Control cells as identified through Ingenuity Pathway Analysis. **B,** Immunoblot of SUM149, MDA-MB-468, and MDA-MB-157 cells depicting siRNA knockdown of IFITM1 and subsequent CD81 protein expression after 48 hours. **C-D,** Western blot of cells treated with 10μg/mL cycloheximide for 2-10 hours and quantification of western blot via ImageJ (**D**). Representative blot of at least two experiments for each cell line shown. **E,** Immunoblot of SUM149, MDA-MB-468 and MDA-MB-157 cells depicting siRNA knockdown of CD81 and subsequent IFITM1 expression. Representative blot of at least two experiments for each cell line shown.

CD81 regulates IFITM1 mediated TNBC growth

Next, we investigated the functional relationship between IFITM1 and CD81 *in vitro*. To determine whether CD81 contributes to IFITM1 mediated TNBC growth, we examined the growth effects of knockdown of CD81 in SUM149 CRISPR/Con, SUM149 IFITM1 KO, and MDA-MB-468 cells with or without siRNA against IFITM1. Similar to SUM149 parental cells, loss of CD81 induced IFITM1 expression in CRISPR/Cas9 SUM149 cells (Figure 3.4 A). By cell counting to assess proliferation in CRISPR/Con and IFITM1 KO SUM149 cells, loss of CD81 decreases proliferation similar to that of IFITM1, but there is no additive effect when both CD81 and IFITM1 are gone (Figure 3.4 B). To assess this effect in another TNBC cell line, MDA-MB-468 cells were used. Though loss of CD81 resulted in a significant decrease in cellular proliferation, this response was not as robust as in SUM149 cells (Figure 3.4 C). However, similar to SUM149 cells, there is no significant difference between loss of CD81 or IFITM1 on cell growth and no additive effect of decreased proliferation when both IFITM1 and CD81 are gone (Figure 3.4 D). These data suggest that in both SUM149 and MDA-MB-468 cells, the presence of IFITM1 expression does not rescue the attenuated proliferative capacity as observed upon knockdown of CD81 and CD81 mediated growth may be partially regulated by IFITM1 expression. Since loss of CD81 in the absence of IFITM1 has no additive effect, these data suggest that both proteins act via a common pathway (143). Collectively, the mechanism whereby IFITM1 mediates TNBC proliferation is in part, due to its relationship with CD81.

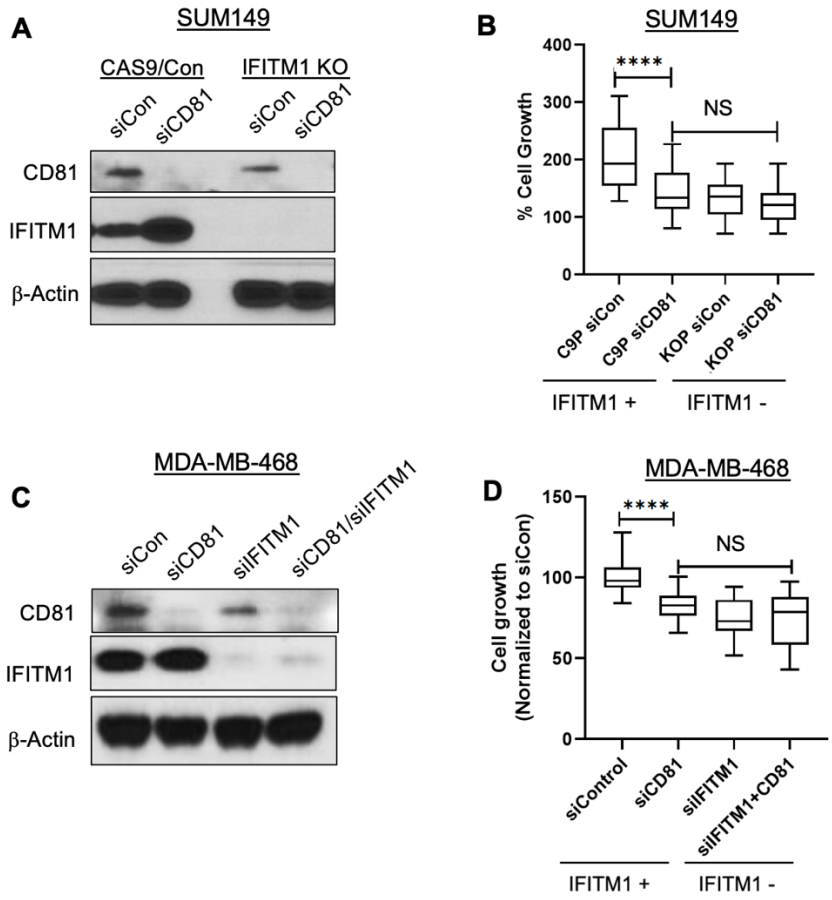

Figure 3.4 IFITM1 utilizes CD81 to regulate TNBC growth
A. Immunoblot of SUM149 CAS9/Control and SUM149 IFITM1 KO cells treated with either siControl or siCD81 and blotted for CD81, IFITM1 and β-actin. **B**. Percent cell growth as assessed by cell counting at 48 hours compared to the 0 hour timepoint of each cell line prior to transfection of CAS9/Control cells treated with siControl or siCD81 and IFITM1 KO cells treated with either siControl or siCD81. **C.** Immunoblot of MDA-MB-468 cells treated with either siControl, siIFITM1, siCD81, or both siCD81 and siIFITM1 and blotted for CD81, IFITM1 and β-actin. **D**. Percent cell growth as normalized to siControl at 48 hours. Cell counting for both SUM149 and MDA-MB-468 experiments were completed >5 times in triplicate. A one-way ANOVA was used to assess significance between groups. ****$p<0.0001$.

IFITM1 regulation of integrins and NFκB genes is mediated by CD81

To identify a mechanism of how IFITM1 utilizes CD81 for cell growth, we first utilized the STRING interaction network to identify functional and physical associations between CD81 and other proteins and compared this against our RNA sequencing data. The STRING interaction network predicts an association between CD81 and ITGB1 and ITGA4 (Figure 3.5 A). Assessment of sequencing data identified that loss of IFITM1 increases ITGB7, ITGB2, ITGA6 and integrin binding proteins ITGB1BP2 and ITGB3BP but decreases integrins ITGAV, ITGB8, ITGB5, ITGB4, and ITGA3 (Figure 3.5 B). Notably, ITGB1 and ITGA4 are known to complex with ITGB5, ITGA6 and ITGA3. Therefore, based on the STRING interaction network and RNA sequencing data we focused on assessing the levels of ITGB1, ITGB5, ITGA3 and ITGA4. Here, we utilized CRISPR/Cas9 Con and IFITM1 KO SUM149 cell lines with and without manipulation of CD81 through siRNA. Through qRT-PCR analysis we identified that expression of integrins ITGB1, ITGB3, and ITGA4 are all mediated by IFITM1 through its relationship with CD81 whereas ITGB5 is CD81 independent (Figure 3.3 C). We further identified RELA, NFKB2, and IL6 (a downstream mediator of NFκB signaling and integrin signaling as identified in Chapter 2) as genes dependent on the IFITM1/CD81 relationship (Figure 3.3 D). Collectively, these data suggest that CD81 is in part, an essential mediator of IFITM1 regulation of integrin, NFκB and IL6 gene expression.

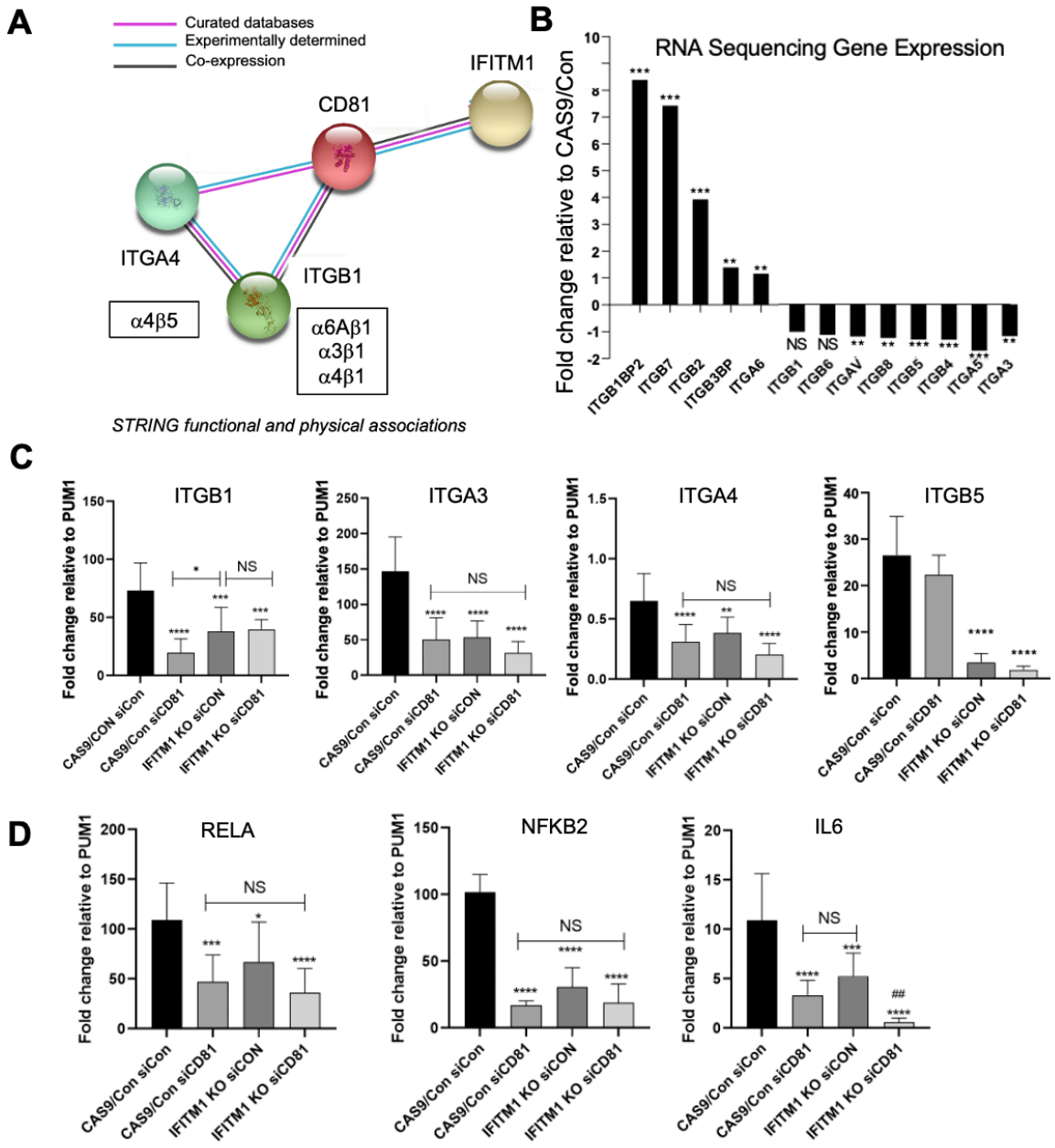

Figure 3.5 IFITM1 regulation of integrins, RELA, NFKB1 and IL6 is mediated by CD81
A, STRING interaction network of functional and physical associations with CD81 derived from experiments, databases, co-expression, gene fusion and co-occurrence with highest confidence. **B,** Gene expression fold change of SUM149 IFITM1 KO cells compared to SUM149 CAS9/Control cells as identified through RNA sequencing analysis. **C-D.** Gene expression of ITGB1, ITGB3, ITGA4, ITGA5 (C), and (D) NFκB mediated genes RELA, NFKB2, IL6, relative to PUM1 as assessed by qRT-PCR analysis. SUM149 CRISPR/Cas9 Control or SUM149 IFITM1 KO cells were treated with either siControl or siCD81. Data represent average ± standard deviation of at least 4 independent experiments with outlier values removed. An ANOVA was used to assess statistical significance. ****p<0.001, ***p<0.001, #p<0.05 when compared to IFITM1 KO cells treated with siControl **E.** Pearson's pairwise correlation plot between IFITM1 and IL6 in TNBC patients as determined by IHC obtained from analyzing RNA sequencing data from bcGenExMiner4.0.

IFITM1 and CD81 are within close proximity but do not interact

The identified functional relationship between IFITM1 and CD81 led us to hypothesize that a direct interaction between IFITM1 and CD81 is occurring in TNBC. In SUM149 and MDA-MB-157 cells, IFITM1 and CD81 have similar subcellular localization as identified through co-immunofluorescence (Figure 3.6 A). However, we did not observe a direct interaction between IFITM1 and CD81 in either SUM149 or MDA-MB-157 cells as assessed by co-immunoprecipitation. Therefore, these data suggest that IFITM1 and CD81 are in very close proximity but do not interact

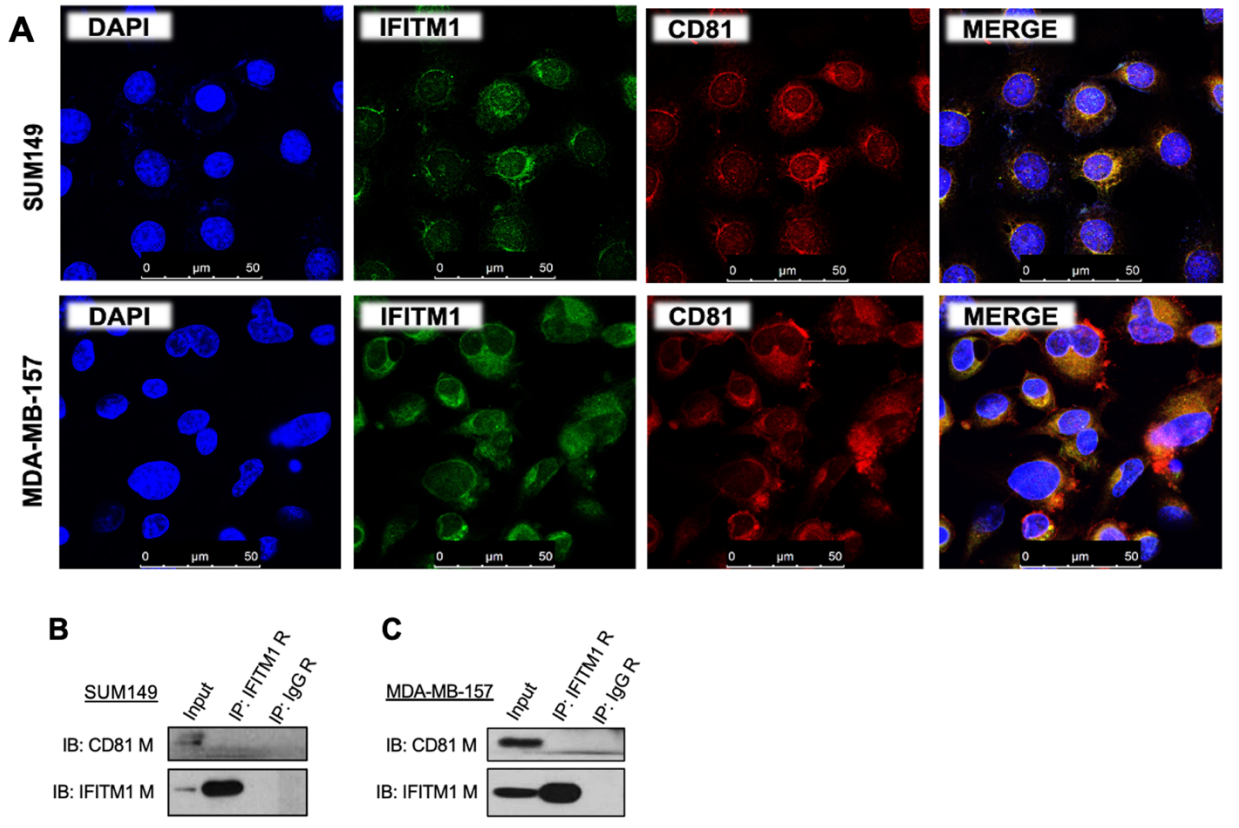

Figure 3.6 IFITM1 and CD81 co-localize but do not directly interact
A, Immunofluorescent images at 60x magnification of co-staining with IFITM1 (green) and CD81 (red) antibodies in SUM149 and MDA-MB-157 cell lines. **B,** Western blot of co-immunoprecipitation of IFITM1 and CD81 in SUM149 cells **C,** Western blot of co-immunoprecipitation of IFITM1 and CD81 in MDA-MB-157 cells.

CAV1 is overexpressed in TNBC and interacts with IFITM1 and CD81

Since IFITM1 and CD81 do not directly interact but appear to be functionally related, we hypothesized that this is perhaps due to interaction with a mediator protein. IFITM1 has a CAV1 binding domain which is represented in Supplemental Figure 3.1 A and both CAV1 and CD81 are structural membrane raft proteins (144). Therefore, we hypothesized that IFITM1, CAV1, and CD81 may form a functional complex in TNBC cells. Clinically, CAV1 and IFITM1 gene transcripts are not correlated in basal-like breast cancer (Supplemental Figure 3.1 B) but CAV1 does contribute to poor overall survival (Supplemental Figure 3.2 C). Furthermore, we found that CAV1 was highly expressed in TNBC cell lines compared to ER+ cell lines (MCF7 and T47D) (Supplemental Figure 3.1 D).

To further investigate this relationship, the co-localization of IFITM1 and CAV1 through co-immunofluorescence was used. IFITM1 and CAV1 show overlap in the perinuclear region of the cell, but not at cell-cell junctions (Supplemental Figure 3.2 A). Though there is limited resolution of confocal imaging, these experiments suggest a possible association between IFITM1 and CAV1, which was then validated by co-immunoprecipitation experiments. Here, IFITM1 and CAV1 directly interact in SUM149, MDA-MB-157 and MDA-MB-468 cells (Supplemental Figure 3.2 B). MDA-MB-157 cells have highest protein levels of CD81 and IFITM1 so we used these cells for a proof of principle complex identification. Through co-immunoprecipitation, we identified that in MDA-MB-157 cells, CAV1 and CD81 directly interact (Supplemental Figure 3.2 C). Therefore, these data suggest that CAV1, IFITM1, and CD81 may form a complex in TNBC. However, future investigations into where, when, and how this complex forms as well as its functionality in TNBC are necessary.

IFITM1 is identified in extracellular vesicles

The IFITM family inhibits viral infection and replication through inhibiting viral fusion on the plasma membrane and by regulating endosome fusion with the lysosome to inhibit viral reproduction (94). The C-terminal end of IFITM1 is essential to regulate cellular susceptibility to viral infection since this domain regulates IFITM1 expression on intracellular vesicles and the plasma membrane (21, 22). Interestingly, native IFITM1 has been shown to localize with Rab5 (92) and to directly bind with AP-3 (96). AP-3 is the adaptor protein that is predominantly responsible for sorting transmembrane proteins within the endocytic pathway (37). Though these processes are essential to limit viral replication, tumor cells use these same pathways for regulation of multiple processes. Extracellular vesicles, in particular, can be formed by the intracellular recycling pathway. Notably, CD81 is a well-known marker of extracellular vesicles and CAV1 localization in exosomes has emerged as a tumor promoter in breast cancer (145). Therefore, we investigated if IFITM1 is localized on intracellular membranes involved in intracellular recycling and in extracellular vesicles. To assess whether IFITM1 may be involved in intracellular recycling we assessed co-immunofluorescence of IFITM1 with the ER apparatus protein marker calnexin, and the early endosomal Rab5 protein. Here, we identified strong co-localization with calnexin and RAB5. Thus, the observations of this experiment and through the results of our fractionation assay suggest that IFITM1 is expressed within the intracellular membranes of TNBC cells. Next, using high density centrifugation, we isolated the extracellular vesicle component of SUM149, MDA-MB-468 and MDA-MB-157 cells (Figure 3.9 B-C). In agreement with other papers, exosomes derived from these TNBC cell lines were shown to express IFITM1, CAV1 and CD81. Though our major findings are focused on the intracellular relationship regarding IFITM1 dependence on CD81 for regulating TNBC growth and integrin expression (Figure 3.8), this exosome data is important to provide rationale for investigating the role of IFITM1 as a serum biomarker, the role of IFITM1 in mediating the microenvironmental response, and providing a novel avenue for IFITM1 biology in TNBC which has yet to be explored

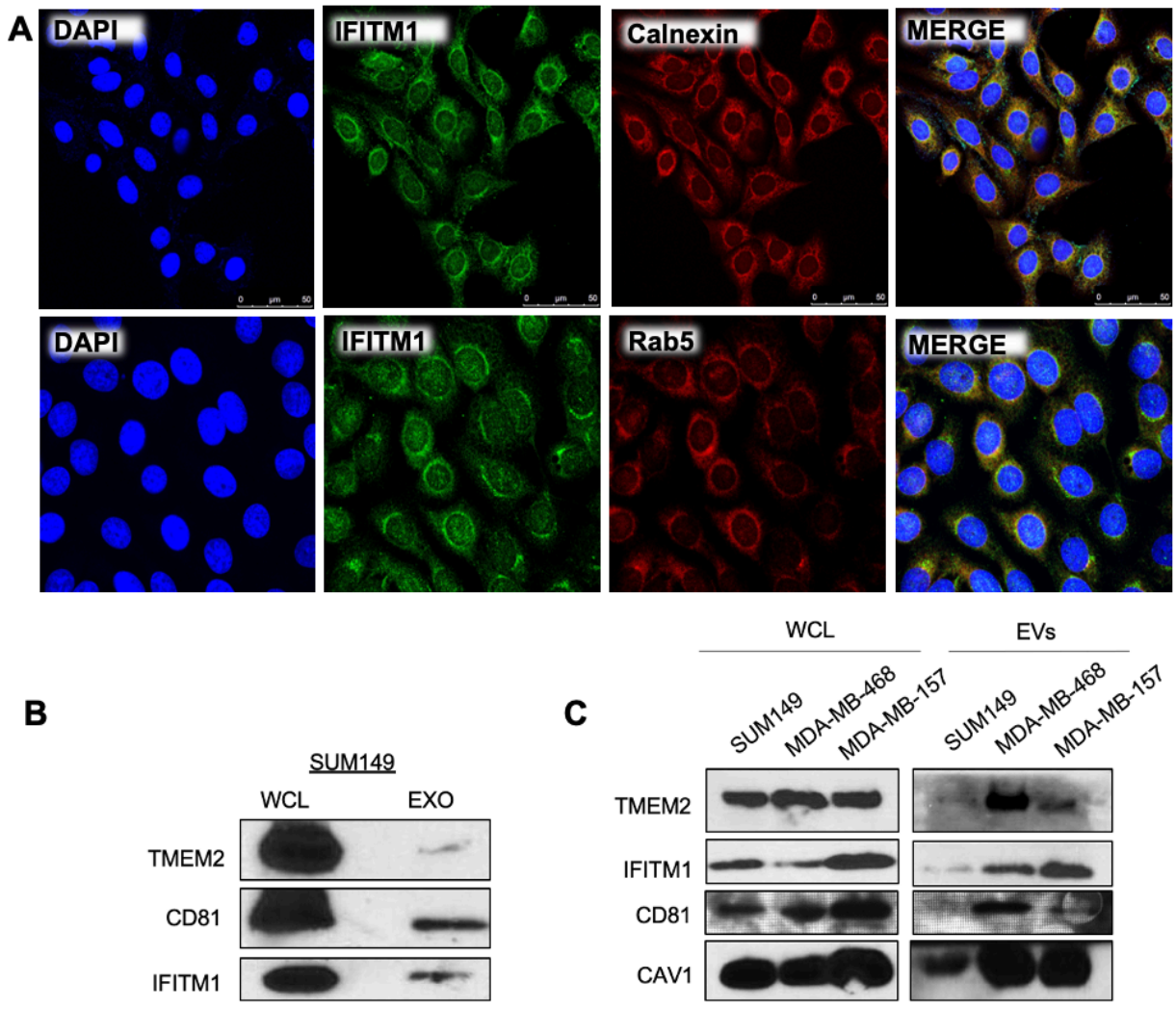

Figure 3.7 IFITM1, CD81 and CAV1 in extracellular vesicles
A. Co-immunofluorescence in SUM149 cells of IFITM1, Calnexin, and RAB5. **B.** Western blot of SUM149 whole cell lysates and isolated extracellular vesicles. TMEM2 and CD81 are key extracellular vesicle markers. **C**. Immunoblot of SUM149, MDA-MB-468, and MDA-MB-157 whole cell lysates and isolated extracellular vesicles.

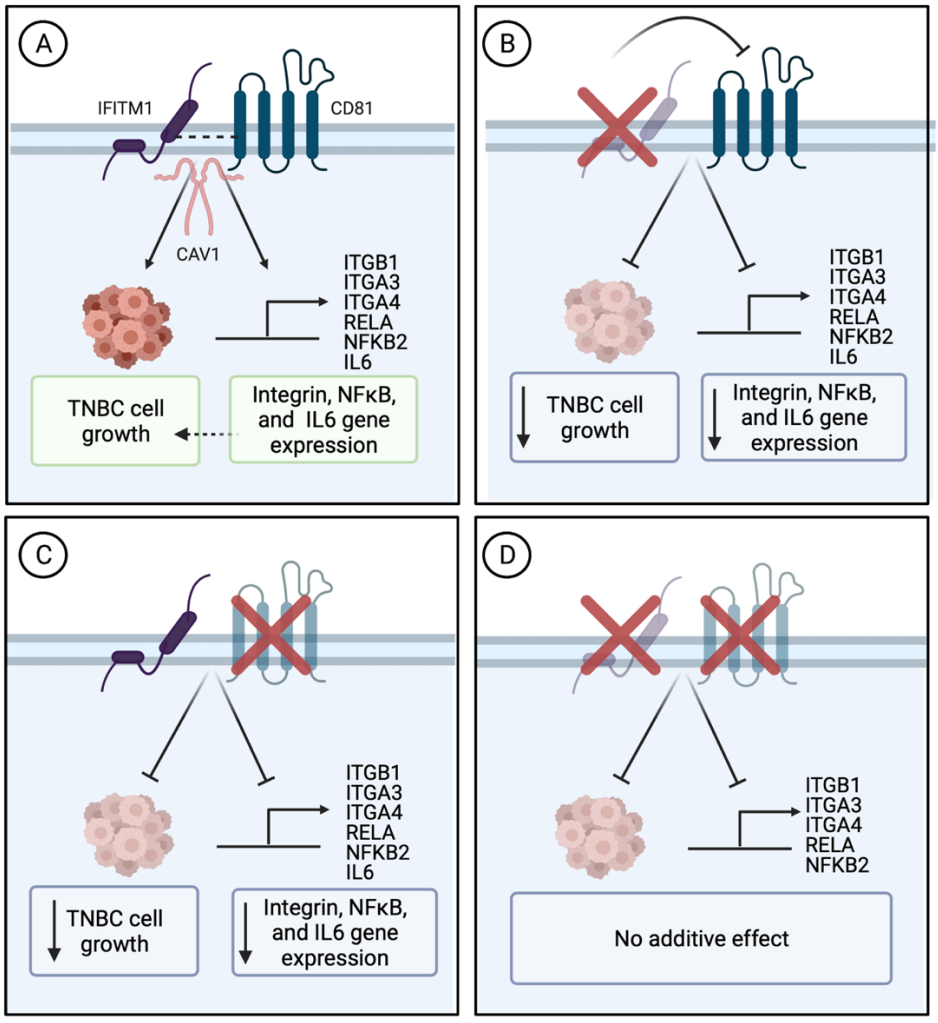

Figure 3.8 Proposed model of IFITM1 and CD81 relationship
A, Generalized model of IFITM1 and CD81 function in TNBC. The presence of IFITM1 and CD81 in SUM149 and MDA-MB-468 cells is important for *in vitro* growth and as observed in SUM149 cells, to regulate the expression of a subset of integrins and IL6, though a direct interaction was not detected (dotted lines to show hypothesized proximity). However, we suspect CAV1 may be important in this interaction though functional analyses were not studied. To generate this model, a series of *in vitro* experiments were performed **(B-D)**. **B,** Loss of IFITM1 reduces CD81 by decreasing CD81 stability and also decreases growth and gene expression of identified genes. This suggests that IFITM1 alone is capable of mediating said responses. **C,** Loss of CD81 does not decrease IFITM1 expression, though growth and gene expression is altered. This suggests that though present, IFITM1 cannot overcome the loss of CD81. **D,** Loss of both CD81 and IFITM1 show no additive effect on downstream targets, with the exception of IL6. Since no additive effect is observed, these data suggest that neither CD81 or IFITM1 is functioning properly without the other. Since IL6 decreases even more dramatically when both CD81 and IFITM1 are gone, this suggests that IL6 can be partially regulated by either CD81 and IFITM1 when individually present. Figure created with BioRender.com.

Discussion

This study is the first to assess the biology and mechanism of IFITM1 in TNBC. Data presented herein show that IFITM1 is resides in the membrane of TNBC cells and co-localizes with CD81. Clinically, CD81 and IFITM1 are positively correlated and high expression of CD81 contributes to poor overall survival in patients with TNBC. Though we did not identify a direct interaction between IFITM1 and CD81, we show that CAV1 may be an important secondary mediator of this relationship. Regarding functional relevance of the IFITM1 and CD81 interaction, our data suggest that IFITM1 may utilize CD81 for cell growth and integrin, NFκB and IL6 gene expression. Another important, but less developed finding, is that IFITM1 and CD81 are secreted into small extracellular vesicles (EV's) in all TNBC cell lines. Overall, these findings suggest that IFITM1 may regulate TNBC growth with help from CD81 and may also play a role in cell-cell communication through EV secretion. Moreover, these findings suggest that IFITM1 does not act alone to mediate TNBC growth and uncovers important biological characteristics that may be harnessed for therapeutic development.

Early reports identified direct interactions between IFITM1 and tetraspanin proteins in a complex comprising CD19, CD21, and CD81 in B-cells (23). These reports also suggest that CD81 and IFITM1 signal through the same pathways which is supported by our work (143). Notably, tetraspanins have gained traction as targets for cancer treatment (146, 147) and in specific, CD81 has been established as a tumor promoter in multiple cancers (25). Though we observed strong co-localization between IFITM1 and CD81 using co-immunofluorescence, we did not observe a direct interaction as assessed by co-immunoprecipitation. Tetraspanins are known for forming both homo- and hetero- dimers, trimers, and tetramers as primary interactions (148). These complexes often come together to form a network of secondary interactions incorporating more non-tetraspanin proteins including integrins and other membrane proteins (148). These secondary interactions are often mediated by protein palmitoylation, a key characteristic of

IFITM1, and implicated in the organization of signaling molecules in the membrane. Though direct interactions are maintained when stringent detergents are used, secondary interactions become disrupted, perhaps providing an experimental reason for the lack of direct interaction detected (148). Supporting the evidence of secondary complex formation including IFITM1 and CD81 is our finding that both IFITM1 and CD81 interact with CAV1 (Supplemental figure 3.2). CD81 is known to interact with cholesterol enriched membrane domains which are enriched in CAV1 (148), though if this is directly related to the function of IFITM1 remains unknown. Therefore, future studies are necessary to determine if IFITM1/CD81 and CAV1 all form a complex and where, as well as when a combination of these interactions are transiently forming. Future studies must also investigate if CAV1 has any functional role in mediating the IFITM1/CD81 relationship in regard to cellular phenotypes, gene expression, or protein localization. Since these studies may be confounded by the likelihood that changes in the specific cell state (i.e: epithelial, mesenchymal, transitioning, etc.) may alter these interactions, it is important to investigate multiple cellular states when assessing these relationships.

CD81 is known to regulate α4β1 and α3β1 integrin-mediated signaling and adhesion to extracellular matrix proteins, resulting in activation of phosphoinositide dependent signaling, AKT signaling, and cytoskeletal rearrangement (101, 142, 149, 150). Regarding IFITM1 and CD81 mediated cancer cell phenotypes there has been only one study that has specifically looked at the role of tetraspanins and IFITM1 in cancer (106). In HNSCC cells loss of IFITM1 does not regulate CD81 levels whereas in our current study, IFITM1 decreases CD81 levels, thus highlighting the context dependent specificity of the relationship. Additionally, in IFITM1 overexpressing HNSCC cells, loss of CD81 significantly inhibited migration thus suggesting that the presence of CD81 mediates the function of IFITM1. Though our study investigated growth, we found similar results. We further contribute to the field through identifying that IFITM utilizes CD81 for regulation of integrins β1, α3, and α4, NFκB transcripts of RELA and NFKB2 and the cytokine IL6. Though our data suggests IFITM1 may need CD81 to mediate cell growth likely

through integrin dependence, future studies investigating how cells respond to forced attachment on different matrices such as fibronectin and laminin with IFITM1 and integrin inhibition are necessary. Moreover, loss of IFITM1 significantly reduces the migratory properties of TNBC cells and loss of CD81 has been shown to reduce lamellipodia formation (150). Therefore, it is possible that IFITM1 may also work with CD81 for integrin mediated migration in TNBC. Lastly, though we identified NFκB gene transcripts to be regulated by the IFITM1/CD81 relationship, it remains unknown if this NFκB signaling is responsible for altering the observed transcriptional differences of integrin expression.

Finally, we identified that IFITM1, CD81, and CAV1 are found in TNBC extracellular vesicles (EVs). Like CD81 and CAV1, IFITM1 has been found in EVs in multiple tumor types (exocarta.org), but this study is the first to identify that IFITM1 is secreted in TNBC EV's. This finding alone suggests that IFITM1 may have an extracellular role in mediating TNBC aggression. A limitation of this finding is that the method used to generate this data is a crude isolation of EVs and is not separated into the multiple subclasses of EVs. Nevertheless, EVs have been identified as a potent regulator of metastatic dissemination for priming distant organs for cancer cell colonization (151). Additionally, EVs have emerged as both a biomarker and a drug-carrier in breast cancer (152). Should the presence of IFITM1 or its interactions be specific for TNBC EVs, IFITM1 may serve as a prognostic biomarker for future treatments to enhance patient outcomes. Though the functional extracellular relationship between CAV1, CD81 and IFITM1 has not been studied, this specific finding opens the door to an alternative realm of IFITM1 function.

Findings presented in this chapter are threefold: 1) In TNBC a functional relationship between CD81 and IFITM1 exist in regulation of growth rate and integrin, NFκB, and IL6 gene expression; 2) IFITM1 and CD81 may be interacting through secondary complex formation mediated by CAV1; and 3) IFITM1 may have an extracellular function in TNBC. Lastly, though CD81 is present in cell lines without IFITM1 expression, this suggests that CD81 may also function independently in some cell types.

Materials and Methods

Cellular fractionation

Cells grown in 10-cm dishes were harvested and subjected to cellular fractionation following the manufacturers protocol (Cell Signaling Technology, #9308) followed by western blot analysis.

Immunofluorescence microscopy

Cells grown on coverslips were washed with PBS and fixed with 100% ice cold methanol for 10 minutes and washed with PBS three times for 10 minutes. After permeabilization by 0.1% Triton-X in PBS for 15 minutes, cells were incubated with either 5% normal horse serum in PBS or 5% BSA in PBS for 1 hour followed by incubation with IFITM1, CD81 or CAV1 antibodies, 2µg/mL in 0.01% Triton X-100/PBS overnight. Cells were stained with fluorescein isothiocyanate (FITC)-conjugated labeled goat anti-rabbit IgG (Fluorescein, FMK2201) or TRIT-C conjugated labeled goat-anti-mouse IgG (Cell Signaling Technologies, #8890S) for 1-hour followed by coverslip mounting with the ProLong® gold anti-fade reagent with DAPI (Life Technologies). Samples were imaged on a Leica TCS SPE confocal microscope in the Confocal Imaging Core at the University of Kansas Medical Center. Images were collected and analyzed using the Leica LAS AF Lite software (Leica Biosystems, Nussloch Germany).

Western blot and co-immunoprecipitation

Western blot protocol is outlined in Chapter 2 Materials and Methods. Here, the CD81 (Santa Cruz Biotechnology: 1:200, #sc-166029, mouse; Cell Signaling Technologies: 1:100, #10037, rabbit) CAV1 (Cell Signaling Technologies: 1:1000, #3238, rabbit) and IFITM1 (Santa Cruz Biotechnology: 1:200, sc-374026, mouse; Cell Signaling Technologies: 1:500, #13126, rabbit) were used.

For co-immunoprecipitation experiments, cell lysates were collected in RIPA buffer (150mM NaCl, 6mM disodium phosphate, 4mM monosodium phosphate, 2mM EDTA pH=8, 1% Triton-X 100,

50mM sodium fluoride) supplemented with supplemented with protease inhibitor cocktail (Roche Diagnostics, Cat#11836–153-001) and phosphatase inhibitor (Sigma, Cat#P0044). Cell lysates containing at least 1000mg/mL concentrations were incubated overnight at 4^{o}C with 20mL of IFITM1 (Santa Cruz Biotechnology: 1:200, sc-374026, mouse) or CD81 (Santa Cruz Biotechnology: 1:200, #sc-166029, mouse) antibodies or 1mL of rabbit IgG per reaction. 30µL of protein A and 30µL Protein G coated magnetic beads (Invitrogen: #10001D) were used per-reaction. Beads were first washed with supplemented RIPA and added in a final volume of 100mL and followed by an incubation time of 2 hours. Immune complexes were washed three times with PBS, resuspended in Laemelli sample buffer containing dithiothreitol and b-mercaptoethanol (Invitrogen, Cat#NP0007), boiled for 5 minutes, and subjected to western blotting. Antibodies used for probing specific proteins were the opposite species.

Clinical Analyses

Overall survival data in regard to CAV1 and CD81 and correlation analysis between CAV1 or CD81 with IFITM1 in TNBC were analyzed using bcGenExMiner (153).

Small interfering RNA (siRNA) transfections:

SUM149 and MDA-MB-468 cells were seeded overnight and transfected at 60-80% confluency with 60-100nM of targeted siRNAs or scrambled RNA (siControl; Santa Cruz Biotechnology: sc-37007) introduced by Lipofectamine 2000^{TM} (Invitrogen: #1668019) in OptiMEM Reduced-Serum Medium (Gibco: #11058-021). After overnight incubation the transfection mixture was replaced with normal culture medium. SUM149 and MDA-MB-468 cells were transfected with pooled siRNA's targeting IFITM1 (Santa Cruz Biotechnology: sc-44549) or CD81 (Santa Cruz Biotechnology: sc-05030) followed by western blot, qRT-PCR or cell-counting.

qRT-PCR

Protocol described in Chapter 2 was followed. Primer sequences from this chapter are below.

Table 3.1 Primer sequences

Gene	Forward (5'-3')	Reverse (3'-5')
PUM1	TCACCGAGGCCCCTCTGAACCCTA	GGCAGTAATCTCCTTCTGCATCCT
IFITM1	GGATTTCGGCTTGTCCCGAG	CCATGTGGAAGGGAGGGCTC
IL6	CCTCCAGAACAGATTTGAGAGTAGT	GGGTCAGGGGTGGTTATTGC
ITGA3	AGCAGGTGAACAGGTCCTCA	TACCAGGAATCGGGTATCCA
ITGA4	CCCCATCAGGTCCGCTCTTG	CCCCACTCCCGGTTTCTGCC
ITGB1	GGGTCTGAGCACAAGCTG	CAGTCCACTTCCCCGTGTT
ITGB5	AAAATGGCTGTGGAGGTGAG	GTGCCGTGTAGGAGAAAGGA
CD81	GGGAGTGGAGGGCTGCACCAAGTGC	GATGCCACAGCACAGCACCATGCTC
RELA	AGCTCAAGATCTGCCGAGTG	ACATCAGCTTGCGAAAAGGA
NFKB2	GGCAGACCAGTGTCATTGAGCA	CAGCAGAAAGCTCACCACACTC

Cycloheximide assay

SUM149 and MDA-MB-468 cells were plated at 150,000 cells/well in a 12-well plate. The next day MDA-MB-468 cells were treated with siControl and siIFITM1for 24-hours whereas SUM149 cells were treated with cycloheximide 24-hours after plating. For cycloheximide treatment, cell culture media was replaced including 10mg/mL of cycloheximide for 10 hours. Samples were harvested every 2-hours and processed for western blot analysis.

Extracellular vesicle isolation

SUM149, MDA-MB-157 and MDA-MB-468 cells were grown in 10cm plates for 48 hours before relacing growth media with 10mL serum free media for 24 hours. 30mL conditioned medium was collected and spun down at 3,000g for 10 minutes to remove cellular debris. Supernatant was transferred to fresh tube and balanced with sterile 1x PBS. Samples were spun at 30,000g for 1 hour in a Thermo Scientific WX Ultracentrifuge. Pellet was resuspended in 70μM storage buffer (2M sucrose, 0.5M MOPS pH 6, sterile water, 1 complete minitab phosphatase/protease inhibitor).

Supplemental Data

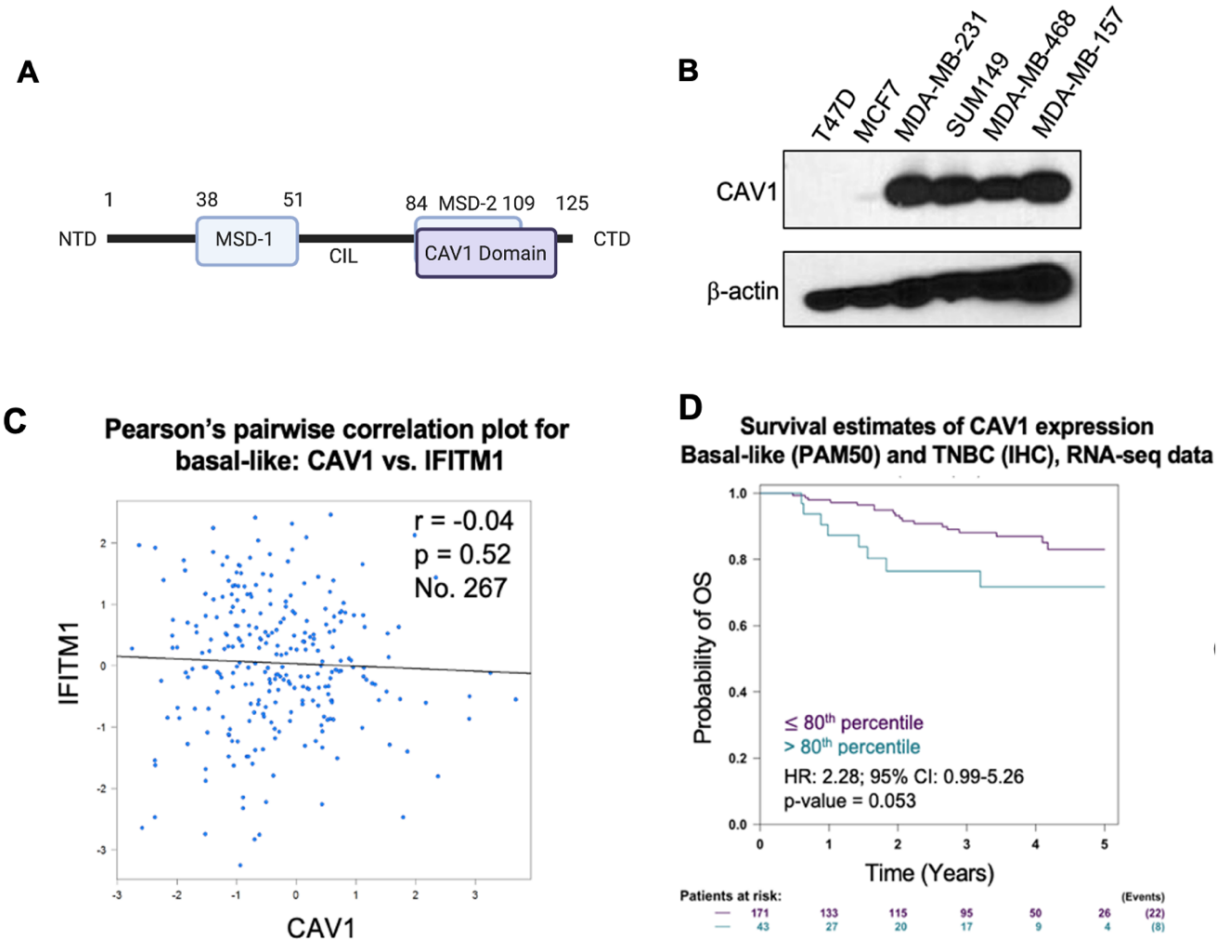

Supplemental Figure 3.1 Relevance of CAV1 in TNBC
A. IFITM1 protein domain representation. B, bcGenExMiner4.0 was used to assess the correlation between CAV1 and IFITM1 DNA expression in basal-like breast cancer C, CAV1 RNA expression on basal-like and TNBC overall survival derived from bcGenExMiner4.0 D, Western blot of CAV1 expression in TNBC and ER+ cell lines.

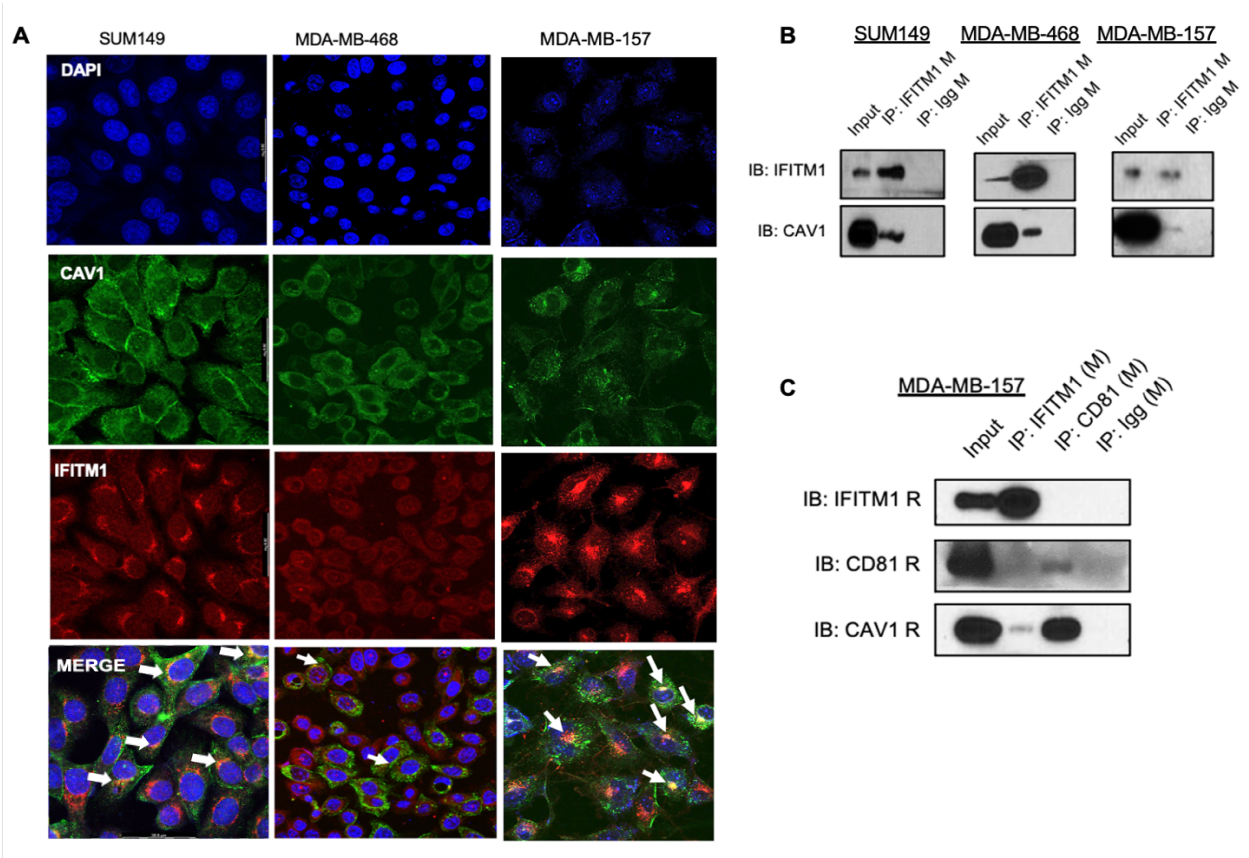

Supplemental Figure 3.2 IFITM1 and CAV1 directly interact

A, Co-immunofluorescence of SUM149, MDA-MB-468 and MDA-MB-157 cell lines with antibodies against CAV1 (green) and IFITM1 (red). **C,** Co-immunoprecipitation of IFITM1 (mouse antibody) or Igg (mouse) in SUM14, MDA-MB-157 and MDA-MB-468 cells and probed for IFITM1 (rabbit) or CAV1 (rabbit). **D,** Co-immunoprecipitation of IFITM1 (mouse), CD81 (mouse), or Igg (mouse) in MDA-MB-157 cells and blotted for IFITM1 (rabbit), CD81 (rabbit), and CAV1 (rabbit).

Chapter 4: IFITM1 is regulated by non-canonical interferon signaling

Parts of this chapter have previously been published as an open access article and are reprinted here alongside never-before published results.

Provance OK, Geanes ES, Lui AJ, Roy A, Holloran SM, Gunewardena S, Hagan CR, Weir S, Lewis-Wambi J: *Disrupting interferon-alpha and NF-kappaB crosstalk suppresses IFITM1 expression attenuating triple negative breast cancer progression.* Cancer Lett. 2021, August 28; 514:12-29. DOI:10.1016/j.canlet.2021.05.006.

Introduction

IFITM1 is an ISG that is regulated by interferon signaling and NFκB activation (37, 154). Our studies and others report that some tumors express elevated levels of IFITM1 compared to normal tissue (106, 109, 118) and that its overexpression correlates with drug resistance (104, 111, 113, 155) and metastasis (106-108). Therefore, elucidating the regulation of IFITM1 in TNBC can provide greater insight into its role in TNBC pathogenesis and possibly pave the way for the development of therapeutics targeting its expression.

IFNs are cytokines that can be released by all cells in the body to inhibit viral infection, through upregulating ISGs as a mechanism of controlling cell death and survival pathways (114). To date, thirteen subtypes of IFNα have been identified. Each member of IFNα lacks distinct introns and is encoded independently with genes located in a 400 kb cluster on chromosome 9q (156). Though IFNα and IFNβ both signal through the interferon alpha receptor-(IFNAR)1 and IFNAR2 complex, they have different binding affinities thus producing distinct anti-viral effects (157), therefore, the biological responses to IFNα and IFNβ are distinct. Though both IFNα and IFNβ are classified as type I IFNs, previous studies suggest a specific role of IFNα in breast cancer biology (55, 70, 104).

Canonically, IFNα activates JAK and TYK for phosphorylation of STAT1 and STAT2 and subsequent formation of the interferon stimulated gene factor-3 (ISGF3) complex consisting of pSTAT1, pSTAT2 and IRF9. Upon formation and nuclear translocation, ISGF3 induces ISG expression through binding to the interferon stimulated response elements (ISRE) in the promoter of ISGs. However, under chronic exposure to IFNα, the ISGF3 complex loses phosphorylation (U-ISGF3) but remains transcriptionally active, transcribing a specific subset of ISGs (37) which regulate cellular events including; apoptosis, senescence, migration or drug resistance (53). Additionally, IFN can also activate NFκB in a dose-dependent mechanism, and doing so, protects cells against apoptosis (63-65). Previous studies suggest crosstalk between IFNα and NFκB such

that the kinetics of IFN signaling and subsequent gene expression depend on concurrent NFκB activation, and vice versa, such that NFκB can regulate the IFN amplification loop (158). Supporting this evidence, multiple ISGs have NFκB binding sites within their promoter, but which ISGs are regulated by both IFNα and NFκB is highly context dependent (63, 66).

In this chapter, through *in vitro* analyses, we provide evidence such that both IFNα/NFκB signaling in mediate IFITM1 expression. Therefore, targeting this crosstalk might be beneficial in a subset of TNBC patients.

Results

IFNα regulates IFITM1 expression through IFNAR

Because previous studies allude to the importance of IFNα in breast cancer and since IFNα regulates IFITM1 under viral stimulated conditions, we validated that IFNα regulates IFITM1 expression in TNBC cell lines. Using SUM149 cells as a model, we assessed multiple doses of IFNα on IFITM1 expression and identified a linear relationship of amount of IFNα to induction of IFITM1 (Figure 4.1 A). We then assessed the functional integrity of the interferon signaling pathway by treating SUM149, MDA-MB-468 and MDA-MB-157 cells with 30 picomolar (500U/mL) exogenous IFNα. IFNα treatment significantly induces IFITM1 expression in SUM149, MDA-MB-468, and MDA-MB-157 (Figure 4.1 B). These data suggest that though IFITM1 is overexpressed in these TNBC cell lines, the cells are still able to respond to IFNα.

The source of IFNα can be derived from the tumor microenvironment or from the tumor cells themselves. To determine if endogenous IFNα is responsible for regulating IFITM1 expression, we first assessed the relative IFNα levels in TNBC cell lines compared to ER+ breast cancer. Here, we focused on the specific IFNα-2a gene since it has been identified to be a potential risk factor associated with female breast cancer (159). Through qRT-PCR analysis we identified variable levels of IFNα-2a among TNBC cell lines with SUM149 having the highest mRNA levels (Figure 4.1 C). To assess the functional role of IFNα on regulating IFITM1

expression siRNA against IFNα-a2 was used. Knocking down IFNα transiently reduced IFITM1 gene and protein expression in SUM149 cells (Figure 4.1 D,E). However, a caveat to this method is that siRNA induces IFITM1 protein expression significantly as compared to the basal levels through activation of a viral response. To further assess autocrine IFN signaling, an IFNAR neutralizing antibody (IFNAR nAb) was used. We confirmed that the neutralizing antibody is specific to the IFN receptor since treatment with the antibody significantly reduces IFNα induction of IFITM1 expression (Figure 4.1 F). We identified that though the levels of IFNα are not as high for MDA-MB-157 and MDA-MB-468 cells, autocrine IFN signaling is important for IFITM1 expression. Neutralizing the IFNAR receptor significantly abrogates IFITM1 expression in all TNBC cell lines (Figure 4.1 G). Collectively, these data suggest that TNBC cells have in-tact IFN signaling and may be regulating IFITM1 expression through continuous production of low levels of IFN signaling through the IFNAR complex.

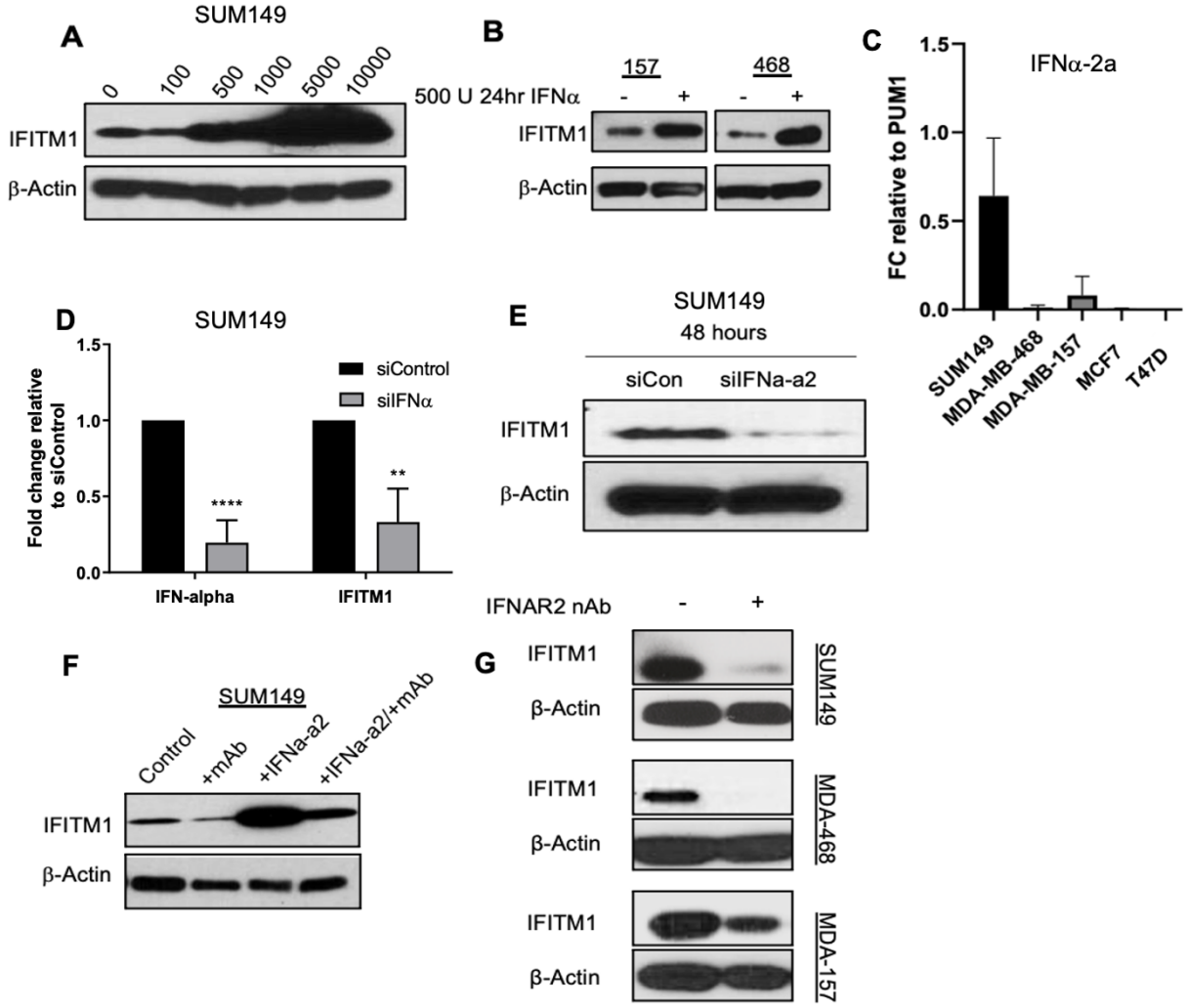

Figure 4.1 IFNα regulates IFITM1 expression through INFAR
A. SUM149 cells were treated with increasing doses of IFNα and run on a western blot 24 hours later. **B.** Western blot of IFITM1 in MDA-MB-157 and MDA-MB-468 after 24 hour treatment with 500 units/mL of IFNα. **C.** qRT-PCR of relative IFNα-2a levels in TNBC and ER+ cell lines. **D.** qRT-PCR of IFITM1 and IFNα in SUM149 cells levels after siRNA targeting of IFNα for 48 hours. Data represent means of three independent experiments ± standard deviation. **E.** Western blot of SUM149 cells after 48 hours of treatment with siIFNα. **F.** Western blot of IFITM1 in SUM149 cells treated with 5μg/mL IFNAR neutralizing antibody IFNAR nAb), 500 units/mL IFNα-a2, or both for 24 hours. **H.** Western blot of IFITM1 in SUM149, MDA-MB-468, and MDA-MB-157 cell lines treated with 5μg/mL IFNAR2 neutralizing antibody for 24 hours.

IFNα does not affect SUM149 phenotype in vitro

SUM149 has the highest levels of IFN gene expression and secreted levels. Since IFNα regulates IFITM1 expression we hypothesized that inhibition of IFNα directly will significantly abrogate SUM149 growth and migration. siRNA mediated inhibition of IFNα through siRNA decreased growth of SUM149 cells at 48-hours (Figure 4.2 A) but did not affect migration (data not shown). We observed that cyclin-e decreases slightly upon siRNA targeting of IFNα (Figure 4.2 B). To assess how endogenous IFNα signaling mediates SUM149 phenotype an IFNAR2 neutralizing antibody was used. Use of the IFNAR neutralizing antibody had no significant effect on cell growth but significantly decreased migration at 48-hours (Figure 4.2 C-D). Since IFNα has been identified to promote cell death, we assessed how the cells respond to exogenous IFNα. Treatment with IFNα did not have a prominent effect on cell growth at 48-hours, nor did treatment alter cell cycle protein expression (Figure 4.2 E-F). Overall, these data suggest that IFN, specifically IFNα-2a, does not have a strong impact on the phenotype of SUM149 cells *in vitro* in short term treatments.

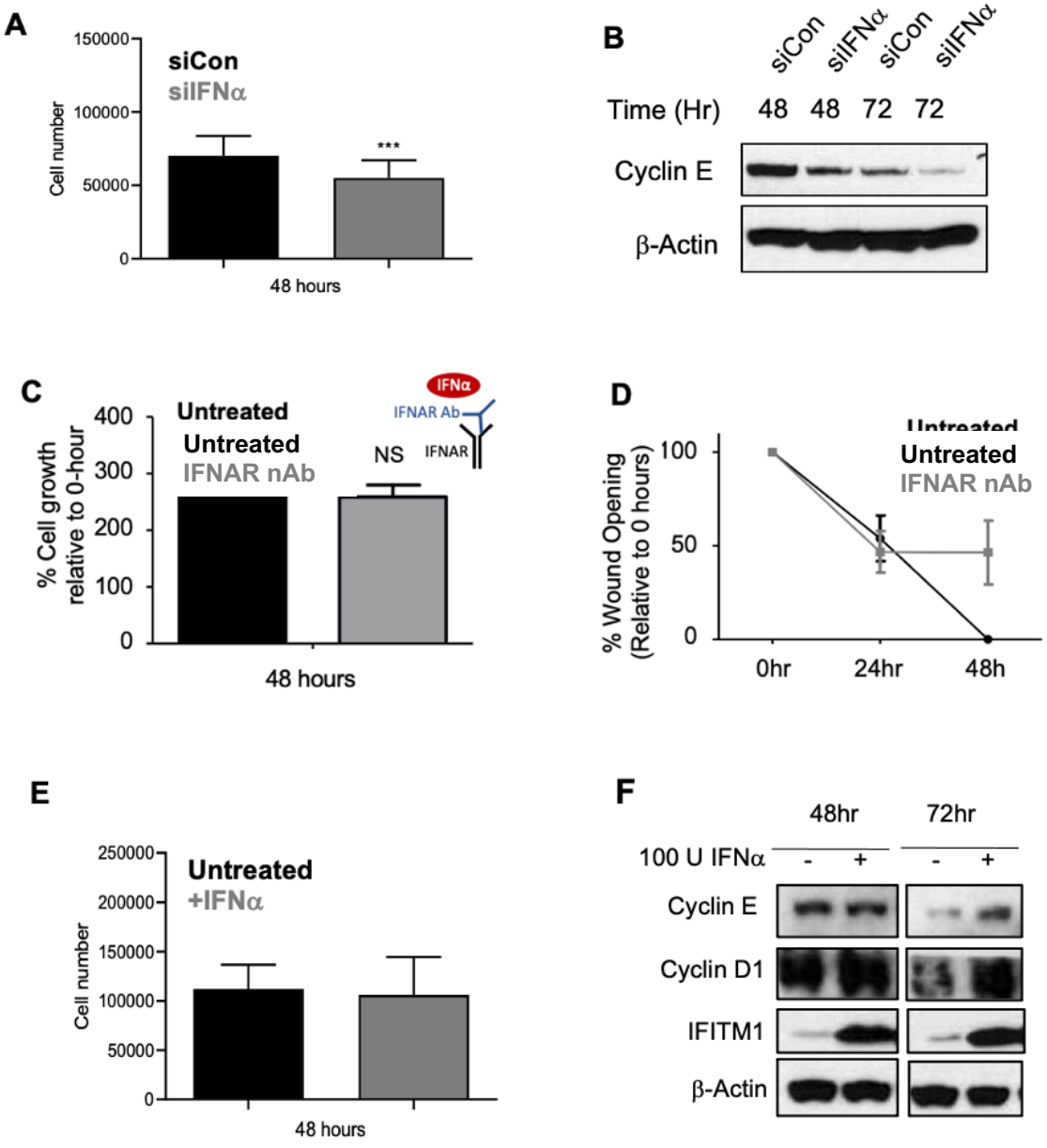

Figure 4.2 The effect of IFNα on SUM149 growth and migration
A. Number of SUM149 cells after 48 hour treatment **B.** Western blot of cyclin-e expression in SUM149 cells after 48 and 72 hour treatment with siIFNA. **C**. Number SUM149 cells after 48 hours and quantification of wound healing (**D**) when treated with 5mg/mL IFNAR2 neutralizing antibody. **E.** Number of SUM149 cells after 48 hour treatment with 500units/mL of IFNα. **F.** Western blot of cyclin e, cyclin D1, and IFITM1 expression after 24, 48, or 72 hour treatment with 500 units/mL IFNα.

STAT2 and IRF9 are critical regulators of IFITM1 expression in TNBC cell lines

IFNα can continually regulate gene expression at very low levels or though kinase independent functions of JAK proteins (66). When this occurs, STAT proteins generally lose their phosphorylation and regulate a specific subset of genes through a non-canonical mechanism. Since SUM149, MDA-MB-468 and MDA-MB-157 cell lines have variable IFNα expression but overexpress IFITM1 which is regulated by autocrine IFN signaling, we hypothesized that these cell lines would regulate IFITM1 through a non-canonical pathway. First, we assessed the basal activity of pSTAT1 and pSTAT2 western blot analysis and confirmed that these cells have undetectable or very low levels of pSTAT2 but with some pSTAT1 observed in SUM149 cells (Figure 4.3 A). Unphosphorylated STAT1 and unphosphorylated STAT2 can form a complex with IRF9 for an unphosphorylated-ISGF3 complex or STAT2 and IRF9 can form a transcriptionally active complex without STAT1. To assess which complex is forming we utilized co-immunoprecipitation and proximity ligation assays. First, we identified that in SUM149 cells, pull down for STAT1 did not bring down STAT2. Further supporting this evidence, IRF9 was immunoprecipitated from all TNBC cell lines on basal levels and upon exogenous addition of IFNα then probed for STAT2 and STAT1 via western blot. Here, we show that STAT2 and IRF9 have direct interaction both on the basal level and in the presence of exogenous IFNα addition without STAT1 (Figure 4.3 C). Moreover, a proximity ligation assay in SUM149 cells suggests that the STAT2:IRF9 complex is occurring both in the cytoplasm and in the nucleus (Figure 4.3 D).

To evaluate the role of specific ISGF3 proteins we used siRNA against STAT1, STAT2 or IRF9 in all three TNBC cell lines. Knockdown of STAT1 does not have a prominent effect on IFITM1 expression, loss of STAT2 results in marked reduction of IFITM1 expression in both SUM149 and 468 where STAT2 did not have as much of an effect in MDA-MB-157, and loss of IRF9 significantly abrogates IFITM1 expression in all cell lines assessed (Figure 4.3 E). Collectively, these data suggest that IFITM1 expression is in part, regulated through non-canonical IFNα signaling specifically through STAT2 and IRF9 interactions.

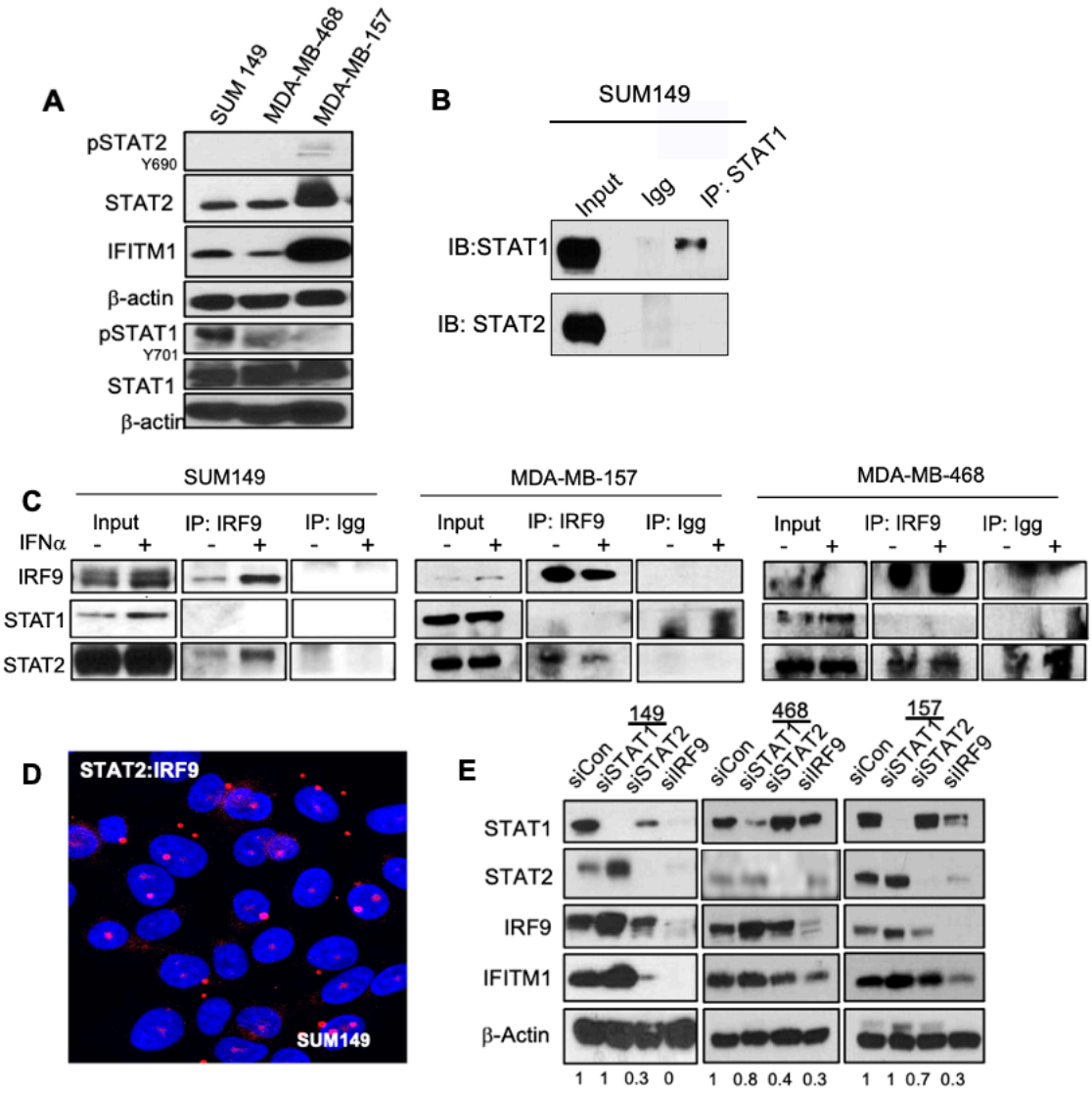

Figure 4.3 STAT2 and IRF9 are essential for IFITM1 expression
A, Immunoblotting was used to assess pSTAT2 and pSTAT1 expression in all TNBC cell lines **B,** Co-immunoprecipitation of STAT2 with STAT1 under untreated conditions. **C,** Co-immunoprecipitation of STAT1 and STAT2 with IRF9 in SUM149 cells treated without or with 500 units/mL IFNα-2a for 2 hours. Data are representative images from at least two independent experiments. **D,** Proximity ligation of STAT2 and IRF9 in SUM149 cells under untreated conditions after 48 hours of cell attachment to slide. **E,** Immunoblotting was used to assess IFITM1 in multiple TNBC cell lines 48 hours after transfection with either siControl, siSTAT1, siSTAT2, or siIRF9. Quantification of IFITM1 values are listed below

Alternative regulation of IFITM1 by AKT and STAT3

PI3K/AKT activation by IFNAR has been shown to occur in the absence of TYK2 activation and subsequent STAT activation (160). Moreover, AKT is essential for regulation of a handful of IFNα stimulated genes. Therefore, we first assessed the involvement of AKT signaling as a potential STAT2/IRF9 independent regulatory mechanism. We identified that treatment with the LY294002 inhibitor significantly inhibits IFITM1 expression in SUM149 cells (Supplemental Fig. 4.1). However, MDA-MB-157 cells do not have pAKT on a basal level (data not shown). Therefore this finding cannot be extrapolated to multiple IFITM1 expressing TNBC cell lines. Next, we assessed if loss of STAT3 which is a key mediator of IFNα and PI3K signaling has an effect on IFITM1 protein expression. We found that siRNA inhibition of STAT3 does not have a prominent effect on IFITM1 expression in any cell line (Supplemental Figure 4.1). These data suggest that targeting pAKT through use of LY294002 can inhibit IFITM1 expression in some cell lines.

NFκB regulates IFITM1 expression

Recently, a selective JAK1/2 inhibitor called Ruxolitinib has been used in clinical trials for metastatic TNBC (161). However, as a single agent, this drug did not meet the primary efficacy endpoints of a partial or complete response though the output of pSTAT3 was reduced by about 45-55%. We next tested the effect of Ruxolitinib in TNBC (Supplemental Figure 4.1 C). Though we identify some inhibition of IFITM1 through ruxolitinib, our finding suggests that other pathways are contributing to the regulation of IFITM1 expression other than active JAK1/2 signaling.

Previous studies suggest signal-induced phosphorylation is non-essential for IRF9 interaction with STAT2 and that JAK1/2 inhibition does not change STAT2/IRF9 nuclear levels (66). Moreover, in support of crosstalk with other signaling pathways, STAT2 and IRF9 have been shown to form a complex with p65 to enhance IL-6 expression in the absence of STAT1 (82) and IFNα can both directly and indirectly signal through NFκB (63). Additionally, some ISGs have NFκB elements in their promoter. By utilizing a luciferase assay with IFITM1 promoter deletion

mutants, we found that loss of the NFκB region significantly impairs IFITM1 promoter activity thus, NFkB may also play a role in regulating IFITM1 expression (13). Therefore, we assessed if p65 mediates IFITM1 expression in TNBC.

To gain a better insight into whether NFκB regulates IFITM1 expression in TNBC cells we utilized siRNA to decrease p65 expression. Reduction of p65 levels in all three TNBC cell lines significantly inhibits IFITM1 protein (Figure 4.4 A) and mRNA expression (Figure 4.4 B). Since IFNα regulates IFITM1 expression (70) and can regulate NFκB activation (63, 65) we assessed whether autocrine IFNα signaling through the IFNAR receptor impacts NFκB activation. TNBC cells were treated with 5μg/mL of IFNAR neutralizing antibody for 24 hours resulting in a reduction of IFITM1 in all three cell lines (Figure 4.4 C) and a trend of decreased phosphorylation of p65 (Figure 4.4 C). Moreover, exogenous IFNα treatment significantly induces NFκB promoter activity through use of an NRE luciferase (Figure 4.4 D).

Interestingly, we identified that treatment of TNBC cell lines with ruxolitinib, significantly enhances NFκB promoter activity as measured by an NRE luciferase (Figure 4.4 E). These findings are twofold. First, these suggest that the NFκB pathway directly regulates IFITM1 expression. And second, they suggest that there is crosstalk occurring between NFκB and IFNα signaling. Perhaps IFNα regulates NFκB directly through exogenous addition and autocrine signaling, but also indirectly in an attempt to counteract JAK1/2 inhibition through overactivation of TYK2, which is not inhibited by Ruxolitinib (78). Though JAK1/2 inhibition and use of the neutralizing antibody both inhibit IFN signaling, perhaps the specific mechanism of inhibition is important for mediating the effects of IFNα on NFκB.

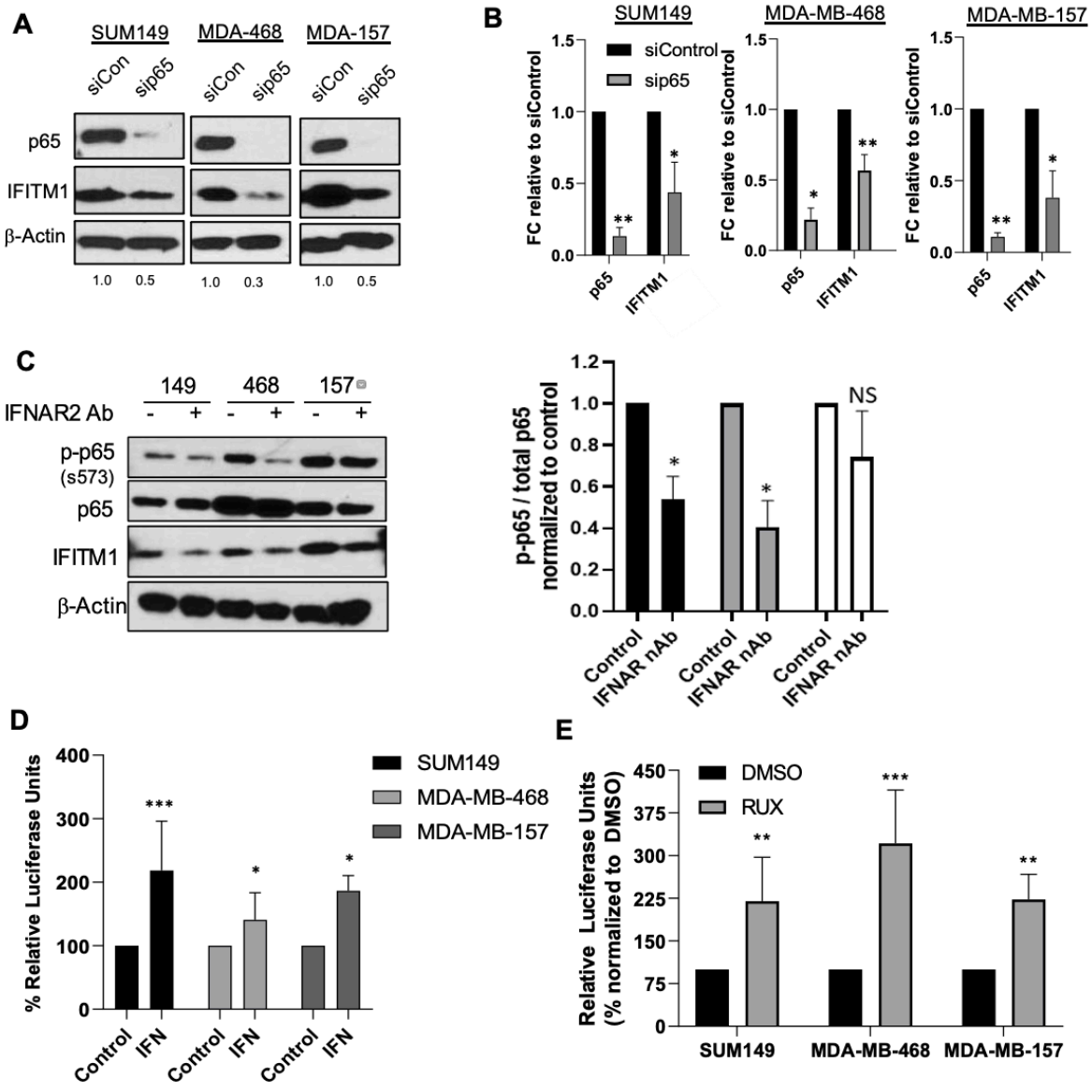

Figure 4.4 IFITM1 is regulated by NFκB signaling in TNBC

A, Immunoblotting assessed IFITM1 in multiple TNBC cell lines 48 hours after transfection with either siControl or sip65. Quantification of IFITM1 values are listed below. **B,** qRT-PCR assessed the gene expression of p65 and IFITM1 after transfection with either siControl or sip65. Data represented as fold change compared to siCon via $2^{\Delta DDCT}$ method. Values represent means ± SD of three independent experiments. Fold change relative to PUM1 was assessed with a t-test *p<0.05, **p<0.01, ***p<0.001. **C,** SUM149(149), MDA-MB-468 (468), and MDA-MB-157 (157) cells were treated with 5mM IFNAR2 neutralizing antibody for 24 hours and immunoblotted for p-p65 and IFITM1. Quantification of IFITM1 values are listed below and the ratio of p-p65/p65 is listed to the right. Values represent means ± SD of three independent experiments. A t-test was used to assess significance *p<0.05. **D,** TNBC cells were treated with 500U IFNa-2a for 24 hours and NRE luciferase activity was measured. E. TNBC cells were transfected with the NRE luciferase vector followed by 24 hour treatment with 10mM ruxolitinib. For **D** and **E**, Values represent means ± SD of at least three independent experiments. Significance was assessed with a t-test on raw values *p<0.05, **p<0.01, ***p<0.001

Discussion

Though treatment for triple-negative breast cancer (TNBC) has improved over the last decade there is still an essential need for development of therapies. To identify novel agents for the treatment of TNBC, it is critical to uncover molecular mechanisms and signaling pathways promoting the aggressive phenotype. We have previously identified that the interferon stimulated gene (ISG), interferon-induced transmembrane protein-1 (IFITM1) is overexpressed in a subset of TNBC patient samples and cell lines, and contributes to increased growth, migration, invasion, and relapse free survival (Chapter 1 and (70)). However, its mechanism of regulation has not been well defined in TNBC. Through promoter sequence analysis, we have identified multiple transcription factor binding sites in the IFITM1 promoter including GAS and ISRE, NFκB, SP1, CREB, and AP1 elements. Therefore, we took the approach of investigating which specific signaling pathways regulate IFITM1 expression to understand how to target its expression and subsequent aggressive phenotypes. Here, we show that IFITM1 is regulated by components of both IFNα and NFκB signaling as observed through blockade of the IFNAR receptor and siRNA against p65 (Fig. 5). Collectively, our data suggest that IFITM1 expression is in part, mediated by NFκB and IFNα crosstalk.

Beginning our study we first wanted to determine how TNBC cells utilize IFNα to regulate cell growth and migration since IFNα is a key regulator of IFITM1. siRNA mediated decrease of IFNα resulted in a decrease of cell proliferation after 48-hours but had no prominent effect on wound healing while the use of the IFNAR neutralizing antibody did not reduce growth but mediated cell migration. Notably, addition of IFN is known to be cytotoxic to multiple cell types including renal cell carcinoma (162), but here we show that addition of exogenous IFNα did not alter growth or cyclin expression in short term studies. Though we identified an intact IFN response in all TNBC cell lines, it is important for future studies to assess long-term depletion and treatment with IFNα to fully understand the role of IFNα signaling in regulating TNBC phenotypes.

Perhaps the inconsistencies in IFNα mediated cellular growth and migration arise from the short-term nature of the experiments or pleiotropic effects of IFNα itself. For example, siRNA was directed against IFNα-2a which is just one of the 13 family members of IFNα (46). IFN signaling has strong positive feedback mechanisms to ensure that upon inhibition of one gene, the viral response can still occur (114). Therefore, though IFNα-2a is inhibited, perhaps other IFNα family members and IFNβ are induced in the process. Moreover, though IFITM1 is suppressed in both experimental methods (siRNA and IFNAR neutralization), we suspect other significant differences in terms of pro-survival and apoptotic ISG expression are occurring thus outweighing the effect of IFITM1 alone. Along these lines, crosstalk between IFNα and other pathways including NFκB, integrin signaling, and p53 has been detected thus regulating cellular response to IFNs and subsequent ISG, cytokine and chemokine expression (114). Additionally, cytokines very rarely act in isolation and the cancer cell is not the only player. Therefore, it is essential to test the involvement of IFNα is through studying the tumor microenvironment. I hypothesize that IFNα is important for tumor growth in the context of its interaction with the immune cells within the microenvironment.

Supporting crosstalk between IFNα and other signaling pathways, our data suggests JAK/STAT involvement in driving IFITM1 expression in TNBC, but evidence presented herein also suggest an alternative mechanism involving IFNα and NFκB crosstalk. We show that inhibition of autocrine IFNα signaling and loss of STAT2 and IRF9 reduces IFITM1 expression; however, loss of p65 reduces IFITM1 expression as well. Previous studies highlight IFITM1 as a non-canonical ISG since it can be regulated independently of the phosphorylated-ISGF3 complex in which our data supports through identification of essential roles for STAT2 and IRF9 (163). STAT2 and IRF9 have a unique relationship. STAT2 is unlike other STAT as it does not recognize a DNA target site as a homodimer but instead provides the transcriptional activation domain essential for induction of target gene transcription (164). Additionally, IRF9 does not have independent transcriptional activity (61, 62). Since we observed the most robust decrease in

IFITM1 expression upon IRF9 inhibition, perhaps IRF9 is also interacting with another co-activator other than STAT2. Furthermore, as previously mentioned in our introduction, in the absence of STAT1, a certain threshold amount of STAT2 and IRF9 must be reached to allow STAT1 independent transcription (61). This is of functional relevance because in the case of prolonged IFNα signaling, STAT2/IRF9 alone could be promoting transcription of pro-tumorigenic ISGs in the absence of phosphorylation and STAT1 and perhaps, in the absence of JAK1/2 activation. This idea has been investigated in previous studies. Phosphorylation is non-essential for IRF9 interaction with STAT2 and JAK1/2 inhibition does not change STAT2/IRF9 nuclear levels (66).

Interestingly, STAT proteins in their unphosphorylated form and the NFκB signaling molecule, p65, have a coordinated effort in driving ISG expression and NFκB can regulate IFITM1 expression (37, 154). This is evidenced by p65 being required for ISG induction in the absence of pSTATs and p65 dependence on unphosphorylated-STAT2 (U-STAT2) for nuclear translocation (165, 166). Notably, the TNBC cells used in this study have very low levels of pSTAT2 on basal level and we have previously shown that the deletion of the region containing the NFκB element in the IFITM1 promoter significantly diminishes promoter activity (70). Perhaps this could be attributed to the recently discovered phenomenon that U-STAT2 can bridge DNA bound p65 and IRF9 to induce full transriptional activation of specific genes (166) since p65 can directly bind to the promoter of IFITM1 (154). Moreover, Pfeffer's group found that in JAK1-deficient cells IFN induces NFκB activation and NFκB dependent gene transcription through TYK2 activaion, but in this model, IFN does not enhance genes only dependent on STATs for transcription (78). This alone provides an explaination into why ruxolitinib may enhance NFκB promoter activity and have poor regulation of IFITM1 expression. Alternatively, the crosstalk between NFκB and IFNα may hinge on IKKα. IKKα is a regulator of NFκB signaling that can induce IRF7 driven IFN activation and subsequent NFκB signaling independent of IκB disassociation resulting in a positive IFN feedback loop (63). Alternative pathways of ISG induction have likely evolved to control infection upon inhibition of canonical JAK/STAT signaling

to minimize the risk of aberrant signaling and infection; however, our evidence suggests that alternative IFN signaling play a role in cancer progression through crosstalk with NFκB and subsequent induction of IFITM1. A limitation of our study is the focus on independent effects of p65 and STAT2:IRF9. Future studies would benefit from investigating the specific interactions between these proteins and how DNA binding is mediated. Moreover, NFκB can signal in a non-canonical fashion similar to IFNα, which could also have a distinct role in mediating IFNα responses. Lastly, potential IFN independent mechanisms driving IFITM1 expression should be investigated, and understanding these processes will help target its expression.

Collectively, we identify that IFITM1 is mediated by components of IFNα and NFκB signaling in TNBC. Both IFNα and NFκB are inflammatory components of the tumor. Perhaps, targeting these inflammatory components simultaneously would be beneficial rather than direct targeting of malignant cell its self which is quick to mutate and acquire resistance. Moreover, IFNα and NFκB are both critical promoters of inflammation linked to chemoresistance so targeting this circuit with could be a promising mechanism of action. However, determining how to best modulate type I IFN response both in isolation and through interrupting other pathways will likely need to be explained based on subtype. Therefore, defining how IFNα is involved in alternative signaling pathways may be harnessed for therapeutic purposes with IFITM1 as a biomarker for this response.

Materials and Methods

Interferon alpha receptor neutralization

SUM149, MDA-MB-468 and MDA-MB-157 cells were pretreated with 5μg/mL anti IFNAR2/MMHAR2 (Millipore: #MAB1155) for either 4 hours followed by overnight treatment with human recombinant IFNα (Sigma: #SRP4595) for 24-hours where indicated. Cells were

harvested by cell scraping for western blot or subjected to phenotypic assays as previously discussed in Chapter 2.

Luciferase assays

For NFκB promoter assay, 0.8 μg of plasmid DNA pGL4.32 NFkB-RE vector (Promega) containing 5x NFkB-RE was co-transfected with the pRL CMV Renilla vector. The NFkB plasmid was a kind gift from Dr. Christy Hagan (University of Kansas Medical Center). After 24 hours, transfection reagent was replaced with normal cell culture media containing 500U/mL IFNa or 10mM of the JAK inhibitor, ruxolitinib, where indicated. Luciferase and Renilla activities were measured 24 hours later using the Dual-Luciferase® reporter assay kit (Promega: E1910) according to the manufacturer's instructions on a BioTek Synergy 4 microplate reader using the Gen 5 data analysis software.

Small interfering RNA (siRNA) transfections

SUM149, MDA-MB-468 and MDA-MB-157 cells were seeded overnight and transfected at 60-80% confluency with 60-100nM of targeted siRNAs or scrambled RNA (siControl Santa Cruz Biotechnology: sc-37007) introduced by Lipofectamine 2000™ (Invitrogen: #1668019) in OptiMEM Reduced-Serum Medium (Gibco: #11058-021). After overnight incubation the transfection mixture was replaced with normal culture medium. MDA-MB-468, MDA-MB-157 and SUM149 cells were transfected with pooled siRNA's targeting STAT1 (Santa Cruz Biotechnology: sc-44123), STAT2 (Santa Cruz Biotechnology: sc-29492), IRF9 (Santa Cruz Biotechnology: sc-38013), p65 (Santa Cruz Biotechnology: sc-29410) or IFN-α2 (Santa Cruz Biotechnology: sc-63324) and harvested 48 hours post transfection for western blot analysis or subjected to phenotypic *in vitro* assays as outlined in Chapter 2 when stated.

Western blotting, fractionation and co-immunoprecipitation

Western blot protocol was followed as previously stated (Chapter 2). Here, target proteins were detected using anti-IFITM1 (1:200, SantaCruz: sc-374026), anti-IRF9 (1:200, SantaCruz: sc-365893), anti-STAT2 (1:200, SantaCruz: sc-1668), anti-STAT1 (1:200, SantaCruz: sc-464) or anti-phospho-p65 (1:500, Cell Signaling Technologies: #3033S) and anti p-65 (1:500, Cell Signaling Technologies: #8242). Membranes were stripped and re-probed for β-actin (1:15,000, Cell Signaling Technologies: #3700).

For fractionation, cells were grown in 10-cm dishes for 48 hours followed to cellular fractionation following the manufacturers protocol (Cell Signaling Technology, #9308) and assessed by western blot.

For co-immunoprecipitation experiments, cell lysates were collected in RIPA buffer (150mM NaCl, 6mM disodium phosphate, 4mM monosodium phosphate, 2mM EDTA pH=8, 1% Triton-X 100, 50mM sodium fluoride) supplemented with supplemented with protease inhibitor cocktail (Roche Diagnostics, Cat#11836–153-001) and phosphatase inhibitor (Sigma, Cat#P0044). Cell lysates containing at least 1000mg/mL concentrations were incubated overnight at 4^{o}C with 5μL of anti-rabbit-IRF9 antibody (Cell Signaling Technology: #76684S) or 1mL of rabbit IgG per reaction. Protein A coated magnetic beads (Invitrogen: #10001D) were washed with supplemented RIPA and added in a final volume of 100mL and followed by an incubation time of 2 hours. Immune complexes were washed three times with PBS, resuspended in Laemelli sample buffer containing dithiothreitol and b-mercaptoethanol (Invitrogen, Cat#NP0007), boiled for 5 minutes, and subjected to western blotting.

Proliferation and wound healing assays

Cell proliferation was measured by cell counting. Cells were seeded onto a 24-well plate at a density of 25,000 cells/well. The next day, cells were either transfected, treated, or harvested for the 0-hour timepoint. Cells were counted every 24 hours and the final values were normalized to the 0-hour timepoint or to vehicle.

Wound healing was assessed by seeding cells onto a 24-well plate at a density of 90,000-120,000 cells/well (approximately 80% confluency) and making a single wound by scratching the attached cells using a 10-µl sterile pipette tip. The plates were washed with complete medium to remove cellular debris. Images of the cells were taken immediately after and 24, 48, and 72 hours later using a phase-contrast microscope and wound area was quantified using the Wound Healing Tool in ImageJ.

Proximity Ligation

SUM149 cells grown on coverslips were washed with PBS and fixed with 100% ice cold methanol for 10 minutes and washed with 1X PBS three times for 10 minutes. After permeabilization by 0.1% Triton-X in 1X PBS for 15 minutes cells were incubated Duolink® blocking solution. For the remainder of the processing the Duolink® PLA Fluorescence (Sigma Aldrich, #DUO92001) was used per manufacturer's instructions. Antibodies used were STAT2 R (Cell Signaling Technologies, #D9J7L,) and IRF9 M (1:200, SantaCruz: sc-365893)

qRT-PCR primers

Table 4.1 Primer sequences

Gene	Forward (5'-3')	Reverse (3'-5')
PUM1	TCACCGAGGCCCCTCTGAACCCTA	GGCAGTAATCTCCTTCTGCATCCT
IFITM1	GGATTTCGGCTTGTCCCGAG	CCATGTGGAAGGGAGGGCTC
IFNα	CTTGAAGGACAGACATGACTTTGGA	GGATGGTTTCAGCCTTTTGGA

Supplemental Data

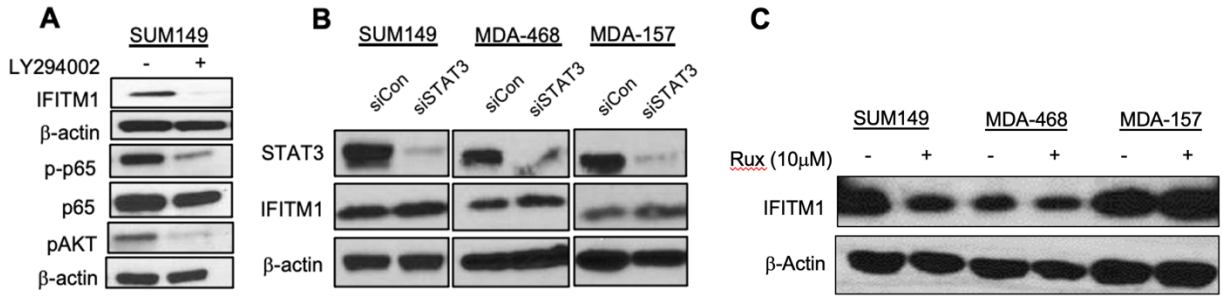

Supplemental Figure 4.1 Effect of AKT, STAT3, and Ruxolitinib on IFITM1 expression
A, SUM149 cells were treated for 24 hours with 30μM of LY294002 or with equal amount of DMSO followed by immunoblotting **B,** SUM149, MDA-MB-468, and MDA-MB-157 cells were co-transfected with siControl or siSTAT3 for 48 hours followed by immunoblotting. Data represents at least two independent experiments and a representative blot is shown. **C,** TNBC cell lines were treated with 10μM ruxolitinib for 24 hours.

Chapter 5: High throughput screen of drug repurposing library identifies inhibitors of IFITM1 positive TNBC.

Parts of this chapter have previously been published as an open access article and are reprinted here alongside never-before published results.

Provance OK, Geanes ES, Lui AJ, Roy A, Holloran SM, Gunewardena S, Hagan CR, Weir S, Lewis-Wambi J: *Disrupting interferon-alpha and NF-kappaB crosstalk suppresses IFITM1 expression attenuating triple negative breast cancer progression.* Cancer Lett. 2021, August 28; 514:12-29. DOI:10.1016/j.canlet.2021.05.006.

Introduction

Patients diagnosed with TNBC have a lower 3-5 year overall survival rate than receptor positive breast tumors and have been reported to have a 12-month median overall survival compared to 20 months for ER/PR positive tumors and 56 months for HER2+ tumors (10, 14, 15). Regardless of treatment, approximately 20-40% of patients with TNBC have tumor recurrence three to five years following diagnosis (167). Perhaps this poor overall survival is due, in part, to the lack of targeted therapy (7, 27, 168). The current standard of care for TNBC patients is treatment with a taxane-anthracycline based systemic chemotherapy (13). However, an interesting phenomenon has emerged from previous clinical studies known as the TNBC paradox. One specific study aimed to assess the potential of pathological complete response (pCR) as a surrogate for long-term outcomes (27). Here, researchers identified that 33% of TNBC patients treated with pre-operative systemic chemotherapy alone achieved a pCR whereas hormone receptor positive tumors had a pCR of 7-16% and HER2+ tumors had a pCR of 18-30%. However, when assessing the correlation between pCR and long-term outcome, researchers found that the TNBC subtype has significantly poorer overall survival in the 70% of patients who fail to achieve a pCR or achieve only a partial response compared to other subtypes. Though more targeted therapies for TNBC are emerging with promising clinical evidence such as BRCA, PI3K/AKT, and immune checkpoint inhibitors, there is still a major unmet need for more efficacious therapies.

In our previous studies we have identified that IFITM1 is an important regulator of TNBC growth, migration, and invasion. Our data also suggest that IFITM1 is regulated by both NFκB and IFN signaling. Therefore, the crosstalk between these two signaling pathways may contribute to poor response to a single pathway inhibitor. For example, in previous studies, the FDA-approved ATP-dependent kinase inhibitor of JAK2, ruxolitinib, has been shown to inhibit interferon signaling and IFITM1 expression (104). However, ruxolitinib often fails to achieve a pathological complete response in these patients (161). Reports reason this occurs through non-canonical

JAK signaling to overcome the effects of JAK2 inhibition (169). Therefore, perhaps by targeting both canonical and non-canonical IFN signaling and subsequent crosstalk would be beneficial in this population.

Identifying new drugs which have the potential to be used outside the scope of the original proposed application through high-throughput drug screening has promising implications for cancer therapeutics (170). This method is known as drug repurposing. Repurposing approved and abandoned drugs allows researchers to capitalize on existing data recorded for these drugs which significantly decreases the cost, time, and risk associated with advancing investigational agents to clinical proof of concept trials (171). The KU Cancer Center has established a formal drug repurposing program. The library of FDA-approved drugs housed at KU is routinely screened for activity against identified drug targets and this program has implemented innovative approaches to advancing repurposed drugs to cancer clinical proof of concept trials. Thus, the cost and time effectiveness of identifying candidate drugs via high throughput drug repurposing screens could expedite the discovery of drugs and agents that are capable of inhibiting both IFITM1 and TNBC.

Through high-throughput screen, we identified TNBC drug repurposing opportunities. One of which, is the drug parthenolide (PN). This study focuses on the identification and characterization of PN which is a sesquiterpene lactone derived from the feverfew plant, historically used as a medicinal Chinese herb to treat migraines, fever, and arthritis (172). In pre-clinical studies of breast cancer, PN has been shown to attenuate tumor progression through increased autophagy, generation of reactive oxygen species, activation of JNK, inhibition of JAK2-STAT3 axis, but mostly through inhibition of NFκB (173-175). Most importantly, PN has tissue protective effects such that it attenuates the negative effect of radiation therapy on neighboring organs (176) and prevents muscular skeletal wasting during chemotherapy in a mouse model of breast cancer (177). Therefore, based on the previously discussed evidence suggesting IFN-alpha and NFκB crosstalk, we hypothesized that if these coordinated efforts drive IFITM1

expression in TNBC cells, then treatment with parthenolide can subdue these signaling processes attenuating IFITM1 expression and subsequent TNBC growth. Through mechanistic analyses, we found that parthenolide is both cytotoxic to TNBC and decreases IFITM1 expression. Additionally, we identified a novel mechanism of parthenolide such that it interrupts type I IFN signaling thus decreasing IFITM1 expression and inducing apoptosis. These data suggest that IFN crosstalk with NFκB and the concurrent regulation of IFITM1 may be a pro-survival mechanism for TNBC, and suggests future investigations into utilizing parthenolide or its derivatives for IFITM1 positive TNBC.

Results

Identification of agents through high-throughput drug repurposing screen

Two TNBC cell lines (SUM149 and MDA-MB-157) and a HER2+ cell line (SUM190) were used for the high-throughput drug screen to identify agents that would be specific to TNBC. The initial screen was performed in all three cell lines with 3,594 drugs from Selleck, Enzo, NIH and Prestwick all of which are either FDA approved or abandoned (Figure 5.1 A). Each cell line was treated with 2.5mM of the drug for 72 hours followed by viability analysis via cell titer glo to assess the percent cytotoxicity. From this screen, we identified 20 drugs that were specific to TNBC, 10 that were specific to SUM149, and 4 that were specific to MDA-MB-157 (Fig. 5.1 B). Of the 20 that were specific to both TNBC cell lines, most were microtubule destabilizers or topoisomerase inhibitors, which are currently used as the standard of care for TNBC patients. Others have been previously investigated in clinical trials including dasatinib and ponatinib. However, through assessing both SUM149 and MDA-MB-157 specific drugs one specifically piqued our interest, parthenolide, as it is known to inhibit NFκB signaling. Therefore, parthenolide (PN) was used for further *in vitro* analysis via a secondary screen with multiple TNBC cell lines

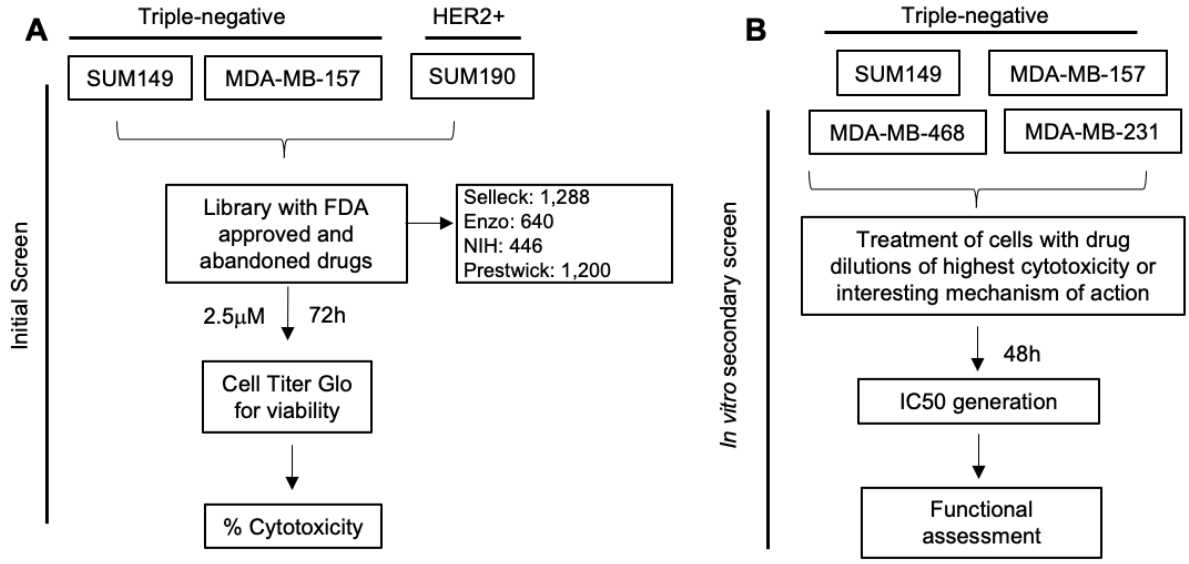

Figure 5.1 Drug repurposing workflow
A: Drug repurposing workflow for initial screen. Three cell lines SUM149 (TNBC), MDA-MB-157 (TNBC), and SUM190 (HER2+) were used. Screen was performed in the High Throughput Screening lab at University of Kansas in Lawrence. Cells were treated once with 2.5μM of each drug/compound for 72 hours followed by Cell Titer Glo for assessment of viability. **B.** Table of results from the initial screen divided by TNBC specific, SUM149 specific, and MDA-MB-157 specific drugs. **C.** Workflow of *in vitro* secondary screen for TNBC cell line IC50.

Parthenolide inhibits TNBC growth and migration and induces apoptosis

Our initial screen identified parthenolide, a naturally derived NFκB inhibitor, as a potent growth inhibitor in SUM149 cells. We then confirmed activity by generating concentration-response curves of parthenolide in four TNBC breast cancer cell lines (SUM149, MDA-MB-468, MDA-MB-157 and MDA-MB-231). As results are depicted in Figure 5.2 A and Supplemental Figure 5.1, SUM149 has the lowest IC50 (4.1mM) followed by MDA-MB-468 (4.5μM), and MDA-MB-157 (6.8μM), while MDA-MB-231 cells, which lack IFITM1, have the highest IC50 (15.8μM).

Next, SUM149, MDA-MB-468, and MDA-MB-157 cell lines were treated with parthenolide at the IC50 and assessed for cellular clonogenicity, proliferation, wound healing, and apoptosis. We found that parthenolide significantly inhibits TNBC colony formation (Figure 5.2 B Supplemental Figure 5.1), proliferation (Figure 5.2 C), and wound healing (Figure 5.2 D). Lastly, parthenolide induces PARP cleavage and increased TUNEL staining which are important markers of apoptosis (Figure 5.2 E-G).

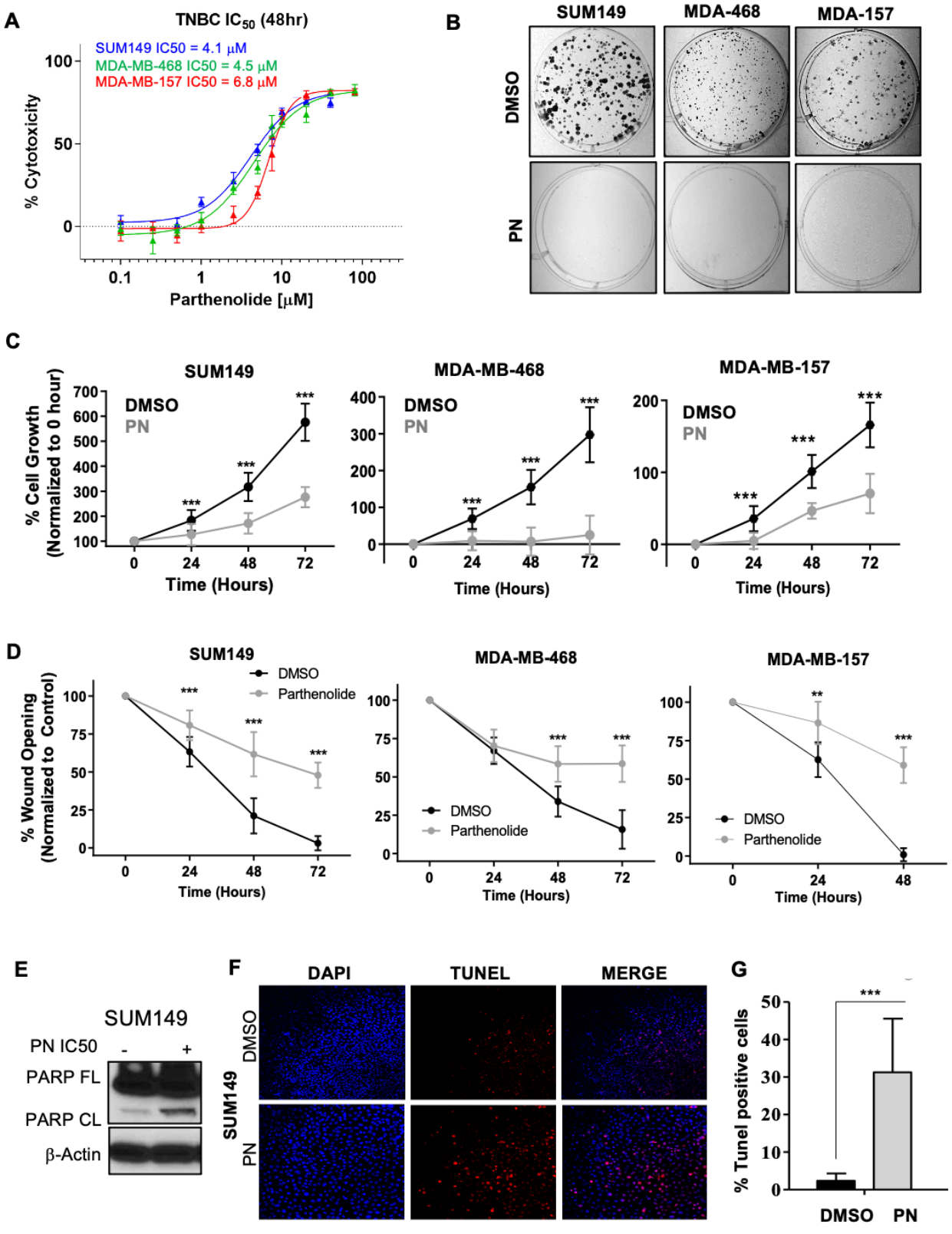
A
TNBC IC50 (48hr)
SUM149 IC50 = 4.1 μM
MDA-MB-468 IC50 = 4.5 μM
MDA-MB-157 IC50 = 6.8 μM
% Cytotoxicity
Parthenolide [μM]
B
SUM149
MDA-468
MDA-157
DMSO
PN
C
SUM149
MDA-MB-468
MDA-MB-157
% Cell Growth (Normalized to 0 hour)
DMSO
PN
Time (Hours)
D
SUM149
MDA-MB-468
MDA-MB-157
% Wound Opening (Normalized to Control)
DMSO
Parthenolide
Time (Hours)
E
SUM149
PN IC50
PARP FL
PARP CL
β-Actin
F
DAPI
TUNEL
MERGE
SUM149
DMSO
PN
G
% Tunel positive cells
DMSO
PN

Figure 5.2 Parthenolide inhibits TNBC growth and migration and induces apoptosis
A, SUM149, MDA-MB-468, MDA-MB-157 cells were seeded onto a 96-well plate at 5,000 cells/well in 100µL. Twenty-four hours later, cells were treated with varying concentrations of parthenolide (PN) (0–80 µM) for 48 hours. The IC50 and the 95% confidence interval were calculated by fitting the non-linear regression curve, log(inhibitor) vs. response – Variable slope (four parameters), to the data. **B,** Images of SUM149, MDA-MB-468 and MDA-MB-157 colony formation when treated with parthenolide at the IC50. Cells were treated every other day with the IC50 dose of parthenolide and grown for 10-14 days when colonies were stained with crystal violet and counted by ImageJ. **C,** SUM149, MDA-MB-468 and MDA-MB-157 breast cancer cells were treated with parthenolide at the IC50 and matched DMSO concentration followed by the cell counting every 24 hours. The 0-hour time point represents cells counted prior to drug treatment. Values are normalized as percent growth from 0 hours. Values represent means ± SD of three independent experiments conducted in triplicate. A t-test was used to assess statistical significance at each timepoint; ***P<0.00. **D,** Parthenolide inhibits wound healing capacity of TNBC cell lines (SUM149, MDA-MB-468 and MDA-MB-157). Cells were plated near confluency and a scratch was made. Media was changed daily. The scratch was monitored for 48-72 hours and the wound area was measured by ImageJ. Statistical significance between vehicle and drug treatment was measured through comparing the means of 3 separate experiments through an unpaired t-test at each time point ***p<0.001 ** P<0.01. **E,** Western blot of SUM149 cells treated with PN IC_{50} showing PARP cleavage. **F-G,** SUM149 breast cancer cells were treated with the IC_{50} of Parthenolide at 48 hours and matched DMSO concentration followed by the TUNEL assay and confocal microscopy, and quantified by ImageJ, ***P<0.001

Parthenolide regulates NFκB signaling and IFITM1 expression

Next, we assessed whether parthenolide can regulate NFκB signaling and IFITM1 expression. For these experiments each cell line was treated with the respective IC50 as determined previously. We found that parthenolide inhibits p65 activation in SUM149, MDA-MB-157 and MDA-MB-468 cells (Figure 5.3 A) and it significantly reduces NFκB promoter activity in SUM149 cells (Figure 5.3 B). Notably, parthenolide significantly inhibits IFITM1 protein (Figure 5.3 C) and mRNA expression (Figure 5.3 D) in all cell lines. These data are in line with our previous data such that loss of p65 decreases IFITM1 expression.

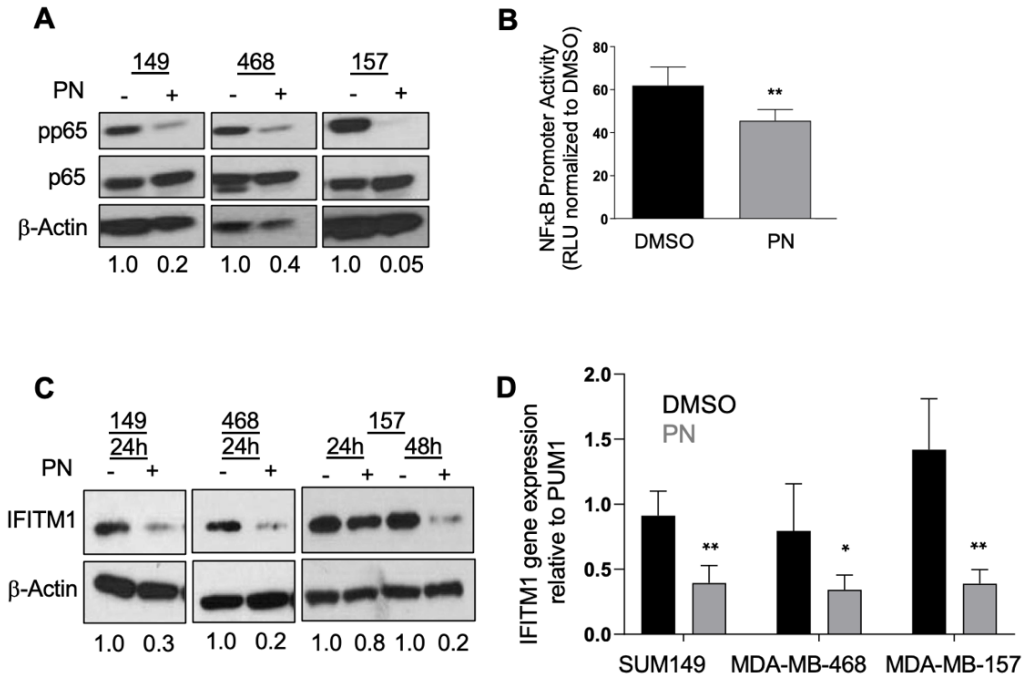

Figure 5.3 Parthenolide inhibits NFkB signaling and IFITM1 expression
A, SUM149, MDA-MB-468 and MDA-MB-157 cells were treated for 24 hours with either parthenolide at the IC50 or with equal amount of DMSO followed by immunoblotting for phospho-p65 (S536) and total-p65. Quantification of pp65/p65 ratios are listed below. **B,** SUM149 cells were co-transfected with the DNA pGL4.32 NFkB-RE and Renilla constructs. Cells were treated with parthenolide at the IC50 or DMSO and luciferase was assayed 24-hours after treatment. Values represent means ± SD of four independent experiments conducted in triplicate. A t-test was used to assess statistical significance; **P<0.01. **C-D,** SUM149, MDA-MB-468, and MDA-MB-157 cells were treated with the parthenolide at the IC50 or with equal amount of DMSO for 24 followed by immunoblotting (quantification of IFITM1 values are listed below) (**C**) or qRT-PCR (**D**) where data represents at least two independent experiments run in triplicate. A t-test was used to assess significance. *p<0.05, **p<0.01.

Parthenolide interrupts IFN mediated activation of IFITM1

Since IFITM1 is tightly regulated by endogenous and exogenous IFNα signaling, we assessed the effect of parthenolide on the IFN response. Here, we found that parthenolide significantly inhibits IFNα mRNA levels in SUM149 cells (Figure 5.4 A). Since parthenolide reduces the cellular response governed by endogenous IFNα we hypothesized that exogenous IFNα could rescue its inhibition. Notably, we found that treatment with parthenolide followed by exogenous IFNα does not rescue the IFITM1 protein expression in SUM149, MDA-MB-468 or MDA-MB-157 cells (Figure 5.4 B) and that this is regulated on a transcriptional level (Figure 5.4 C). We therefore hypothesized that other genes within the IFNα response would be altered as well. qRT-PCR data suggest that parthenolide interrupts IFNα mediated induction of multiple ISGs including OAS1, IFI27, MX1, and IFIT1 (Figure 5.4 D). To assess if this gene expression is mediated by NFκB promoter activity, we assessed the NFκB response element (NRE) through a luciferase assay. We found that addition of IFNα induces NRE activity in SUM149 and MDA-MB-468 cells, addition of parthenolide substantially decreases NRE activity, and co-treatment results in a lack of induction by IFNα (Figure 5.4 E-F). Previous studies suggest that IFNα can mediate cell growth through regulation of the NFκB pathway. Therefore, we hypothesized that pre-treating the cells with parthenolide followed by IFNα would enhance cell death. Through western blot analysis we identified a decrease in p65 activity and increased in cleaved PARP with the co-treatment suggestive of elevated cell death (Figure 5.4 G). Therefore, these data suggest that IFNα and NFkB signaling cooperate to drive IFITM1 expression and subsequent IFITM1 mediated phenotypes.

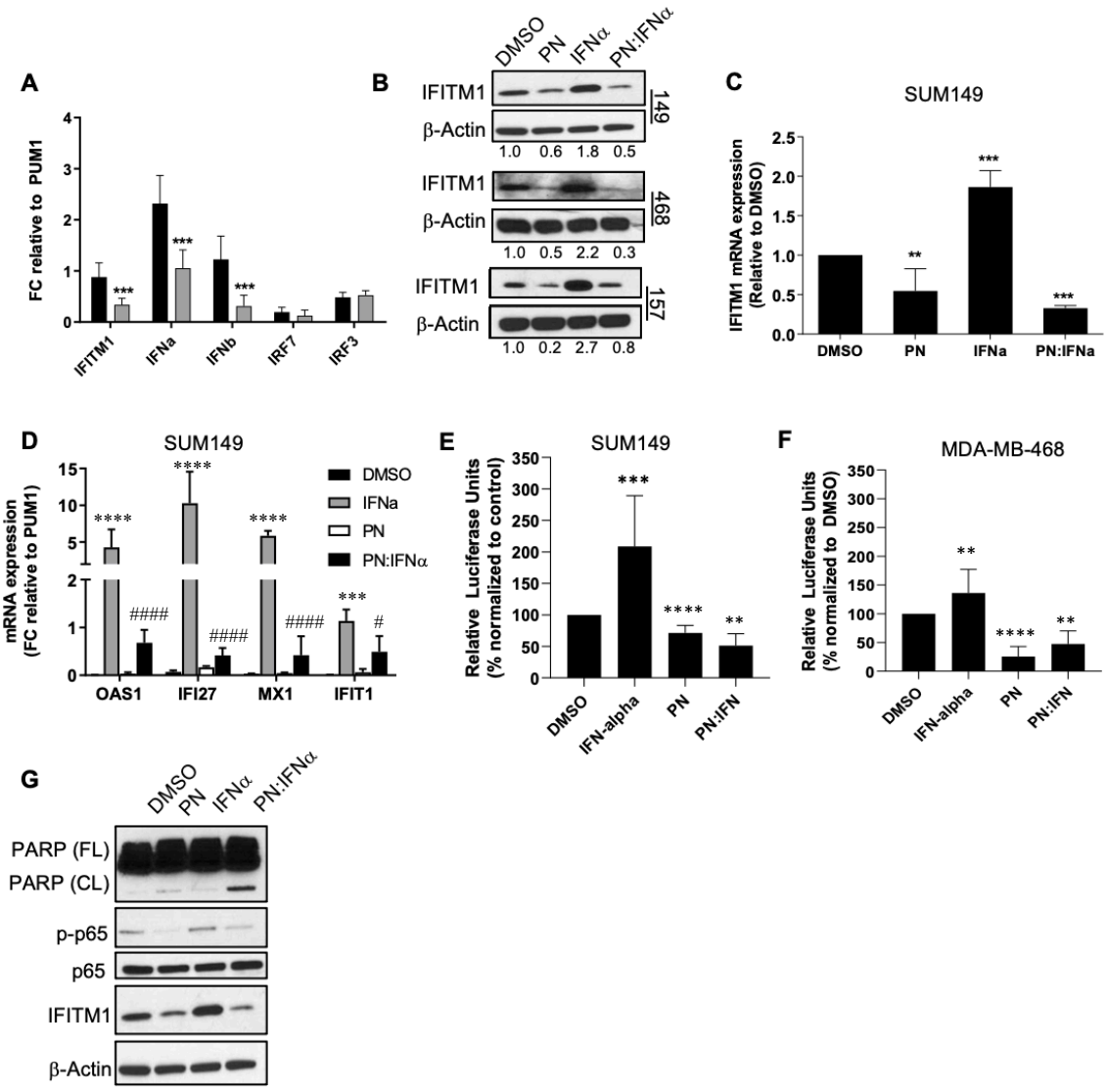

Figure 5.4 Parthenolide interrupts IFN signaling

A. qRT-PCR of IFN regulated genes after 24 hour treatment with PN at the IC50. Data represented are means ± standard deviation of three independent experiments ***p<0.001. **B,** SUM149, MDA-MB-468 and MDA-MB-157 cells were treated with DMSO, PN at the IC50, 500 units/mL IFNα-2a or pre-treated for 4 hours with PN at the IC50 followed by 20 hours treatment with 500 units/mL IFNa-2a. Samples were immunoblotted for IFITM1 expression and a representative blot with IFITM1 quantification is shown. **C.** IFITM1 mRNA expression and other ISG expression (**D**) was assessed in SUM149 cells after treatment with either DMSO, PN at the IC50, 500 units/mL IFNα-2a or pre-treated for 4 hours with parthenolide at the IC50 followed by 20 hours treatment with 500 units/mL IFNα-2a. Values are displayed as fold change relative to either DMSO (**C**) or PUM1 (**D**). Data represents at least two independent experiments run in triplicate. A t-test was used to assess significance. *p<0.05, ***p<0.001, ****p<0.0001. For **D**, Asterisks mark significance between DMSO and IFNα treatment and number signs mark significance between IFNα and the co-treatment of IFNα and PN. **E-F,** SUM149 and MDA-MB-468 cells were co-transfected with the DNA pGL4.32 NFkB-RE and Renilla constructs. Cells were treated with PN at the IC50 or DMSO and luciferase was assayed 24 hours after treatment. Values represent means ± SD of three independent experiments conducted in triplicate. A t-test was used to assess statistical significance; **P<0.01. **G.** PARP, phospho-p65 and IFITM1 expression in SUM149 cells depicted via western blot after treatment with either DMSO, PN at the IC50, 500 units/mL IFNα-2a, or pre-treated for 4 hours with PN at the IC50 followed by 20 hours treatment with 500 units/mL IFNα-2a.

In vivo effects of parthenolide

To assess the effect of parthenolide *in vivo*, the orthotopic fat pad model was used. Tumors were developed through bilateral injection of SUM149 or MDA-MB-468 cell lines into the mammary fat-pads of 7-week old female NSG mice. Mice were treated intraperitoneally with a 10% DMSO solution or 30mg/kg/day parthenolide for 14-21 days. Parthenolide treatment significantly decreased MDA-MB-468 tumor volume from 500mm^3 to 200mm^3 and tumor weight from 175mg to 130mg after 14 days of treatment (Figure 5.5 A-B). An increase in apoptosis as measured by TUNEL staining (Figure 5.5 C) and a decrease in Ki67 staining (Figure 5.5 D) suggests parthenolide reduces proliferation and induces cell death *in vivo*. Moreover, IHC analysis suggests that this is due to a slight decrease in phospho-p65 and IFITM1 expression (Figure 5.5 D). Similarly, parthenolide significantly reduces SUM149 tumor volume from 1,200mm^3 to 550mm^3 (Figure 5.5 E) and tumor weight from 900mg to 400mg (Fig. 7F) after 21 days of treatment. In SUM149 cells, PN only slightly decreases IFITM1 and the ratio of phospho-p65 to p65 as depicted by Western blot analysis (Figure 5.5 G, Supplemental Figure 5.2). We should note that there were no adverse effects or potential toxicity associated with parthenolide treatment as demonstrated by no significant body weight loss in the mice (Figure 5.5 H). These data suggest that parthenolide has a similar effect *in vivo* as it does *in vitro*.

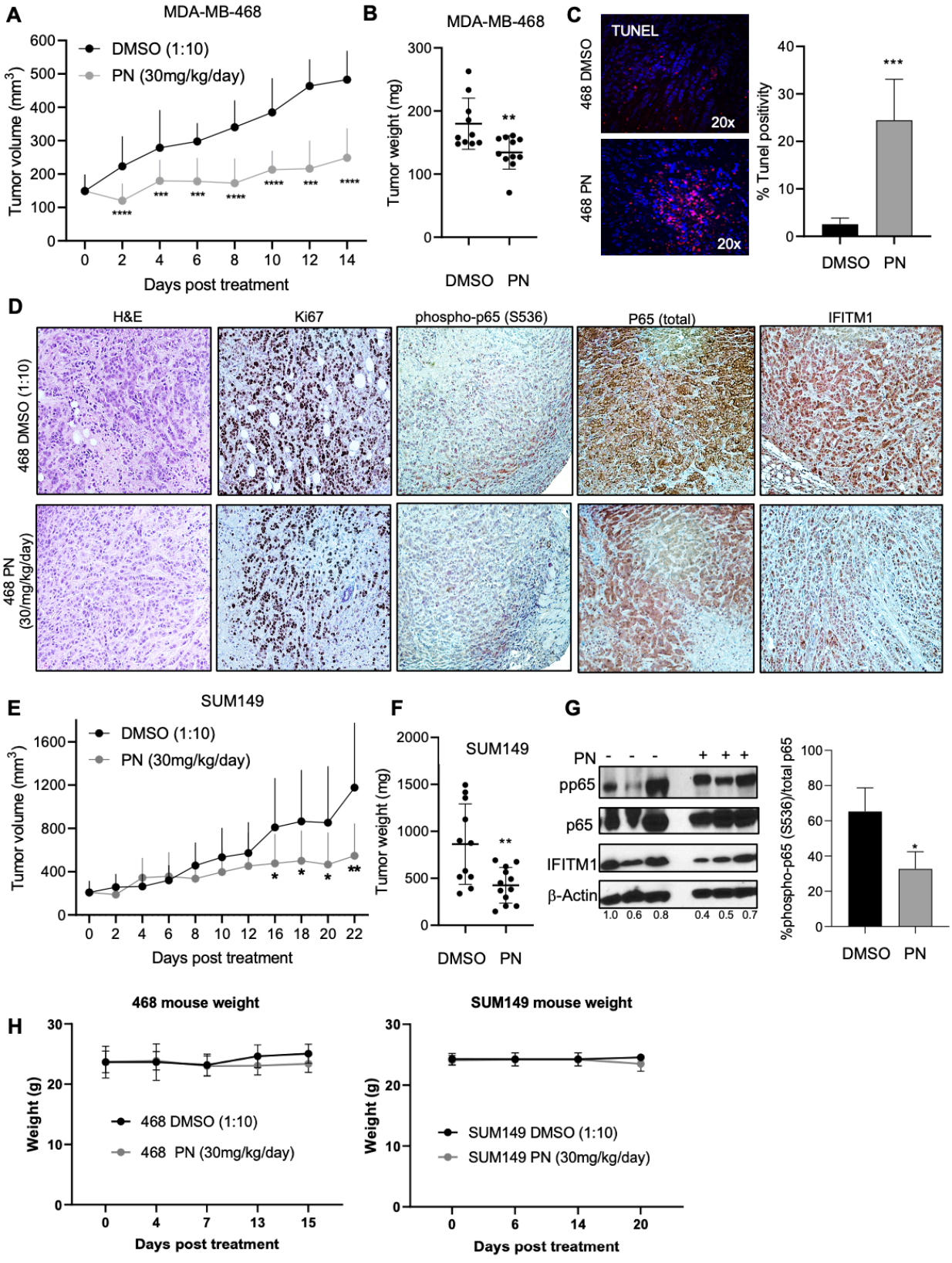
A
MDA-MB-468
DMSO (1:10)
PN (30mg/kg/day)
Tumor volume (mm3)
Days post treatment
B
MDA-MB-468
Tumor weight (mg)
DMSO PN
C
TUNEL
468 DMSO
468 PN
20x
% Tunel positivity
DMSO PN
D
H&E
Ki67
phospho-p65 (S536)
P65 (total)
IFITM1
468 DMSO (1:10)
468 PN (30/mg/kg/day)
E
SUM149
DMSO (1:10)
PN (30mg/kg/day)
Tumor volume (mm3)
Days post treatment
F
SUM149
Tumor weight (mg)
DMSO PN
G
PN
pp65
p65
IFITM1
β-Actin
%phospho-p65 (S536)/total p65
DMSO PN
H
468 mouse weight
468 DMSO (1:10)
468 PN (30mg/kg/day)
Weight (g)
Days post treatment
SUM149 mouse weight
SUM149 DMSO (1:10)
SUM149 PN (30mg/kg/day)
Weight (g)
Days post treatment

Figure 5.5 Parthenolide decreases TNBC tumor growth *in vivo*
A, $3x10^6$ MDA-MB-468 cells were injected bilaterally into the fat pad of 7-week old female NSG mice. Mice were treated with a 10% DMSO solution or 30mg/kg/day parthenolide for 14 days once tumors reached a mean volume of $150mm^3$. Tumors were measured every 48-hours and volume was calculated by $W^2/2L$. **B**, Final tumor weight of MDA-MB-468 DMSO and parthenolide treated tumors. **C,** The Click-iT™ Plus TUNEL kit was used to stain for apoptotic cells within the MDA-MB-468 tumor. Quantification (left) was completed using ImageJ software and a t-test was used to assess the significance of the percentage of cells with TUNEL staining ***p<0.001. **D,** IHC analysis was used to assess phospho-and total p65, IFITM1 and Ki67 in DMSO and parthenolide treated MDA-MB-468 tumors. **C**, $3x10^6$ SUM149 cells were injected bilaterally into the fat pad of 7-week old female NSG mice and the same MDA-MB-468 experimental design was followed. **F**, Final tumor weight after 21 days of either DMSO or parthenolide treatment in SUM149 cells. **G**, Western blot of three DMSO treated tumors and three parthenolide treated tumors. IFITM1 expression was quantified below and phospho-p65/p65 ratio was plotted as a bar chart to assess significance (right). **H**, Mice were weighed at least 1x/week after parthenolide treatment started. Weight is represented in grams (g).

IFITM1 is an indirect target of parthenolide

To determine whether parthenolide inhibits tumor cell growth through direct targeting of IFITM1, we assessed the effect of parthenolide in SUM149 and MDA-MB-157 CRISPR/Con and IFITM1 KO cells. We found that loss of IFITM1 in SUM149 cells (Figure 5.6 A) and in MDA-MB-157 cells (Figure 5.6 B) significantly enhances sensitivity to parthenolide when treated with both half the IC50 and the full IC50 values at 72-hours as assessed by cell growth. This data is further supported by 2D colony formation which shows that loss of IFITM1 significantly reduces colony formation upon fractionated doses of parthenolide treatment in both SUM149 cells (Figure 5.6 D-E) and in MDA-MB-157 cells (Figure 5.6 F). The fact that TNBC cells retain their sensitivity to parthenolide despite their loss of endogenous IFITM1 suggests that parthenolide may not directly target IFITM1, but rather, targets the upstream regulators of IFITM1: NFκB and IFNα.

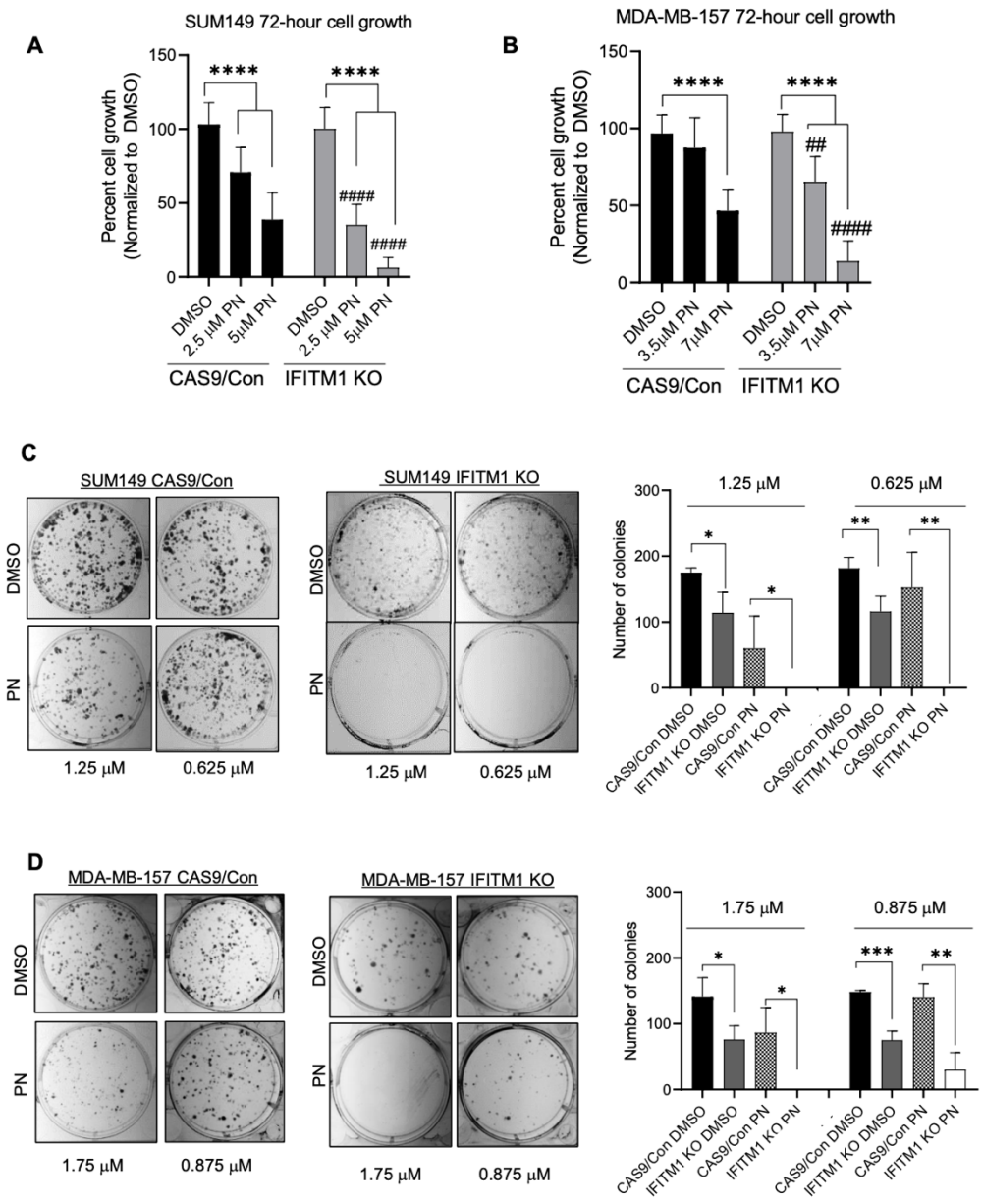

Figure 5.6 Loss of IFITM1 sensitizes SUM149 and MDA-MB-157 cells to parthenolide
A, SUM149 and MDA-MB-157 (**B**) CAS9/Con and IFITM1 KO cells were treated with parthenolide at the IC50 and ½ IC50 followed by cell counting at 72-hours. Values are normalized to DMSO and represent means ± SD of four independent experiments conducted in triplicate. A t-test was used to assess statistical significance. Asterisks (*) represent significance within the specific clone assessed (CRISPR/Con or IFITM1 KO) while number signs (#) represent significance of the percent change between CRISPR/Con and IFITM1 KO cells.****p<0.0001, ####p<0.001, ## p<0.01. **C-D,** Images of SUM149 (**C**) and MDA-MB-157 (**D**) CAS9/Con and IFITM1 KO colony formation when treated with fractionated doses of parthenolide. Cells were treated every other day with either 1/4 or 1/8 IC50 dose of parthenolide and grown for 10-14 days when colonies were stained with crystal violet and counted by ImageJ. Quantifications are to the right of the images. Values represent means ± SD of three independent experiments. *p<0.05, **p<0.01, ***p<0.005.

Discussion

The absence of well characterized, druggable targets and disease heterogeneity in TNBC provide significant therapeutic barriers. Here, we discovered that the naturally derived NFκB inhibitor, parthenolide, inhibits both IFNα and NFκB pathways, subsequently inhibiting IFITM1 expression and inducing TNBC cell death (Fig. 6). These findings suggest that targeting both IFNα and NFκB signaling with parthenolide might be a novel therapeutic strategy for a subset of TNBC that overexpress IFITM1.

High-throughput drug cytotoxicity screening is a method used for rapid profiling of FDA-approved and abandoned drugs which have the potential to be repurposed outside of the scope of the original proposed application (170). Our high throughput screen identified parthenolide, a sesquiterpene lactone derived from the feverfew plant, and a known NFκB inhibitor, as a potent growth inhibitor of TNBC cells. Moreover, further mechanistic studies identified parthenolide has the ability to suppress IFITM1 expression. Sesquiterpene lactones can directly inhibit NFκB through modification of the p65 subunit (178). Parthenolide is best known for its inhibition of p65 phosphorylation by targeting both IKKα and IKKβ and subsequent p65 nuclear translocation, but additional reports suggest that parthenolide directly alkylates p65 preventing its DNA binding (178). Prior to our study, parthenolide was tested in breast cancer cells using the MDA-MB-231 cell line where it was shown to promote cell death, inhibit metastasis, and decrease *in vivo* growth (173, 174, 179). Similarly, we show that parthenolide significantly reduces tumor growth and increases apoptosis in MDA-MB-468 and SUM149 cells *in vivo* which is associated with a decrease in phospho-p65 and IFITM1 expression. Notably, the inhibitory effect of parthenolide on IFITM1 and phospho-p65 *in vivo* was less pronounced than its effect on these proteins *in vitro*, thus highlighting the importance of the tumor microenvironment in impacting the efficacy of parthenolide *in vivo*. Also, altered metabolism of parthenolide *in vivo* (180, 181) may impact its efficacy thus requiring a higher dose of the drug to produce similar effects to those seen *in vitro*. Therefore, though parthenolide has a growth inhibitory effect in IFITM1 positive TNBC, a higher

dose might be necessary for a more robust decrease in p-p65 and IFITM1. In regard to metabolism differences, use of the water soluble analogue, dimethylaminoparthenolide, should be investigated in regard to IFITM1 regulation.

An interesting finding is that MDA-MB-231 cells, which lack endogenous IFITM1, have a significantly higher IC50 of parthenolide compared SUM149, MDA-MB-157 and MDA-MB-468 TNBC cells which express IFITM1 (Supplemental Table 1), suggesting that the presence of IFITM1 might sensitize TNBC cells to parthenolide. This assertion, however, is contradicted by our observation that knockout of IFITM1 in SUM149 and MDA-MB-157 cells enhances their sensitivity to parthenolide, suggesting that parthenolide does not directly target IFITM1 but rather targets NFkB to suppress IFITM1. Supporting this evidence, IFITM1 has been identified as an ISG involved in the interferon related DNA damage response signature, suggesting that IFITM1 may function as an important mediator of the cell response to external stressors including drug treatment (87). Though this specific phenomenon was not examined *in vivo*, future studies are essential to confirm how the loss of IFITM1 alters TNBC response to specific treatment strategies. Perhaps loss of IFITM1 and its subsequent decrease in NFκB gene expression (Chapter 1) decreases the threshold of parthenolide necessary to elicit a phenotypic effect. Alternatively, though our findings suggest that IFITM1 is not a direct target of parthenolide, the presence of IFITM1 has the potential to be used as a predictive biomarker for targeting alternative IFNα signaling.

Aside from NFκB inhibition, parthenolide has been shown to have multiple targets in tumor cells including: binding directly to focal adhesion kinase in MDA-MB-231 breast cancer cells when treated with high doses (179), increasing autophagy, generating reactive oxygen species, activating of JNK, or inhibiting the JAK2-STAT3 axis (173-175, 182); though each of these pathways can regulate NFκB. Ultimately, these data suggest that parthenolide indirectly targets IFITM1 but highlights an important crosstalk between NFκB signaling and IFNα in TNBC cell lines. Therefore, future medicinal chemistry campaigns or another high-throughput screen utilizing

CRISPR/Cas9 Control and IFITM1 KO cells to determine if analogues of parthenolide or other drugs directly targeting IFITM1 would be beneficial.

Tumor acquired drug resistance and off target effects of cancer drugs are essential determinants of drug efficacy. Approximately 70% of TNBC patients do not respond to conventional chemotherapy (27) and an elevated IFN signature, including IFITM1 overexpression, contributes to drug and radiation resistance in breast cancer (87). Supporting this evidence, past unpublished data from our laboratory suggest that targeting IFITM1 expression in SUM149 TNBC cells enhances their sensitivity to doxorubicin (data not shown). Regarding parthenolide, studies have reported that it has the ability to synergize and cooperate with anti-cancer agents in multiple malignancies including breast cancer (182). Use of MDA-MB-231 cells shows a synergistic effect of parthenolide with docetaxel, paclitaxel, doxorubicin, SAHA, TRAIL, and vinorelbine while use of parthenolide in MCF-7 cells has a synergistic effect with 4-hydroxytamoxifen, tamoxifen, and fulvestrant. Additional studies provide evidence of parthenolide protecting neighboring organs from radiation therapy (176) and preventing muscular skeletal wasting during chemotherapy (177), perhaps through limiting systemic inflammation. Though parthenolide represents an opportunity to further validate IFITM1 as a promising drug target for TNBC, future studies investigating resistance mechanisms are essential. Specifically, it will be important to investigate how long-term treatment with parthenolide alters JAK/STAT signaling due to the proposed mechanistic crosstalk between NFκB and IFN signaling. Lastly, parthenolide is highly lipophilic which limits its bioavailability, however, derivatives with improved solubility have been developed such as dimethylaminoparthenolide, which could eventually be used in patient populations (173, 183).

Collectively, evidence presented herein demonstrate that targeting IFITM1 expression through interrupting IFNα/NFκB crosstalk with parthenolide, substantially attenuates TNBC tumor growth and migration and induces cell death. Parthenolide has historically been used for its anti-inflammatory and anti-migraine effects but is potentially beneficial for patients with TNBC (182).

We acknowledge that IFNα/NFκB crosstalk has been introduced in previous studies (63, 64, 184), however, the novelty of our findings are that they suggest that both pathways play a critical role in regulating IFITM1 expression, thus providing additional insight into the pathogenesis of TNBC.

Materials and methods

Reagents and antibodies

Parthenolide was obtained from Acros Organics (Code: 462151000; Lot: A0386092) and stored as lyophilized powder in -20 when not in use. Prior to *in vitro* experiments a 10mM stock of parthenolide in DMSO was made. Aliquots of 10mM stock were stored in -20 and used to prevent freeze-thaw cycling. Phospho-p65 and p65 antibodies were purchased from Cell Signaling Technology: anti-phospho-p65 (1:500, Cell Signaling Technologies: #3033S) and anti p-65 (1:500, Cell Signaling Technologies: #8242).

qRT-PCR

qRT-PCR protocol was followed as outlined in Chapter 2. Primers used in this chapter are below:

Table 5.1 Primer sequences

Gene	Forward Primer (5'-3')	Reverse Primer (5'-3')
PUM1	TCACCGAGGCCCCTCTGAACCCTA	GGCAGTAATCTCCTTCTGCATCCT
IFITM1	GGATTTCGGCTTGTCCCGAG	CCATGTGGAAGGGAGGGCTC
IFNα	CTTGAAGGACAGACATGACTTTGGA	GGATGGTTTCAGCCTTTTGGA
IFNβ	GTCTCCTCCAAATTGCTCTC	ACAGGAGCTTCTGACACTGA
IRF3	AGGACCCTCACGACCCACATAA	GGCCAACACCATGTTACCCAGT
IRF7	GAGCCCTTACCTCCCCTGTTAT	CCACTGCAGCCCCTCATAG
IFI27	GCCTCTGG CTCTGCCGTAGTT	ATGGAGGACGAGGCGATTCC
IFIT1	TCTCAGAGGAGCCTGGCTAA	CCAGACTA TCCTTGACCTGA TGA
MX1	CTTTCCAGTCCAGCTCGGCA	AGCTGCTGGCCGTACGT CTG
OAS1	TGAGGTCCAGGCTCCACGCT	GCAGGTC GGTGCACTCCTCG

High Throughput Drug Screen

The drug repurposing collection at KUCC contains 3,574 FDA-approved and abandoned drugs from the following vendors: Selleck (1288), Enzo (640), NIH (446) and Prestwick (1,200). The drugs are stored at 10 mM in 100% dimethyl sulfoxide (DMSO). KUCC maintains and continues to grow an internal, integrated database describing activities (and, lack thereof) of FDA-approved and abandoned drugs evaluated in high throughput screens across many proposed drug targets employing cell-based and biochemical assays. For the screen, SUM149 and MDA-MB-157 (1000 cells/well) plated in 384-well microplates. The drugs and DMSO controls were added to the plates using Echo 555 (Labcyte Inc.) at a final concentration of 2.5μM. After 72 hours incubation at 37°C, cytotoxicity was measured using the luminescence-based CellTiter-Glo reagent (Promega Inc.). The luminescence was read on Enspire plate reader (PerkinElmer Inc.) and percent cytotoxicity was normalized to positive and negative controls on each assay plate. The Z' scores of the two repurposing screens were: (A) SUM149 screen, average Z'= 0.91 ± 0.018 , (B) MDA-MB157 screen, average Z'= 0.81 ± 0.034, (C) SUM190 screen, average Z'= 0.81 ± 0.034, indicating a good separation of positive and negative controls across all assay plates and suitability of the assay for compound screening. In addition to the assay performance criteria described above, cytotoxicity was defined as drugs demonstrating greater than 50% inhibition of cell viability in one or both breast cancer cell lines screened with no observed toxicity in normal cells. Parthenolide was one of the compounds identified for further *in vitro* analyses.

IC50 calculations

SUM149, MDA-MB-468, MDA-MB-157 cells were seeded onto a 96-well plate at 5,000 cells/well in 100μL. Twenty-four hours later, cells were treated with varying concentrations of parthenolide (PN) (0–80 μM) for 48 hours. After 48 hours, 10μL solution of 5 mg/mL 3-(4,5-dimethylthiazol-2-yl)-2,5-diphenyltetrazolium bromide (MTT) and incubated for 3 h at 37ºC. The medium was then

aspirated and 100µL of the solubilizing solution of a 1:1 solution of dimethyl sulfoxide and ethanol was added to dissolve blue formazan crystals. Results were obtained by reading the plate at 570 nm. IC50 values were calculated by first normalizing each well to the average of the untreated wells which were then imported into GraphPad Prism version 5 for Windows (GraphPad Software, La Jolla, CA). The drug concentrations (X values) were transformed to a logarithmic scale while the Y values were transformed to percentages by multiplying these values by 100. To represent as percent cytotoxicity, Y values were further transformed using the equation, Y=K-Y. The IC50 and the 95% confidence interval were calculated by fitting the non-linear regression curve, log(inhibitor) vs. response – Variable slope (four parameters), to the data.

Proliferation, colony formation, and wound healing assays

Cell proliferation was measured by cell counting. Cells were seeded onto a 24-well plate at a density of 25,000 cells/well. The next day, cells were treated or harvested for the 0-hour timepoint. Cells were counted every 24 hours and the final values were normalized to the 0-hour timepoint or to DMSO. Cells were re-treated with parthenolide at the IC50 or with equivalent concentrations of DMSO every 48 hours when indicated.

For colony formation, cells were seeded onto a 6-well plate at 1,000 cells/well. For experiments using parthenolide, cells were treated 24 hours after plating and re-treated every 48 hours. Cells were grown for 10-14 days prior to staining colonies with 5% crystal violet and imaged using the ChemiDoc™ XRS system equipped with Image Lab™ software.

Wound healing was assessed by seeding cells onto a 24-well plate at a density of 90,000-120,000 cells/well (approximately 80% confluency) and making a single wound by scratching the attached cells using a 10-µl sterile pipette tip. The plates were washed with complete medium to remove

cellular debris. Images of the cells were taken immediately after and 24, 48, and 72 hours later using a phase-contrast microscope and wound area was quantified using the Wound Healing Tool in ImageJ. Cells were re-treated with the parthenolide at the IC50 every 24 hours when indicated.

TUNEL staining

TUNEL staining was performed using the Click-iT™ Plus TUNEL assay kit (Thermo Fisher: #C10617) on deparaffinized tissue or methanol fixed cell lines grown on chamber slides following the manufacturer's instructions. The average number of TUNEL positive cells was quantified using the binary transformation and cell counting method in ImageJ.

Luciferase assays

For NFκB promoter assay, 0.8 μg of plasmid DNA pGL4.32 NFκB-RE vector (Promega) containing 5x NFkB-RE was co-transfected with the pRL CMV Renilla vector. The NFkB plasmid was a kind gift from Dr. Christy Hagan (University of Kansas Medical Center). For ISRE promoter assay, 1μg of plasmid DNA containing the ISRE luciferase was used. After 24 hours, transfection reagent was replaced with normal cell culture media containing DMSO, ruxolitinib, parthenolide, or IFNα where indicated. Luciferase and Renilla activities were measured 24 hours later using the Dual-Luciferase® reporter assay kit (Promega: E1910) according to the manufacturer's instructions on a BioTek Synergy 4 microplate reader using the Gen 5 data analysis software.

Supplemental Data

A

***In vitro* parthenolide IC_{50} in TNBC cell lines at 48 hours.**

Cell Line	Subtype	Gene Cluster	IFITM1 Status	IC50 (μM)	95% CI
SUM149	TNBC	Mixed	+++	4.1	3.61-4.63
MDA-MB-468	TNBC	Basal	++	4.5	4.07-5.14
MDA-MB-157	TNBC	Mesenchymal	++++	6.8	6.49-7.2
MDA-MB-231	TNBC	Mesenchymal	-	15.79	12.47-20.0

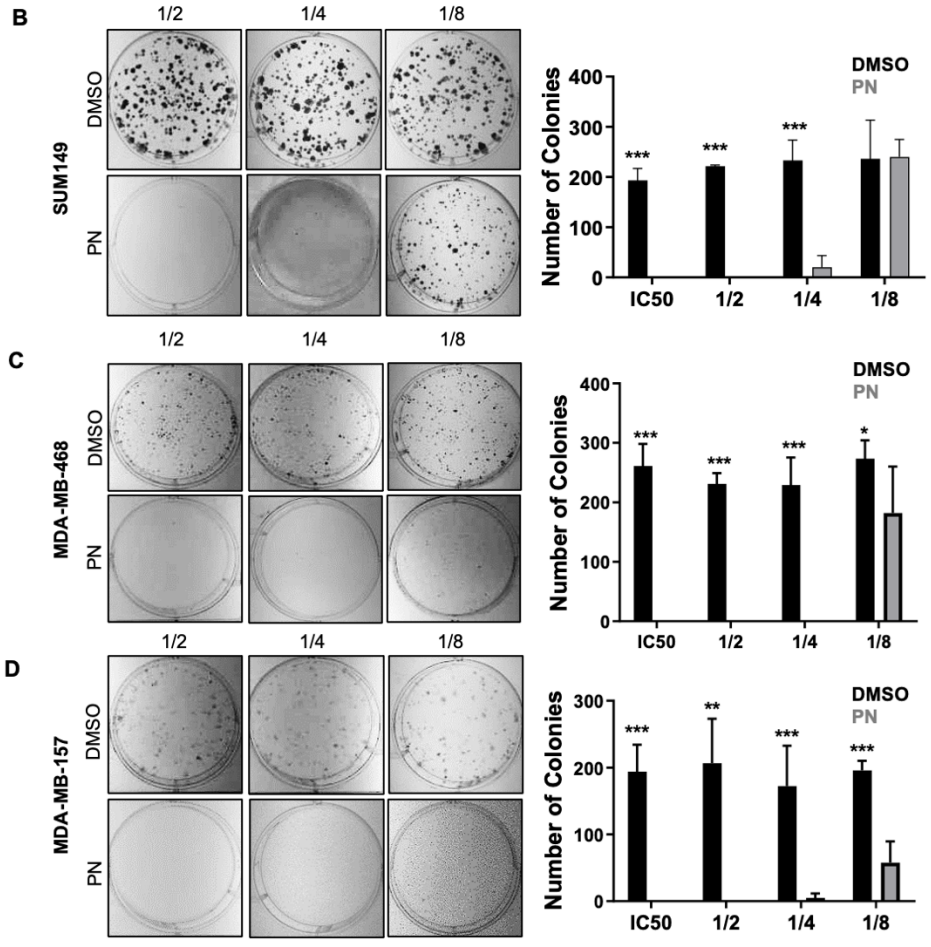

Supplemental Figure 5.1 IC50 values and colony formation with fractionated PN doses
A. Table of in vitro IC50 parthenolide values in multiple cell lines. **B-D,** cells were plated at 1000 cells per 6 well dish, treated every other day with fractionated doses of the parthenolide IC50 for the respective cell lines and allowed to grow for 10-14 days. After colonies formed, media was removed, cells were washed with PBS, stained with crystal violet and counted by ImageJ. Values represent means ± SD of four independent experiments conducted in duplicate. A t-test was used to assess statistical significance;***p<0.001.

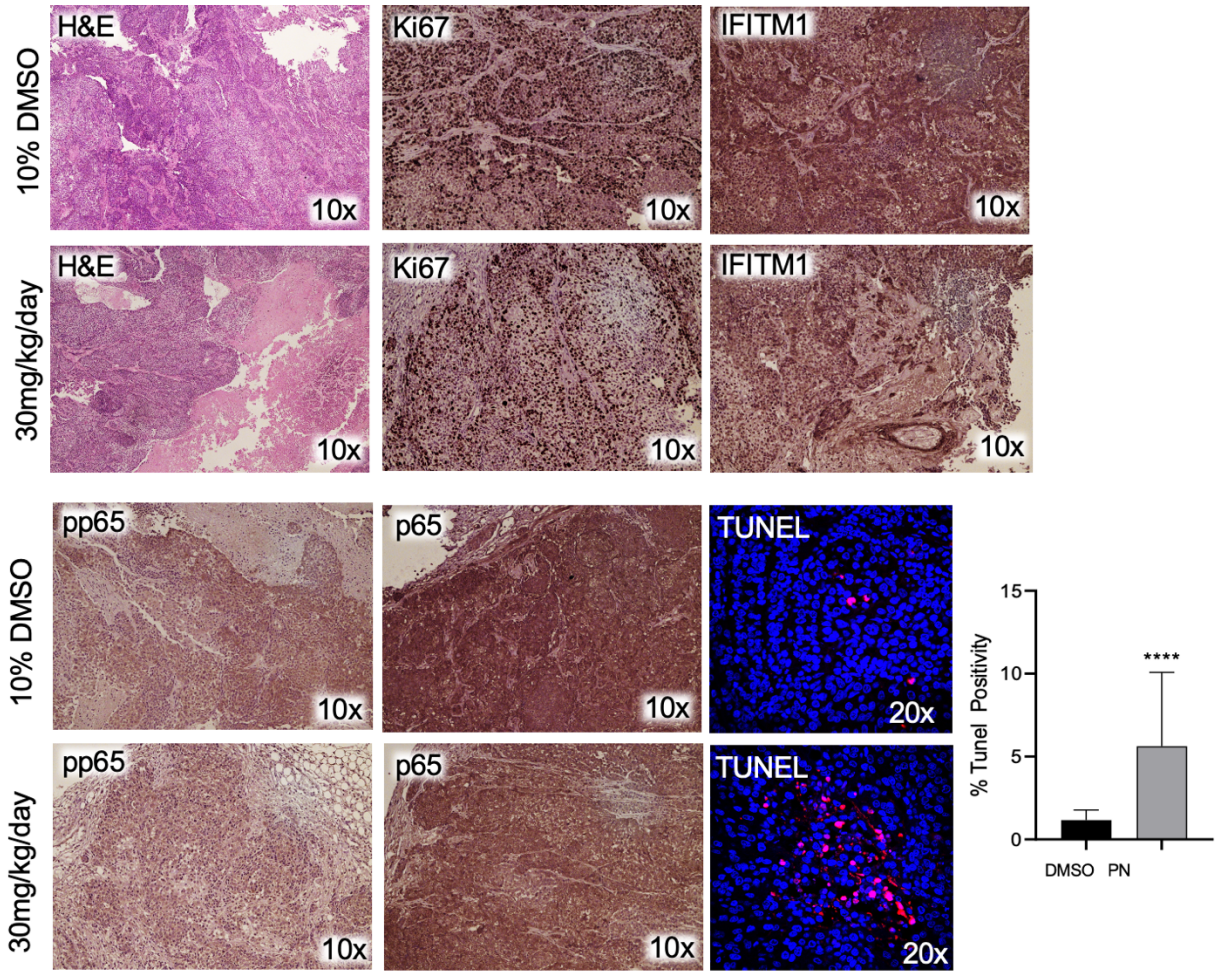

Supplemental Figure 5.2 H&E, IHC and TUNEL stain of SUM149 DMSO and parthenolide treated tumors

H&E staining and IHC analysis was used to assess Ki67, IFITM1, phospho-and total p65 in DMSO and parthenolide treated SUM149 tumors. The Click-iT™ Plus TUNEL kit was used to stain for apoptotic cells within the SUM149 tumor. Quantification (left) was completed using ImageJ software and a t-test was used to assess the significance of the percentage of cells with TUNEL staining ****$p<0.001$.

Chapter 6: Conclusions and Future Directions

Parts of this chapter are adapted from work previously published as an open access article.

Provance, OK, Lewis-Wambi, J. (2019). *Deciphering the role of interferon alpha signaling and microenvironment crosstalk in inflammatory breast cancer. Breast Cancer Res, 2019. 21(1):59.* PMCID*:* PMC6501286. doi: 10.1186/s13058-019-1140-1.

Due to the poor overall survival of patients diagnosed with TNBC, we sought to determine novel mechanisms and subsequent targets that could be harnessed for therapeutic development. Previous studies have shown that the ISG, IFITM1, has a central role in mediating tumor progression from early stages of tumor onset and local invasion to metastatic dissemination; however, prior to this study the relevance and function of IFITM1 in TNBC was unknown. Evidence presented in this thesis demonstrate that overexpression of IFITM1 in TNBC contributes to poor overall survival in a subset of TNBC patients (Figure 6.1 A). Results obtained from a combination of *in vitro* and *in vivo* functional and mechanistic analyses suggest that IFITM1 mediates TNBC progression, perhaps through its relationship with CD81, and may have both intracellular and extracellular roles (Figure 6.1 A). Lastly, IFITM1 expression can be targeted by interrupting its upstream drivers, IFNα and NFκB, by the naturally derived compound parthenolide (Figure 6.1 B). Collectively, data presented herein suggest that TNBC tumors expressing IFITM1 could benefit from therapies inhibiting IFITM1 expression.

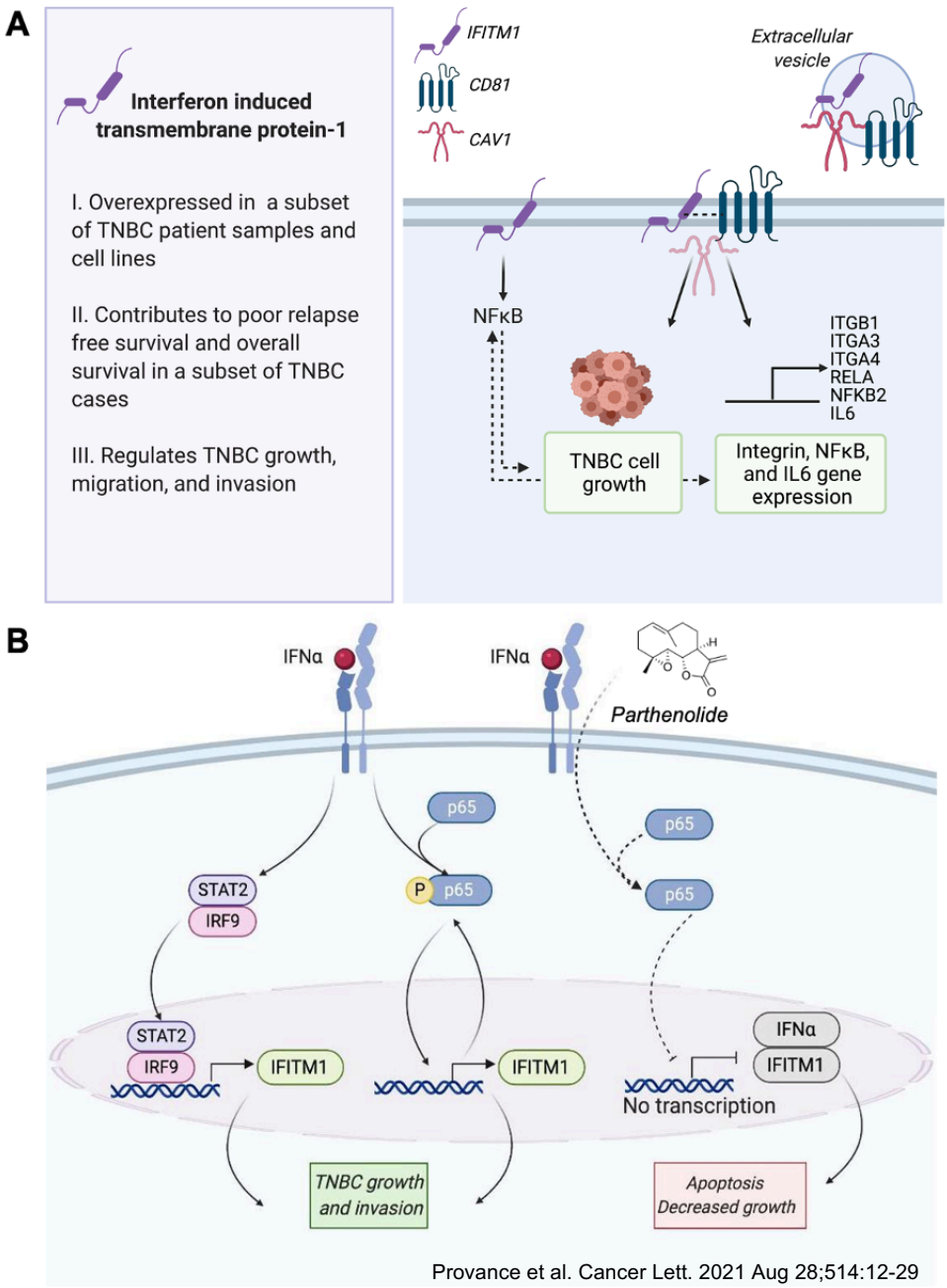

Figure 6.1 Project summary
A, *Right,* General overview of Aim1. *Left,* Depiction of how IFITM1 may function with dependence on CD81 for integrin and IL6 expression and subsequent AKT/NFκB signaling to promote IL6 expression contributing to cell growth. Depicted also is the presence of IFITM1/CAV1/CD81 in extracellular vesicles. RNA sequencing analysis identified that loss of IFITM1 inhibits NFκB signaling which we hypothesize (dotted line) to contribute to decreased growth and integrin expression **B,** Schematic representation of IFNα and NFκB signaling regulating IFITM1 expression in TNBC. *Left*, Non-canonical IFNa signaling through STAT2-IRF9 drives IFITM1 expression which promotes TNBC tumor growth and invasion. *Middle,* IFNa signaling contributes to a positive feedback loop activating p-p65 to promote IFITM1 expression. *Right*, Parthenolide targets p-p65/NFκB activation and inhibits IFNa signaling thus suppressing IFITM1 expression and inducing apoptosis and growth inhibition. Figure created with BioRender.com.

A major limitation in the treatment of TNBC is the inherent heterogeneity of the disease. Though we found IFITM1 to be an important mediator of TNBC progression, not all TNBC cell lines express IFITM1. This phenomenon is further supported in patient data. For example, IFITM1 contributes to significantly reduced overall survival in the mesenchymal, mesenchymal stem- like and basal-like-1 subtypes, but contributes to better overall survival in the immunomodulatory subtype (Chapter 2). These differences likely arise due to the contribution of the cells in the tumor microenvironment included in these analyses. It is well established that the tumor microenvironment is a major contributor of tumor progression and response to therapy in TNBC (185). Therefore, a limitation of the data presented in this thesis is our focus on the TNBC cell intrinsic function of IFITM1, and not the roles of IFITM1 in the TNBC tumor microenvironment. IFITM1 is expressed in the tumor stroma (53) and we show here, that IFITM1 can be secreted in TNBC extracellular vesicles, suggesting the potential for alternative roles of IFITM1 in the TME. Studies assessing the function of the relationship of IFITM1 with the TME in TNBC are non-existent. However, immune cell signaling in TNBC has been investigated and we suspect IFITM1 may play a role. TNBC tumors are known as “hot” tumors since they have higher levels of CD8+ T-cells compared to other breast-cancer subtypes (i.e: “cold” tumors). This T-cell infiltration has been identified as predictive marker for treatment response in TNBC (186). In relation to our findings regarding the mechanism of IFITM1, a previous study identified that integrin targeted monotherapy enhances infiltration of CD8+ T-cells contributing to a better therapeutic response (187). Therefore, since our studies suggest IFITM1 regulates integrin mRNA levels, loss of IFITM1 expression may also contribute to a better therapeutic response due to this mechanism. Moreover, a subsequent study found that TNBC can be stratified based on the amount of CD8+ T-cell levels and extent of infiltration contributing to distinct microenvironment metasignatures which correlate with TNBC specific subtypes and IFITM1 expression (126). For example, immune deficient tumors and those with T-cells that are restricted to tumor margins are enriched in the mesenchymal TNBC subtype, tumors with stromal restriction of T-cells are enriched in the basal-

like and immunomodulatory TNBC subtypes, and the fully inflamed tumors defined by T-cell infiltration into the tumor core are enriched in the immunomodulatory TNBC subtype. As previously mentioned, IFITM1 contributes to poor relapse free survival in mesenchymal, mesenchymal-stem like, and basal-like tumors but enhances relapse free survival in immunomodulatory tumors. The stroma of the fully inflamed, immunomodulatory tumors characterized in this study have higher levels of IFITM1 expression but we hypothesize that IFITM1 has a distinct biological and functional role in this subtype due to interactions with or IFITM1 expression in immune cells. These studies highlight the importance of assessing the biology, function, mechanism, and regulation of IFITM1 in the TNBC tumor microenvironment specifically. Though only assessed *in vitro,* our studies (Chapter 5) and others (87, 104) have shown that IFITM1 expression may contribute to chemotherapy, radiotherapy, and aromatase inhibitor resistance. We propose that IFITM1 inhibitors in combination with other therapies may enhance patient response rate which should first be assessed by pre-clinical investigations. Further uncovering TNBC specific function of IFITM1 down to which protein domains are functional, could perhaps provide a mechanism for tumor cell IFITM1 targeting while sparing normal tissue. Should IFITM1 inhibitors be developed in future studies, the potential off target effects in the microenvironment in response to targeting IFITM1 must be considered.

Similar to the studies of IFITM1, our understanding of IFNα in TNBC has been limited to its effects on TNBC cells alone. *In vitro*, inhibition of IFNα and subsequent signaling does not have a large impact on the TNBC phenotype. Perhaps this is a result of the other ISG's that are regulated by IFNα, modulation of only a single IFNα gene (IFNα-2a), or of the isolated *in vitro system*. Understanding and subsequently targeting tumor produced IFNα or downstream signaling is new territory. Therefore, future studies investigating the roles of IFNα in the tumor microenvironment are necessary. For example, one study identified that 63.3% of breast cancers are positive for IFNα but that stage III breast cancers had no IFNα binding to the receptor complex

suggesting constitutive secretion of IFNα but a lack of autocrine signaling (159). However, JAK/STAT signaling is known to be both a cell intrinsic and cell extrinsic mechanism of aggressive breast cancer (Figure 6.2) (188). Perhaps IFNα could contribute to tumor promoting paracrine signaling in the TNBC microenvironment where if understood and appropriately targeted, could be beneficial for a subset of patients diagnosed with TNBC. Supporting this hypothesis, one of the major contributions of IFNα to the TNBC tumor is educating the tumor microenvironent through immunoediting for eventual tumor progression, of which is not assessed *in vitro* (Figure 6.2). For example, TNBC tumors have high levels of tumor infiltrating lymphocytes in the stroma but also increased levels of PD-L1 expression on both tumor and immune cells (32-35). Notably, only 21.4% of patients of patients with 100% PD-L1 expression achieved the expected overall response rate when treated with immune checkpoint blockade (ICB) therapy (31, 189-192). A potential explanation for this response is such that IFNα can regulate the expression of immune checkpoints perhaps used as a feedback mechanism to overcome selective PD-L1 inhibition (36). Additionally, IFNs have been implicated in enhancing tumor cell DNA damage resistance in multiple cancer types including breast cancer (37). These findings suggest IFNα may contribute to the relatively poor response to ICB or other therapies in TNBC through modulation of the microenvironment. Alternatively, TNBC tumors express higher levels of ISGs compared to other breast cancer subtypes (91), suggestive of in-tact IFN signaling mechanisms that if overstimulated, could lead to a growth inhibitory phenotype or cell death. Therefore, the role of IFNα signaling in TNBC is not black and white, but instead, occurs on a spectrum and is cell dependent, both of which much be considered in future studies.

Regardless, our data suggest that the specific mechanism of IFNα signaling utilized by TNBC cells to transcribe IFITM1 contributes valuable information to the responsiveness of TNBC cells to specific therapies. For example, in an effort to target multiple IFN and cytokine stimulated gens, the selective JAK1/JAK2 inhibitor, Ruxolitinib, was investigated in clinical trials for treatment

of metastatic triple-negative breast cancer (161). Ruxolitinib was well tolerated and as expected, decreased activation of JAK target genes and pSTAT3 activity; however, no patient achieved a partial or complete response. The authors suggest intratumoral heterogeneity contributes to resistance to Ruxolitinib, but perhaps, this could be due to alternative signaling mechanisms as outlined in Figure 6.1 B. Supporting this hypothesis, data presented herein identify that ruxolitinib does not robustly decrease IFITM1 expression in TNBC cells perhaps since TNBC cells appear to utilize non-canonical STAT2/IRF9 mediated signaling to drive IFITM1 expression. Though STAT2 is unphosphorylated, this ISGF3-like complex of STAT2 and IRF9 still forms on a basal level in TNBC cells. This finding is translatable since the transcriptional activation of the STAT2/IRF9 complex can occur independent of active JAK activity. This is because IRF9 lacks the autoinhibitory element such that signal induced phosphorylation is non-essential for interaction with STAT2 (66). Therefore, a subset of ISGs, including IFITM1, regulated by JAK independent mechanisms through U-ISGF3 or STAT2/IRF9 could be detrimental to the host by contributing to tumorigenicity and lack of responsiveness to specific JAK inhibitors or eventual JAK mutations. Furthermore, overexpression of IRF9 has been observed in breast tumors contributing to resistance against microtubule destabilizers (72), providing more evidence into the importance of understanding this pathway. Uncovering the context dependent nuances of non-canonical IFNα signaling mechanism would provide rationale into undertaking an investigative medicinal chemistry campaign for specific STAT2 and or IRF9 inhibitors.

Our data suggests a role of both non-canonical IFNα signaling expression and NFκB signaling in regulating IFITM1 expression. Loss of p65 significantly reduces IFITM1 expression and the naturally derived NFκB inhibitor, parthenolide, reduces IFITM1 expression levels and tumor growth *in vivo*. Moreover, data presented herein suggest IFNα mediated gene expression is regulated, in part, through NFκB signaling. Though the exact mechanism whereby these signaling processes converge is unknow, perhaps it hinges upon non-canonical IFN signaling. Previous studies suggest that unphosphorylated-STAT2 and IRF9 work with p65 to regulate gene

expression (82). This finding provides another explanation into the importance of assessing non-canonical IFN crosstalk with other pathways perhaps contributing to drug resistance through specific ISG regulation. Utilization of RNA sequencing in TNBC cells with modulation of IFNα with and without NFκB inhibitors, or the combination, would provide evidence into pathway convergence in TNBC. Lastly, it is important for future studies to investigate the potential non-IFNα mediated drivers of IFITM1 in TNBC as well.

Though our data suggest that the use of parthenolide may be a novel therapeutic avenue in patients with IFITM1 positive TNBC, there are additional pre-clinical obstacles to assess. To overcome the limitation of the low solubility of parthenolide in vivo, analogues including dimethylaminoparthenolide have been developed which have higher water solubility. Though parthenolide significantly inhibited tumor growth and induced death in both SUM149 and MDA-MB-468 cell lines, the effect on IFITM1 and NFkB signaling was not as pronounced in vivo as it was in vitro. Moving forward, characterization of TNBC responsiveness to dimethylaminoparthenolide in regard to IFITM1 expression *in vivo* would be essential prior moving forward with more clinical applications.

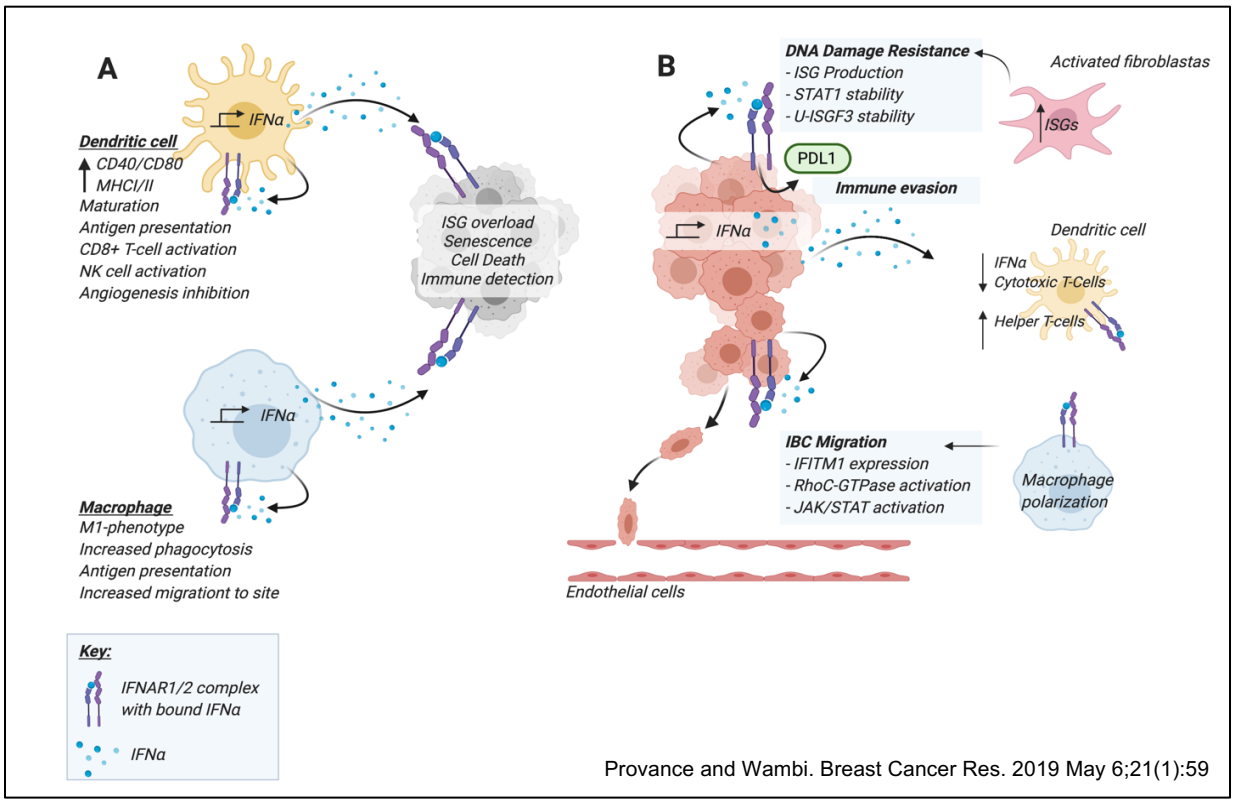

Figure 6.3 Proposed implications of IFNα signaling between the aggressive breast cancer tumor and the tumor microenvironment

A. During canonical IFNα signaling which often occurs during the first steps of immunosurveillance, dendritic cells and macrophages promote tumor cell killing through release of high levels of IFNα. Dendritic cells have high levels of MHC class I and II as well as co-activators (CD40/CD80) which promote the cytotoxic T cell response against the tumor. Macrophages are often polarized to be more M1-like in this scenario. IFNα promotes increased migration of M1-macrophages to the inflamed tissue to aid in antigen presentation. **B.** Hypothesized alterations due to chronic IFNα signaling. IFNα secreted from the tumor cells may act in an autocrine or paracrine manner. In an autocrine fashion, IFNα binds to the receptors on IBC tumor cells increasing PD-L1 expression and upregulating canonical and non-canonical JAK/STAT signaling. Immune evasion may occur through release of IFNα and the paracrine effect on dendritic cells. We hypothesize that increased levels of IFNα produced in the tumor and secreted into the TME in a chronic manner essentially exhausts dendritic cells inhibiting their capability of simulating cytotoxic T cells while instead the helper T cell population is expanded. Furthermore, regulation of JAK/STAT signaling by IFNα may increase DNA damage resistance through increasing ISG production. Additionally, IBC migration is altered through interaction with macrophages. Tumor-associated macrophages in IBC are shown to enhance RhoC-GTPase activation and JAK/STAT signaling by macrophages makes these cells highly aggressive due to their invasion into the blood vessels and the high rate of angiogenesis in IBC. Fibroblasts and endothelial cells in IBC remain understudied; however, macrophages may have the capability to increase the activation of these cells. It is known that type I interferons normally have anti-angiogenic properties (193). However, complex crosstalk between immune cells and stromal cells regulate tumor vasculature (57, 194). Perhaps the tumor cells do not directly act on the endothelial cells via IFNα signaling, but instead the interplay between the other immune and stromal cells previously discussed promotes increased infiltration. The direct relationship between IFNα, IBC, and endothelial cells is elusive. Adapted from Lim et al. Figure created with BioRender.com.

Collectively, this work suggests that some combination of NFκB and JAK/STAT inhibitors can be harnessed as an alternative treatment strategy for TNBC. This proposed alternative strategy has implications in facilitating the response to both chemotherapy and immunotherapy. Primarily, interferon signaling and specific ISG expression has emerged as a predictive indicator for responsiveness to chemotherapy in TNBC (195). Since ISGs can be regulated by both IFNα and NFκB, we hypothesize that inhibition of IFNα and NFκB signaling through the use of parthenolide could enhance the responsiveness to current standard of care agents. This method of IFNα and NFκB inhibition may circumvent the induction of ISGs implicated in DNA damage resistance which are enhanced by current standard of care, perhaps due to microenvironment inflammation. Similarly, data presented herein identify that loss of IFITM1 enhances the sensitivity to parthenolide while additional data obtained from our lab suggest that loss of IFITM1 sensitizes SUM149 cells to doxorubicin. Secondarily, modifying the IFN response in TNBC through use of parthenolide or specifically targeting IFN or IFITM1 will impact the immune microenvironment though the exact mechanisms are unknown. We hypothesize that blocking these proposed mechanisms have the potential to facilitate therapeutic effectiveness to immune checkpoint blockade through altering the expression of PDL1. As previously mentioned, though TNBC cells have high levels of TILs and PDL1, the responsiveness to PDL1 checkpoint inhibitors is low. IFNα has been identified as a regulator of PDL1 expression (Figure 6.2) and loss of IFITM1 increases the levels of MHC molecules and decreases PDL1 as assessed through our RNA sequencing data (data not shown). Therefore, not only could IFNα be contributing to low responsiveness to PDL1 therapies, we hypothesize that inhibition of IFNα signaling whether through parthenolide treatment or developing novel agents to target non-canonical signaling, coupled with additional ICB therapies (i.e: CTLA4 inhibition) has the potential to circumvent ICB resistance through enhancing T-cell responsiveness.

Our long-term goal is to characterize molecular drivers of TNBC aggression as a means for identifying therapeutic targets. Herein we have shown that IFITM1 and its upstream regulators, IFNα and NFκB, are potential therapeutic targets for TNBC. Collectively, the knowledge obtained by continued investigation of the role of type I interferon signaling and downstream gene expression in TNBC not only sheds light on the molecular underpinnings of disease but also provides novel mechanisms of targeted therapy and drug resistance to be considered in the context of translational medicine.

References

1. Bloom HJ, Richardson WW. Histological grading and prognosis in breast cancer; a study of 1409 cases of which 359 have been followed for 15 years. British journal of cancer. 1957;11(3):359-77.
2. Prat A, Pineda E, Adamo B, Galván P, Fernández A, Gaba L, et al. Clinical implications of the intrinsic molecular subtypes of breast cancer. Breast (Edinburgh, Scotland). 2015;24 Suppl 2:S26-35.
3. Prat A, Karginova O, Parker JS, Fan C, He X, Bixby L, et al. Characterization of cell lines derived from breast cancers and normal mammary tissues for the study of the intrinsic molecular subtypes. Breast cancer research and treatment. 2013;142(2):237-55.
4. Prat A, Perou CM. Deconstructing the molecular portraits of breast cancer. Molecular oncology. 2011;5(1):5-23.
5. Perou CM, Sørlie T, Eisen MB, van de Rijn M, Jeffrey SS, Rees CA, et al. Molecular portraits of human breast tumours. Nature. 2000;406(6797):747-52.
6. Sørlie T. The Impact of Gene Expression Patterns in Breast Cancer. Clinical Chemistry. 2016;62(8):1150-1.
7. Lehmann BD, Bauer JA, Chen X, Sanders ME, Chakravarthy AB, Shyr Y, et al. Identification of human triple-negative breast cancer subtypes and preclinical models for selection of targeted therapies. The Journal of clinical investigation. 2011;121(7):2750-67.
8. Bianchini G, Balko JM, Mayer IA, Sanders ME, Gianni L. Triple-negative breast cancer: challenges and opportunities of a heterogeneous disease. Nature reviews Clinical oncology. 2016;13(11):674-90.
9. Denkert C, Liedtke C, Tutt A, von Minckwitz G. Molecular alterations in triple-negative breast cancer-the road to new treatment strategies. Lancet. 2017;389(10087):2430-42.
10. Foulkes WD, Smith IE, Reis-Filho JS. Triple-negative breast cancer. The New England journal of medicine. 2010;363(20):1938-48.
11. Fang WB, Yao M, Brummer G, Acevedo D, Alhakamy N, Berkland C, et al. Targeted gene silencing of CCL2 inhibits triple negative breast cancer progression by blocking cancer stem cell renewal and M2 macrophage recruitment. Oncotarget. 2016;7(31):49349-67.
12. Li X, Yang J, Peng L, Sahin AA, Huo L, Ward KC, et al. Triple-negative breast cancer has worse overall survival and cause-specific survival than non-triple-negative breast cancer. Breast cancer research and treatment. 2017;161(2):279-87.
13. Sharma P. Biology and Management of Patients With Triple-Negative Breast Cancer. Oncologist. 2016;21(9):1050-62.
14. Cejalvo JM, Martinez de Duenas E, Galvan P, Garcia-Recio S, Burgues Gasion O, Pare L, et al. Intrinsic Subtypes and Gene Expression Profiles in Primary and Metastatic Breast Cancer. Cancer research. 2017;77(9):2213-21.
15. Prado-Vazquez G, Gamez-Pozo A, Trilla-Fuertes L, Arevalillo JM, Zapater-Moros A, Ferrer-Gomez M, et al. A novel approach to triple-negative breast cancer molecular classification reveals a luminal immune-positive subgroup with good prognoses. Scientific reports. 2019;9(1):1538.

16. Ismail-Khan R, Bui MM. A review of triple-negative breast cancer. Cancer Control. 2010;17(3):173-6.
17. Prat A, Adamo B, Cheang MC, Anders CK, Carey LA, Perou CM. Molecular characterization of basal-like and non-basal-like triple-negative breast cancer. Oncologist. 2013;18(2):123-33.
18. Jhan JR, Andrechek ER. Triple-negative breast cancer and the potential for targeted therapy. Pharmacogenomics. 2017;18(17):1595-609.
19. Ahn SG, Kim SJ, Kim C, Jeong J. Molecular Classification of Triple-Negative Breast Cancer. Journal of breast cancer. 2016;19(3):223-30.
20. Pareja F, Geyer FC, Marchiò C, Burke KA, Weigelt B, Reis-Filho JS. Triple-negative breast cancer: the importance of molecular and histologic subtyping, and recognition of low-grade variants. NPJ breast cancer. 2016;2:16036.
21. Masuda H, Baggerly KA, Wang Y, Zhang Y, Gonzalez-Angulo AM, Meric-Bernstam F, et al. Differential response to neoadjuvant chemotherapy among 7 triple-negative breast cancer molecular subtypes. Clinical cancer research : an official journal of the American Association for Cancer Research. 2013;19(19):5533-40.
22. Lyons TG. Targeted Therapies for Triple-Negative Breast Cancer. Curr Treat Options Oncol. 2019;20(11):82.
23. Senkus E, Kyriakides S, Penault-Llorca F, Poortmans P, Thompson A, Zackrisson S, et al. Primary breast cancer: ESMO Clinical Practice Guidelines for diagnosis, treatment and follow-up. Annals of oncology : official journal of the European Society for Medical Oncology. 2013;24 Suppl 6:vi7-23.
24. Coates AS, Winer EP, Goldhirsch A, Gelber RD, Gnant M, Piccart-Gebhart M, et al. Tailoring therapies--improving the management of early breast cancer: St Gallen International Expert Consensus on the Primary Therapy of Early Breast Cancer 2015. Annals of oncology : official journal of the European Society for Medical Oncology. 2015;26(8):1533-46.
25. Carey LA, Dees EC, Sawyer L, Gatti L, Moore DT, Collichio F, et al. The triple negative paradox: primary tumor chemosensitivity of breast cancer subtypes. Clinical cancer research : an official journal of the American Association for Cancer Research. 2007;13(8):2329-34.
26. Liedtke C, Mazouni C, Hess KR, André F, Tordai A, Mejia JA, et al. Response to neoadjuvant therapy and long-term survival in patients with triple-negative breast cancer. Journal of clinical oncology : official journal of the American Society of Clinical Oncology. 2008;26(8):1275-81.
27. Cortazar P, Zhang L, Untch M, Mehta K, Costantino JP, Wolmark N, et al. Pathological complete response and long-term clinical benefit in breast cancer: the CTNeoBC pooled analysis. Lancet. 2014;384(9938):164-72.
28. Steward L, Conant L, Gao F, Margenthaler JA. Predictive factors and patterns of recurrence in patients with triple negative breast cancer. Annals of surgical oncology. 2014;21(7):2165-71.
29. Brufsky A, Valero V, Tiangco B, Dakhil S, Brize A, Rugo HS, et al. Second-line bevacizumab-containing therapy in patients with triple-negative breast cancer: subgroup analysis of the RIBBON-2 trial. Breast cancer research and treatment. 2012;133(3):1067-75.

30. Cameron D, Brown J, Dent R, Jackisch C, Mackey J, Pivot X, et al. Adjuvant bevacizumab-containing therapy in triple-negative breast cancer (BEATRICE): primary results of a randomised, phase 3 trial. The Lancet Oncology. 2013;14(10):933-42.
31. Keenan TE, Tolaney SM. Role of Immunotherapy in Triple-Negative Breast Cancer. J Natl Compr Canc Netw. 2020;18(4):479-89.
32. Mittendorf EA, Philips AV, Meric-Bernstam F, Qiao N, Wu Y, Harrington S, et al. PD-L1 expression in triple-negative breast cancer. Cancer Immunology Research. 2014;2(4):361-70.
33. Lotfinejad P, Asghari Jafarabadi M, Abdoli Shadbad M, Kazemi T, Pashazadeh F, Sandoghchian Shotorbani S, et al. Prognostic Role and Clinical Significance of Tumor-Infiltrating Lymphocyte (TIL) and Programmed Death Ligand 1 (PD-L1) Expression in Triple-Negative Breast Cancer (TNBC): A Systematic Review and Meta-Analysis Study. Diagnostics (Basel). 2020;10(9).
34. Soliman H, Khalil F, Antonia S. PD-L1 expression is increased in a subset of basal type breast cancer cells. PloS one. 2014;9(2):e88557.
35. Ghebeh H, Mohammed S, Al-Omair A, Qattan A, Lehe C, Al-Qudaihi G, et al. The B7-H1 (PD-L1) T lymphocyte-inhibitory molecule is expressed in breast cancer patients with infiltrating ductal carcinoma: correlation with important high-risk prognostic factors. Neoplasia. 2006;8(3):190-8.
36. Saleiro D, Platanias LC. Interferon signaling in cancer. Non-canonical pathways and control of intracellular immune checkpoints. Semin Immunol. 2019;43:101299.
37. Cheon H, Holvey-Bates EG, Schoggins JW, Forster S, Hertzog P, Imanaka N, et al. IFNbeta-dependent increases in STAT1, STAT2, and IRF9 mediate resistance to viruses and DNA damage. The EMBO journal. 2013;32(20):2751-63.
38. Chow KT, Gale M, Jr. SnapShot: Interferon Signaling. Cell. 2015;163(7):1808-.e1.
39. Walter MR. The Role of Structure in the Biology of Interferon Signaling. Frontiers in immunology. 2020;11:606489.
40. Bonjardim CA, Ferreira PC, Kroon EG. Interferons: signaling, antiviral and viral evasion. Immunology letters. 2009;122(1):1-11.
41. Stark GR, Kerr IM, Williams BR, Silverman RH, Schreiber RD. How cells respond to interferons. Annual review of biochemistry. 1998;67:227-64.
42. Savan R. Post-transcriptional regulation of interferons and their signaling pathways. Journal of interferon & cytokine research : the official journal of the International Society for Interferon and Cytokine Research. 2014;34(5):318-29.
43. Andzinski L, Spanier J, Kasnitz N, Kroger A, Jin L, Brinkmann MM, et al. Growing tumors induce a local STING dependent Type I IFN response in dendritic cells. International journal of cancer. 2016;139(6):1350-7.
44. Schreiber RD, Old LJ, Smyth MJ. Cancer immunoediting: integrating immunity's roles in cancer suppression and promotion. Science (New York, NY). 2011;331(6024):1565-70.
45. Leplina OY, Tyrinova TV, Tikhonova MA, Ostanin AA, Chernykh ER. Interferon alpha induces generation of semi-mature dendritic cells with high pro-inflammatory and cytotoxic potential. Cytokine. 2015;71(1):1-7.
46. Snell LM, McGaha TL, Brooks DG. Type I Interferon in Chronic Virus Infection and Cancer. Trends Immunol. 2017;38(8):542-57.

47. Ma H, Jin S, Yang W, Zhou G, Zhao M, Fang S, et al. Interferon-alpha enhances the antitumour activity of EGFR-targeted therapies by upregulating RIG-I in head and neck squamous cell carcinoma. British journal of cancer. 2018;118(4):509-21.
48. Brockwell NK, Rautela J, Owen KL, Gearing LJ, Deb S, Harvey K, et al. Tumor inherent interferon regulators as biomarkers of long-term chemotherapeutic response in TNBC. NPJ Precis Oncol. 2019;3:21.
49. Coppe JP, Desprez PY, Krtolica A, Campisi J. The senescence-associated secretory phenotype: the dark side of tumor suppression. Annual review of pathology. 2010;5:99-118.
50. Ma H, Yang W, Zhang L, Liu S, Zhao M, Zhou G, et al. Interferon-alpha promotes immunosuppression through IFNAR1/STAT1 signalling in head and neck squamous cell carcinoma. British journal of cancer. 2019;120(3):317-30.
51. Gato-Cañas M, Zuazo M, Arasanz H, Ibañez-Vea M, Lorenzo L, Fernandez-Hinojal G, et al. PDL1 Signals through Conserved Sequence Motifs to Overcome Interferon-Mediated Cytotoxicity. Cell reports. 2017;20(8):1818-29.
52. Bakhoum SF, Ngo B, Laughney AM, Cavallo JA, Murphy CJ, Ly P, et al. Chromosomal instability drives metastasis through a cytosolic DNA response. Nature. 2018;553(7689):467-72.
53. Provance OK, Lewis-Wambi J. Deciphering the role of interferon alpha signaling and microenvironment crosstalk in inflammatory breast cancer. Breast cancer research : BCR. 2019;21(1):59.
54. Smid M, Hoes M, Sieuwerts AM, Sleijfer S, Zhang Y, Wang Y, et al. Patterns and incidence of chromosomal instability and their prognostic relevance in breast cancer subtypes. Breast cancer research and treatment. 2011;128(1):23-30.
55. Bertucci F, Finetti P, Vermeulen P, Van Dam P, Dirix L, Birnbaum D, et al. Genomic profiling of inflammatory breast cancer: a review. Breast (Edinburgh, Scotland). 2014;23(5):538-45.
56. Cheon H, Borden EC, Stark GR. Interferons and their stimulated genes in the tumor microenvironment. Seminars in oncology. 2014;41(2):156-73.
57. Medrano R, Hunger A, Mendonca S, Barbuto J, Strauss B. Immunomodulatory and antitumor effects of type I interferons and their application in cancer therapy. Oncotarget. 2017;8(41):71249-84.
58. Schneider WM, Chevillotte MD, Rice CM. Interferon-stimulated genes: a complex web of host defenses. Annual review of immunology. 2014;32:513-45.
59. Platanias LC. Mechanisms of type-I- and type-II-interferon-mediated signalling. Nature reviews Immunology. 2005;5(5):375-86.
60. Bluyssen HA, Levy DE. Stat2 is a transcriptional activator that requires sequence-specific contacts provided by stat1 and p48 for stable interaction with DNA. The Journal of biological chemistry. 1997;272(7):4600-5.
61. Blaszczyk K, Nowicka H, Kostyrko K, Antonczyk A, Wesoly J, Bluyssen HA. The unique role of STAT2 in constitutive and IFN-induced transcription and antiviral responses. Cytokine & growth factor reviews. 2016;29:71-81.
62. Blaszczyk K, Olejnik A, Nowicka H, Ozgyin L, Chen YL, Chmielewski S, et al. STAT2/IRF9 directs a prolonged ISGF3-like transcriptional response and antiviral activity in the absence of STAT1. Biochem J. 2015;466(3):511-24.

63. Pfeffer LM. The role of nuclear factor kappaB in the interferon response. Journal of interferon & cytokine research : the official journal of the International Society for Interferon and Cytokine Research. 2011;31(7):553-9.
64. Yang CH, Murti A, Pfeffer SR, Kim JG, Donner DB, Pfeffer LM. Interferon alpha /beta promotes cell survival by activating nuclear factor kappa B through phosphatidylinositol 3-kinase and Akt. The Journal of biological chemistry. 2001;276(17):13756-61.
65. Wienerroither S, Shukla P, Farlik M, Majoros A, Stych B, Vogl C, et al. Cooperative Transcriptional Activation of Antimicrobial Genes by STAT and NF-kappaB Pathways by Concerted Recruitment of the Mediator Complex. Cell reports. 2015;12(2):300-12.
66. Csumita M, Csermely A, Horvath A, Nagy G, Monori F, Göczi L, et al. Specific enhancer selection by IRF3, IRF5 and IRF9 is determined by ISRE half-sites, 5' and 3' flanking bases, collaborating transcription factors and the chromatin environment in a combinatorial fashion. Nucleic Acids Res. 2020;48(2):589-604.
67. Bailey CC, Zhong G, Huang IC, Farzan M. IFITM-Family Proteins: The Cell's First Line of Antiviral Defense. Annual review of virology. 2014;1:261-83.
68. van Boxel-Dezaire AH, Rani MR, Stark GR. Complex modulation of cell type-specific signaling in response to type I interferons. Immunity. 2006;25(3):361-72.
69. Fink K, Grandvaux N. STAT2 and IRF9: Beyond ISGF3. Jak-stat. 2013;2(4):e27521.
70. Ogony J, Choi HJ, Lui A, Cristofanilli M, Lewis-Wambi J. Interferon-induced transmembrane protein 1 (IFITM1) overexpression enhances the aggressive phenotype of SUM149 inflammatory breast cancer cells in a signal transducer and activator of transcription 2 (STAT2)-dependent manner. Breast cancer research : BCR. 2016;18(1):25.
71. Walter KR, Balko JM, Hagan CR. Progesterone receptor promotes degradation of STAT2 to inhibit the interferon response in breast cancer. Oncoimmunology. 2020;9(1):1758547.
72. Luker KE, Pica CM, Schreiber RD, Piwnica-Worms D. Overexpression of IRF9 confers resistance to antimicrotubule agents in breast cancer cells. Cancer research. 2001;61(17):6540-7.
73. Leung S, Qureshi SA, Kerr IM, Darnell JE, Jr., Stark GR. Role of STAT2 in the alpha interferon signaling pathway. Molecular and Cellular Biology. 1995;15(3):1312-7.
74. Hartlova A, Erttmann SF, Raffi FA, Schmalz AM, Resch U, Anugula S, et al. DNA damage primes the type I interferon system via the cytosolic DNA sensor STING to promote anti-microbial innate immunity. Immunity. 2015;42(2):332-43.
75. Honda K, Yanai H, Mizutani T, Negishi H, Shimada N, Suzuki N, et al. Role of a transductional-transcriptional processor complex involving MyD88 and IRF-7 in Toll-like receptor signaling. Proceedings of the National Academy of Sciences of the United States of America. 2004;101(43):15416-21.
76. Platanitis E, Decker T. Regulatory Networks Involving STATs, IRFs, and NFkappaB in Inflammation. Frontiers in immunology. 2018;9:2542.
77. Panne D, Maniatis T, Harrison SC. An atomic model of the interferon-beta enhanceosome. Cell. 2007;129(6):1111-23.

78. Yang CH, Murti A, Valentine WJ, Du Z, Pfeffer LM. Interferon alpha activates NF-kappaB in JAK1-deficient cells through a TYK2-dependent pathway. The Journal of biological chemistry. 2005;280(27):25849-53.
79. Peri S, Devarajan K, Yang DH, Knudson AG, Balachandran S. Meta-analysis identifies NF-κB as a therapeutic target in renal cancer. PloS one. 2013;8(10):e76746.
80. Au-Yeung N, Horvath CM. Transcriptional and chromatin regulation in interferon and innate antiviral gene expression. Cytokine & growth factor reviews. 2018;44:11-7.
81. Platanitis E, Decker T. Regulatory Networks Involving STATs, IRFs, and NFκB in Inflammation. Frontiers in immunology. 2018;9:2542.
82. Nan J, Wang Y, Yang J, Stark GR. IRF9 and unphosphorylated STAT2 cooperate with NF-κB to drive IL6 expression. Proceedings of the National Academy of Sciences of the United States of America. 2018;115(15):3906-11.
83. Aaronson DS, Horvath CM. A road map for those who don't know JAK-STAT. Science (New York, NY). 2002;296(5573):1653-5.
84. He L, Hannon GJ. MicroRNAs: small RNAs with a big role in gene regulation. Nature reviews Genetics. 2004;5(7):522-31.
85. Desai SD, Reed RE, Burks J, Wood LM, Pullikuth AK, Haas AL, et al. ISG15 disrupts cytoskeletal architecture and promotes motility in human breast cancer cells. Experimental biology and medicine (Maywood, NJ). 2012;237(1):38-49.
86. Khodarev NN, Roizman B, Weichselbaum RR. Molecular pathways: interferon/stat1 pathway: role in the tumor resistance to genotoxic stress and aggressive growth. Clin Cancer Res. 2012;18(11):3015-21.
87. Weichselbaum RR, Ishwaran H, Yoon T, Nuyten DS, Baker SW, Khodarev N, et al. An interferon-related gene signature for DNA damage resistance is a predictive marker for chemotherapy and radiation for breast cancer. Proc Natl Acad Sci U S A. 2008;105(47):18490-5.
88. Cervantes-Badillo MG, Paredes-Villa A, Gómez-Romero V, Cervantes-Roldán R, Arias-Romero LE, Villamar-Cruz O, et al. IFI27/ISG12 Downregulates Estrogen Receptor α Transactivation by Facilitating Its Interaction With CRM1/XPO1 in Breast Cancer Cells. Front Endocrinol (Lausanne). 2020;11:568375.
89. Legrier ME, Bièche I, Gaston J, Beurdeley A, Yvonnet V, Déas O, et al. Activation of IFN/STAT1 signalling predicts response to chemotherapy in oestrogen receptor-negative breast cancer. British journal of cancer. 2016;114(2):177-87.
90. Aljohani AI, Joseph C, Kurozumi S, Mohammed OJ, Miligy IM, Green AR, et al. Myxovirus resistance 1 (MX1) is an independent predictor of poor outcome in invasive breast cancer. Breast cancer research and treatment. 2020;181(3):541-51.
91. Buess M, Nuyten DS, Hastie T, Nielsen T, Pesich R, Brown PO. Characterization of heterotypic interaction effects in vitro to deconvolute global gene expression profiles in cancer. Genome biology. 2007;8(9):R191.
92. Jia R, Ding S, Pan Q, Liu SL, Qiao W, Liang C. The C-terminal sequence of IFITM1 regulates its anti-HIV-1 activity. PloS one. 2015;10(3):e0118794.
93. Zhao X, Li J, Winkler CA, An P, Guo JT. IFITM Genes, Variants, and Their Roles in the Control and Pathogenesis of Viral Infections. Front Microbiol. 2018;9:3228.

94. Smith SE, Busse DC, Binter S, Weston S, Diaz Soria C, Laksono BM, et al. Interferon-Induced Transmembrane Protein 1 Restricts Replication of Viruses That Enter Cells via the Plasma Membrane. Journal of virology. 2019;93(6).
95. Hach JC, McMichael T, Chesarino NM, Yount JS. Palmitoylation on conserved and nonconserved cysteines of murine IFITM1 regulates its stability and anti-influenza A virus activity. Journal of virology. 2013;87(17):9923-7.
96. Li K, Jia R, Li M, Zheng YM, Miao C, Yao Y, et al. A sorting signal suppresses IFITM1 restriction of viral entry. The Journal of biological chemistry. 2015;290(7):4248-59.
97. Jia R, Pan Q, Ding S, Rong L, Liu SL, Geng Y, et al. The N-terminal region of IFITM3 modulates its antiviral activity by regulating IFITM3 cellular localization. Journal of virology. 2012;86(24):13697-707.
98. Narayana SK, Helbig KJ, McCartney EM, Eyre NS, Bull RA, Eltahla A, et al. The Interferon-induced Transmembrane Proteins, IFITM1, IFITM2, and IFITM3 Inhibit Hepatitis C Virus Entry. The Journal of biological chemistry. 2015;290(43):25946-59.
99. Wilkins C, Woodward J, Lau DT, Barnes A, Joyce M, McFarlane N, et al. IFITM1 is a tight junction protein that inhibits hepatitis C virus entry. Hepatology. 2013;57(2):461-9.
100. Matsumoto AK, Martin DR, Carter RH, Klickstein LB, Ahearn JM, Fearon DT. Functional dissection of the CD21/CD19/TAPA-1/Leu-13 complex of B lymphocytes. The Journal of experimental medicine. 1993;178(4):1407-17.
101. Hong IK, Byun HJ, Lee J, Jin YJ, Wang SJ, Jeoung DI, et al. The tetraspanin CD81 protein increases melanoma cell motility by up-regulating metalloproteinase MT1-MMP expression through the pro-oncogenic Akt-dependent Sp1 activation signaling pathways. The Journal of biological chemistry. 2014;289(22):15691-704.
102. Vences-Catalán F, Rajapaksa R, Srivastava MK, Marabelle A, Kuo CC, Levy R, et al. Tetraspanin CD81 promotes tumor growth and metastasis by modulating the functions of T regulatory and myeloid-derived suppressor cells. Cancer research. 2015;75(21):4517-26.
103. Zhang N, Zuo L, Zheng H, Li G, Hu X. Increased Expression of CD81 in Breast Cancer Tissue is Associated with Reduced Patient Prognosis and Increased Cell Migration and Proliferation in MDA-MB-231 and MDA-MB-435S Human Breast Cancer Cell Lines In Vitro. Medical science monitor : international medical journal of experimental and clinical research. 2018;24:5739-47.
104. Lui AJ, Geanes ES, Ogony J, Behbod F, Marquess J, Valdez K, et al. IFITM1 suppression blocks proliferation and invasion of aromatase inhibitor-resistant breast cancer in vivo by JAK/STAT-mediated induction of p21. Cancer letters. 2017;399:29-43.
105. Yu F, Ng SS, Chow BK, Sze J, Lu G, Poon WS, et al. Knockdown of interferon-induced transmembrane protein 1 (IFITM1) inhibits proliferation, migration, and invasion of glioma cells. Journal of neuro-oncology. 2011;103(2):187-95.
106. Hatano H, Kudo Y, Ogawa I, Tsunematsu T, Kikuchi A, Abiko Y, et al. IFN-induced transmembrane protein 1 promotes invasion at early stage of head and neck cancer progression. Clinical cancer research : an official journal of the American Association for Cancer Research. 2008;14(19):6097-105.

107. Kim NH, Sung HY, Choi EN, Lyu D, Choi HJ, Ju W, et al. Aberrant DNA methylation in the IFITM1 promoter enhances the metastatic phenotype in an intraperitoneal xenograft model of human ovarian cancer. Oncology reports. 2014;31(5):2139-46.
108. Sari IN, Yang YG, Phi LT, Kim H, Baek MJ, Jeong D, et al. Interferon-induced transmembrane protein 1 (IFITM1) is required for the progression of colorectal cancer. Oncotarget. 2016;7(52):86039-50.
109. Yu F, Xie D, Ng SS, Lum CT, Cai MY, Cheung WK, et al. IFITM1 promotes the metastasis of human colorectal cancer via CAV-1. Cancer letters. 2015;368(1):135-43.
110. Yuan ZY, Luo RZ, Peng RJ, Wang SS, Xue C. High infiltration of tumor-associated macrophages in triple-negative breast cancer is associated with a higher risk of distant metastasis. OncoTargets and therapy. 2014;7:1475-80.
111. Xu YY, Yu HR, Sun JY, Zhao Z, Li S, Zhang XF, et al. Upregulation of PITX2 Promotes Letrozole Resistance Via Transcriptional Activation of IFITM1 Signaling in Breast Cancer Cells. Cancer Res Treat. 2019;51(2):576-92.
112. Zacharias AL, Lewandoski M, Rudnicki MA, Gage PJ. Pitx2 is an upstream activator of extraocular myogenesis and survival. Dev Biol. 2011;349(2):395-405.
113. Yang J, Li L, Xi Y, Sun R, Wang H, Ren Y, et al. Combination of IFITM1 knockdown and radiotherapy inhibits the growth of oral cancer. Cancer science. 2018;109(10):3115-28.
114. Theofilopoulos AN, Baccala R, Beutler B, Kono DH. Type I interferons (alpha/beta) in immunity and autoimmunity. Annual review of immunology. 2005;23:307-36.
115. Győrffy B, Lanczky A, Eklund AC, Denkert C, Budczies J, Li Q, et al. An online survival analysis tool to rapidly assess the effect of 22,277 genes on breast cancer prognosis using microarray data of 1,809 patients. Breast cancer research and treatment. 2010;123(3):725-31.
116. Behbod F, Kittrell FS, LaMarca H, Edwards D, Kerbawy S, Heestand JC, et al. An intraductal human-in-mouse transplantation model mimics the subtypes of ductal carcinoma in situ. Breast cancer research : BCR. 2009;11(5):R66.
117. Chang CS, Kitamura E, Johnson J, Bollag R, Hawthorn L. Genomic analysis of racial differences in triple negative breast cancer. Genomics. 2019;111(6):1529-42.
118. Lee J, Goh SH, Song N, Hwang JA, Nam S, Choi IJ, et al. Overexpression of IFITM1 has clinicopathologic effects on gastric cancer and is regulated by an epigenetic mechanism. The American journal of pathology. 2012;181(1):43-52.
119. Wang M, Zhang Y, Xu Z, Qian P, Sun W, Wang X, et al. RelB sustains endocrine resistant malignancy: an insight of noncanonical NF-κB pathway into breast Cancer progression. Cell communication and signaling : CCS. 2020;18(1):128.
120. Sovak MA, Bellas RE, Kim DW, Zanieski GJ, Rogers AE, Traish AM, et al. Aberrant nuclear factor-kappaB/Rel expression and the pathogenesis of breast cancer. The Journal of clinical investigation. 1997;100(12):2952-60.
121. Yang YG, Koh YW, Sari IN, Jun N, Lee S, Phi LTH, et al. Interferon-induced transmembrane protein 1-mediated EGFR/SOX2 signaling axis is essential for progression of non-small cell lung cancer. International journal of cancer. 2018.
122. Vences-Catalan F, Duault C, Kuo CC, Rajapaksa R, Levy R, Levy S. CD81 as a tumor target. Biochem Soc Trans. 2017;45(2):531-5.

123. Wright MD, Moseley GW, van Spriel AB. Tetraspanin microdomains in immune cell signalling and malignant disease. Tissue Antigens. 2004;64(5):533-42.
124. Siegrist F, Ebeling M, Certa U. The small interferon-induced transmembrane genes and proteins. Journal of interferon & cytokine research : the official journal of the International Society for Interferon and Cytokine Research. 2011;31(1):183-97.
125. Kim JY, Kim H, Suk K, Lee WH. Activation of CD147 with cyclophilin a induces the expression of IFITM1 through ERK and PI3K in THP-1 cells. Mediators of inflammation. 2010;2010:821940.
126. Gruosso T, Gigoux M, Manem VSK, Bertos N, Zuo D, Perlitch I, et al. Spatially distinct tumor immune microenvironments stratify triple-negative breast cancers. The Journal of clinical investigation. 2019;129(4):1785-800.
127. Chandrashekar DS, Bashel B, Balasubramanya SAH, Creighton CJ, Ponce-Rodriguez I, Chakravarthi B, et al. UALCAN: A Portal for Facilitating Tumor Subgroup Gene Expression and Survival Analyses. Neoplasia (New York, NY). 2017;19(8):649-58.
128. Rhodes DR, Kalyana-Sundaram S, Mahavisno V, Varambally R, Yu J, Briggs BB, et al. Oncomine 3.0: genes, pathways, and networks in a collection of 18,000 cancer gene expression profiles. Neoplasia (New York, NY). 2007;9(2):166-80.
129. Rhodes DR, Yu J, Shanker K, Deshpande N, Varambally R, Ghosh D, et al. ONCOMINE: a cancer microarray database and integrated data-mining platform. Neoplasia (New York, NY). 2004;6(1):1-6.
130. Lewis JS, Meeke K, Osipo C, Ross EA, Kidawi N, Li T, et al. Intrinsic mechanism of estradiol-induced apoptosis in breast cancer cells resistant to estrogen deprivation. Journal of the National Cancer Institute. 2005;97(23):1746-59.
131. Andrews S. FastQC: a quality control tool for high throughput sequence data. Available online at: http://www.bioinformatics.babraham.ac.uk/projects/fastqc. 2010.
132. Benjamini Y, Hochberg Y. Controlling the false discovery rate: a practical and powerful approach to multiple testing. Journal of the Royal Statistical Society Series B (Methodological). 1995:289-300.
133. Krogh A, Larsson B, von Heijne G, Sonnhammer EL. Predicting transmembrane protein topology with a hidden Markov model: application to complete genomes. J Mol Biol. 2001;305(3):567-80.
134. Evans SS, Lee DB, Han T, Tomasi TB, Evans RL. Monoclonal antibody to the interferon-inducible protein Leu-13 triggers aggregation and inhibits proliferation of leukemic B cells. Blood. 1990;76(12):2583-93.
135. Paksa A, Bandemer J, Hoeckendorf B, Razin N, Tarbashevich K, Minina S, et al. Repulsive cues combined with physical barriers and cell-cell adhesion determine progenitor cell positioning during organogenesis. Nature communications. 2016;7:11288.
136. Wylie C. IFITM1-mediated cell repulsion controls the initial steps of germ cell migration in the mouse. Dev Cell. 2005;9(6):723-4.
137. Savidis G, Perreira JM, Portmann JM, Meraner P, Guo Z, Green S, et al. The IFITMs Inhibit Zika Virus Replication. Cell reports. 2016;15(11):2323-30.

138. Brass AL, Huang IC, Benita Y, John SP, Krishnan MN, Feeley EM, et al. The IFITM proteins mediate cellular resistance to influenza A H1N1 virus, West Nile virus, and dengue virus. Cell. 2009;139(7):1243-54.
139. Sun F, Xia Z, Han Y, Gao M, Wang L, Wu Y, et al. Topology, Antiviral Functional Residues and Mechanism of IFITM1. Viruses. 2020;12(3).
140. Kowal EJK, Ter-Ovanesyan D, Regev A, Church GM. Extracellular Vesicle Isolation and Analysis by Western Blotting. Methods in molecular biology (Clifton, NJ). 2017;1660:143-52.
141. Uretmen Kagiali ZC, Sanal E, Karayel Ö, Polat AN, Saatci Ö, Ersan PG, et al. Systems-level Analysis Reveals Multiple Modulators of Epithelial-mesenchymal Transition and Identifies DNAJB4 and CD81 as Novel Metastasis Inducers in Breast Cancer. Molecular & cellular proteomics : MCP. 2019;18(9):1756-71.
142. Levy S, Todd SC, Maecker HT. CD81 (TAPA-1): a molecule involved in signal transduction and cell adhesion in the immune system. Annual review of immunology. 1998;16:89-109.
143. Takahashi S, Doss C, Levy S, Levy R. TAPA-1, the target of an antiproliferative antibody, is associated on the cell surface with the Leu-13 antigen. Journal of immunology (Baltimore, Md : 1950). 1990;145(7):2207-13.
144. Cherukuri A, Shoham T, Sohn HW, Levy S, Brooks S, Carter R, et al. The tetraspanin CD81 is necessary for partitioning of coligated CD19/CD21-B cell antigen receptor complexes into signaling-active lipid rafts. Journal of immunology (Baltimore, Md : 1950). 2004;172(1):370-80.
145. Campos A, Salomon C, Bustos R, Díaz J, Martínez S, Silva V, et al. Caveolin-1-containing extracellular vesicles transport adhesion proteins and promote malignancy in breast cancer cell lines. Nanomedicine (Lond). 2018;13(20):2597-609.
146. Vences-Catalan F, Levy S. Immune Targeting of Tetraspanins Involved in Cell Invasion and Metastasis. Frontiers in immunology. 2018;9:1277.
147. Detchokul S, Williams ED, Parker MW, Frauman AG. Tetraspanins as regulators of the tumour microenvironment: implications for metastasis and therapeutic strategies. Br J Pharmacol. 2014;171(24):5462-90.
148. Hemler ME. Tetraspanin functions and associated microdomains. Nat Rev Mol Cell Biol. 2005;6(10):801-11.
149. Sala-Valdes M, Ailane N, Greco C, Rubinstein E, Boucheix C. Targeting tetraspanins in cancer. Expert Opin Ther Targets. 2012;16(10):985-97.
150. Quast T, Eppler F, Semmling V, Schild C, Homsi Y, Levy S, et al. CD81 is essential for the formation of membrane protrusions and regulates Rac1-activation in adhesion-dependent immune cell migration. Blood. 2011;118(7):1818-27.
151. Becker A, Thakur BK, Weiss JM, Kim HS, Peinado H, Lyden D. Extracellular Vesicles in Cancer: Cell-to-Cell Mediators of Metastasis. Cancer cell. 2016;30(6):836-48.
152. Jabbari N, Akbariazar E, Feqhhi M, Rahbarghazi R, Rezaie J. Breast cancer-derived exosomes: Tumor progression and therapeutic agents. Journal of cellular physiology. 2020;235(10):6345-56.

153. Jezequel P, Campone M, Gouraud W, Guerin-Charbonnel C, Leux C, Ricolleau G, et al. bc-GenExMiner: an easy-to-use online platform for gene prognostic analyses in breast cancer. Breast cancer research and treatment. 2012;131(3):765-75.
154. Kim SH, In Choi H, Choi MR, An GY, Binas B, Jung KH, et al. Epigenetic regulation of IFITM1 expression in lipopolysaccharide-stimulated human mesenchymal stromal cells. Stem Cell Res Ther. 2020;11(1):16.
155. Escher TE, Lui AJ, Geanes ES, Walter KR, Tawfik O, Hagan CR, et al. Interaction Between MUC1 and STAT1 Drives IFITM1 Overexpression in Aromatase Inhibitor-Resistant Breast Cancer Cells and Mediates Estrogen-Induced Apoptosis. Molecular cancer research : MCR. 2019;17(5):1180-94.
156. Bordens R, Grossberg SE, Trotta PP, Nagabbushan TL. Molecular and biologic charaterization of recombinant interferon-a2b. Seminars in oncology. 1997;24 (9):41-51.
157. Schreiber G. The molecular basis for differential type I interferon signaling. The Journal of biological chemistry. 2017;292(18):7285-94.
158. Iwanaszko M, Kimmel M. NF-κB and IRF pathways: cross-regulation on target genes promoter level. BMC genomics. 2015;16(1):307.
159. Ahmed F, Mahmood N, Shahid S, Hussain Z, Ahmed I, Jalal A, et al. Mutations in Human Interferon alpha2b Gene and Potential as Risk Factor Associated with Female Breast Cancer. Cancer biotherapy & radiopharmaceuticals. 2016;31(6):199-208.
160. Majoros A, Platanitis E, Kernbauer-Hölzl E, Rosebrock F, Müller M, Decker T. Canonical and Non-Canonical Aspects of JAK-STAT Signaling: Lessons from Interferons for Cytokine Responses. Frontiers in immunology. 2017;8:29.
161. Stover DG, Gil Del Alcazar CR, Brock J, Guo H, Overmoyer B, Balko J, et al. Phase II study of ruxolitinib, a selective JAK1/2 inhibitor, in patients with metastatic triple-negative breast cancer. NPJ breast cancer. 2018;4:10.
162. Shang D, Yang P, Liu Y, Song J, Zhang F, Tian Y. Interferon-alpha induces G1 cell-cycle arrest in renal cell carcinoma cells via activation of Jak-Stat signaling. Cancer investigation. 2011;29(5):347-52.
163. Rong L, Li R, Li S, Luo R. Immunosuppression of breast cancer cells mediated by transforming growth factor-beta in exosomes from cancer cells. Oncology letters. 2016;11(1):500-4.
164. Wesoly J, Szweykowska-Kulinska Z, Bluyssen HA. STAT activation and differential complex formation dictate selectivity of interferon responses. Acta Biochim Pol. 2007;54(1):27-38.
165. Alazawi W, Heath H, Waters JA, Woodfin A, O'Brien AJ, Scarzello AJ, et al. Stat2 loss leads to cytokine-independent, cell-mediated lethality in LPS-induced sepsis. Proceedings of the National Academy of Sciences of the United States of America. 2013;110(21):8656-61.
166. Nan J, Wang Y, Yang J, Stark GR. IRF9 and unphosphorylated STAT2 cooperate with NF-kappaB to drive IL6 expression. Proceedings of the National Academy of Sciences of the United States of America. 2018;115(15):3906-11.
167. Tan DS, Marchio C, Jones RL, Savage K, Smith IE, Dowsett M, et al. Triple negative breast cancer: molecular profiling and prognostic impact in adjuvant

anthracycline-treated patients. Breast cancer research and treatment. 2008;111(1):27-44.
168. Sakuma K, Kurosumi M, Oba H, Kobayashi Y, Takei H, Inoue K, et al. Pathological tumor response to neoadjuvant chemotherapy using anthracycline and taxanes in patients with triple-negative breast cancer. Exp Ther Med. 2011;2(2):257-64.
169. Koppikar P, Bhagwat N, Kilpivaara O, Manshouri T, Adli M, Hricik T, et al. Heterodimeric JAK-STAT activation as a mechanism of persistence to JAK2 inhibitor therapy. Nature. 2012;489(7414):155-9.
170. Pushpakom S, Iorio F, Eyers PA, Escott KJ, Hopper S, Wells A, et al. Drug repurposing: progress, challenges and recommendations. Nature reviews Drug discovery. 2019;18(1):41-58.
171. Weir SJ, DeGennaro LJ, Austin CP. Repurposing approved and abandoned drugs for the treatment and prevention of cancer through public-private partnership. Cancer research. 2012;72(5):1055-8.
172. Kishida Y, Yoshikawa H, Myoui A. Parthenolide, a natural inhibitor of Nuclear Factor-kappaB, inhibits lung colonization of murine osteosarcoma cells. Clinical cancer research : an official journal of the American Association for Cancer Research. 2007;13(1):59-67.
173. D'Anneo A, Carlisi D, Lauricella M, Puleio R, Martinez R, Di Bella S, et al. Parthenolide generates reactive oxygen species and autophagy in MDA-MB231 cells. A soluble parthenolide analogue inhibits tumour growth and metastasis in a xenograft model of breast cancer. Cell death & disease. 2013;4:e891.
174. Carlisi D, Buttitta G, Di Fiore R, Scerri C, Drago-Ferrante R, Vento R, et al. Parthenolide and DMAPT exert cytotoxic effects on breast cancer stem-like cells by inducing oxidative stress, mitochondrial dysfunction and necrosis. Cell death & disease. 2016;7:e2194.
175. Liu M, Xiao C, Sun M, Tan M, Hu L, Yu Q. Parthenolide Inhibits STAT3 Signaling by Covalently Targeting Janus Kinases. Molecules. 2018;23(6).
176. Morel KL, Ormsby RJ, Bezak E, Sweeney CJ, Sykes PJ. Parthenolide Selectively Sensitizes Prostate Tumor Tissue to Radiotherapy while Protecting Healthy Tissues In Vivo. Radiat Res. 2017;187(5):501-12.
177. Yang Q, Wan L, Zhou Z, Li Y, Yu Q, Liu L, et al. Parthenolide from Parthenium integrifolium reduces tumor burden and alleviate cachexia symptoms in the murine CT-26 model of colorectal carcinoma. Phytomedicine. 2013;20(11):992-8.
178. Kreuger MR, Grootjans S, Biavatti MW, Vandenabeele P, D'Herde K. Sesquiterpene lactones as drugs with multiple targets in cancer treatment: focus on parthenolide. Anticancer Drugs. 2012;23(9):883-96.
179. Berdan CA, Ho R, Lehtola HS, To M, Hu X, Huffman TR, et al. Parthenolide Covalently Targets and Inhibits Focal Adhesion Kinase in Breast Cancer Cells. Cell chemical biology. 2019.
180. D'Anneo A, Carlisi D, Lauricella M, Puleio R, Martinez R, Di Bella S, et al. Parthenolide generates reactive oxygen species and autophagy in MDA-MB231 cells. A soluble parthenolide analogue inhibits tumour growth and metastasis in a xenograft model of breast cancer. Cell death & disease. 2013;4(10):e891.
181. Carlisi D, Buttitta G, Di Fiore R, Scerri C, Drago-Ferrante R, Vento R, et al. Parthenolide and DMAPT exert cytotoxic effects on breast cancer stem-like cells

by inducing oxidative stress, mitochondrial dysfunction and necrosis. Cell death & disease. 2016;7(4):e2194.
182. Sztiller-Sikorska M, Czyz M. Parthenolide as Cooperating Agent for Anti-Cancer Treatment of Various Malignancies. Pharmaceuticals (Basel). 2020;13(8).
183. Freund RRA, Gobrecht P, Fischer D, Arndt HD. Advances in chemistry and bioactivity of parthenolide. Nat Prod Rep. 2020;37(4):541-65.
184. Kwok BH, Koh B, Ndubuisi MI, Elofsson M, Crews CM. The anti-inflammatory natural product parthenolide from the medicinal herb Feverfew directly binds to and inhibits IkappaB kinase. Chemistry & biology. 2001;8(8):759-66.
185. Yu T, Di G. Role of tumor microenvironment in triple-negative breast cancer and its prognostic significance. Chinese journal of cancer research = Chung-kuo yen cheng yen chiu. 2017;29(3):237-52.
186. Oshi M, Asaoka M, Tokumaru Y, Yan L, Matsuyama R, Ishikawa T, et al. CD8 T Cell Score as a Prognostic Biomarker for Triple Negative Breast Cancer. International journal of molecular sciences. 2020;21(18).
187. Bagati A, Kumar S, Jiang P, Pyrdol J, Zou AE, Godicelj A, et al. Integrin αvβ6-TGFβ-SOX4 Pathway Drives Immune Evasion in Triple-Negative Breast Cancer. Cancer cell. 2021;39(1):54-67.e9.
188. Lim B, Woodward WA, Wang X, Reuben JM, Ueno NT. Inflammatory breast cancer biology: the tumour microenvironment is key. Nature reviews Cancer. 2018.
189. Bergin ART, Loi S. Triple-negative breast cancer: recent treatment advances. F1000Res. 2019;8.
190. Roux C, Jafari SM, Shinde R, Duncan G, Cescon DW, Silvester J, et al. Reactive oxygen species modulate macrophage immunosuppressive phenotype through the up-regulation of PD-L1. Proceedings of the National Academy of Sciences of the United States of America. 2019;116(10):4326-35.
191. Vinayak S, Tolaney SM, Schwartzberg L, Mita M, McCann G, Tan AR, et al. Open-Label Clinical Trial of Niraparib Combined With Pembrolizumab for Treatment of Advanced or Metastatic Triple-Negative Breast Cancer. JAMA Oncol. 2019;5(8):1132-40.
192. Gaynor N, Crown J, Collins DM. Immune checkpoint inhibitors: Key trials and an emerging role in breast cancer. Semin Cancer Biol. 2020.
193. Indraccolo S. Interferon-alpha as angiogenesis inhibitor: learning from tumor models. Autoimmunity. 2010;43(3):244-7.
194. Norton KA, Jin K, Popel AS. Modeling triple-negative breast cancer heterogeneity: Effects of stromal macrophages, fibroblasts and tumor vasculature. Journal of theoretical biology. 2018;452:56-68.
195. Erdal E, Haider S, Rehwinkel J, Harris AL, McHugh PJ. A prosurvival DNA damage-induced cytoplasmic interferon response is mediated by end resection factors and is limited by Trex1. Genes & development. 2017;31(4):353-69.